UNIVERSITY OF SOUTHAMPTON

FACULTY OF ENGINEERING, SCIENCE & MATHEMATICS

School of Ocean & Earth Sciences

An Investigation Into The Dynamics Of The Ocean Current System Off Southern Greenland

By

David Wilkinson

Thesis for the degree of Doctor of Philosophy

September 2008

UNIVERSITY OF SOUTHAMPTON

ABSTRACT

FACULTY OF ENGINEERING, SCIENCE & MATHEMATICS

SCHOOL OF OCEAN & EARTH SCIENCES

Doctor of Philosophy

AN INVESTIGATION INTO THE DYNAMICS OF THE OCEAN CURRENT SYSTEM OFF SOUTHERN GREENLAND

By David Wilkinson

The ocean current system off Southern Greenland is a key component of the Earth's climate system due to its role in the regulation of the global thermohaline circulation. A combination of historic and new observational data, supported by modelling simulations, has revealed great complexity in both the surface and deep currents of the area. A comprehensive review of the available hydrographic data for the South-East Greenland shelf has shown that the observed spatial variability in the transport of the on-shelf East Greenland Coastal Current is inconsistent with the theory that it is primarily driven by local fjord runoff. A high resolution regional modelling study supports these observations and suggests that the East Greenland Coastal Current is primarily the result of a bifurcation of the East Greenland Current in the vicinity of Denmark Strait. Model simulations also suggest that the pathways followed by the low salinity output of the region's fjord complexes are influenced by the strength and position of the main East Greenland Current. New data collected in the vicinity of Cape Farewell, on the southern tip of Greenland, has also revealed more complex behaviour in the Deep Western Boundary Current. The significant spatial variability in Deep Western Boundary Current transport observed in the region of Cape Farewell suggests that the confluence of Denmark Strait Overflow Water and Iceland Scotland Overflow Water occurs over a wider geographic area than is commonly suggested. A review of historic data indicates that these spatial patterns vary over timescales of months and upwards. It is hypothesised that strands of overflow water follow different depth controlled pathways dependent on their relative water density in comparison with the surrounding water masses. This has significance for the way deep current strength proxies in the region are interpreted in relation to climatic variations. Time series data for a single location may well overestimate the variability in the Deep Western Boundary Current further south due to path switching of the flow. In the future more complete observational datasets combined with more advanced oceanographic and coupled climate models will provide a better understanding of the interaction between the regional current system, the global current system and the climate system. This will enable more reliable prediction of the impact of global warming and, in particular, the potential influence of accelerated Greenland ice cap melting on the global ocean circulation.

CONTENTS

1. Introduction 11

2. Thesis Layout 15

3. Background 16
   - 3.1 The Global Thermohaline Circulation
   - 3.2 Modern Physical Oceanography Of The Northern North Atlantic
   - 3.3 Characteristic Water Masses Of The Region
   - 3.4 The Evolution Of The East Greenland And Deep Western Boundary Currents
   - 3.5 Palaeoclimate And Palaeocirculation Records From North Atlantic Contourite Sediments

4 Observational Studies 53
   - 4.1 The East Greenland Coastal Current
   - 4.2 Appendices To EGCC Paper
   - 4.3 The Deep Western Boundary Current
   - 4.4 Appendices To DWBC Paper

5 Modelling Studies 124
   - 5.1 The East Greenland Current System

6. Concluding Remarks 162
   - 6.1 Overview
   - 6.2 Summary of results
   - 6.3 Future work
   - 6.4 An introduction to modelling the deep flows of the northern North Atlantic

7. References 172

FIGURES & TABLES

Figures

1.1	Key ocean currents of the northern North Atlantic	11
1.2	Key geographic features of the northern North Atlantic	13
3.1.1	The global thermohaline circulation after Broecker (1991)	16
3.1.2	Predicted changes in global mean temperature from coupled climate models running standard scenarios	20
3.1.3	Changes in atmospheric greenhouse gas concentrations	20
3.4.1	The East Greenland Current: its interaction with the waters of the Nordic Seas its contributions to the Denmark Strait overflow	32
3.4.2	The different water masses as they flow along the Greenland slope shown on a density axis	35
3.4.3	The major current systems of the northern North Atlantic between Denmark Strait and the Grand Banks	42
3.4.4	Cross section of DWBC and NAC off the Grand Banks	45
3.5.1	Sediment drifts in the northern North Atlantic (Wold, 1994)	49
GRL1	Map of the SE Greenland region showing the EGCC	58
GRL2	Plot of model derived freshwater transport against total transport calculated from combined observations and model data.	60
GRL3	Plot of percentage error in model derived transport	61
GRL4	Plot of total transport versus depth of EGCC as defined by the maximum observed depth of the 33.5 isohaline	64
GRL5	Plot of total transport versus year with period means	65
DSR1	Pathways of the main deep and intermediate water masses contributing to the DWBC	73
DSR2	Bathymetric map of the Eirik Drift and schematic cross-section of the northern drift flank	78
DSR3	Swath bathymetric map of the southern of the two newly discovered seamounts	79
DSR4	a) Location of hydrographic data and b) Location of geological and geophysical data from cruise D298	81

DSR5 Schematic demonstration of the problems associated with the calculation of geostrophic current velocities for a bottom-intensified current on a sloping bottom. 82

DSR6 Geostrophic velocity and water property contour plots for the D298 sections 87

DSR7. Cross-plots of salinity versus oxygen saturation for a) all D298 sections and b) section D2. 90

DSR8 Plots of salinity versus silicate concentration for all D298 samples taken within 600 m of the bottom and in depths of over 1500m. 92

DSR9 Depth profiles of silicate concentration for D298 sections 93

DSR10 Comparison of velocity cross-sections and water-mass characteristics between new and historic sections 97

DSR11 a) Spatial distribution of sedimentation regimes determined from echo-character data. b) Spatial distribuition of DWBC characteristics determined from the D298 hydrographic data. 102

DSR12 Echo characteristics of the upper Eirik Drift 104

DSR 13 Sidescan sonar line crossing the drift crest, with the corresponding 3.5 kHz section shown below 106

DSR 14 Echo characteristics of the deep-water, southeastern flank of the Eirik Drift, with fine surface sediments in the deep ET2 zone 108

DSR15 Echo characteristics of the deep-water western drift toe and Labrador abyssal plain, with grain size distribution data from core D298-P3. 109

DSR16 3.5 kHz section from the vicinity of core D298-P2 along with the core log and magnetic susceptibility record from D298-P2 110

DSR17 a) Schematic representation of the path of the DWBC through the Irminger and Labrador Basins b) Silicate (μmol l^{-1}) of the deep silicate maximum. 113

4.4.1 Schematic of CTD section over a sloping bottom 120

5.1.1 Map of the South-East Greenland region 127

5.1.2 Example model domains showing the rotated grid 130

5.1.3 The impact of a simplified shelf bathymetry on a 2SV barotropic current of 25km width 136

5.1.4 Plot of potential density along a section taken perpendicular from the East Greenland coast at a latitude of 68.5^{o}N 137

5.1.5 Current characteristics for two baroclinic currents of different depths and strengths 138
5.1.6 Detailed sections at i=200 for model runs 5 and 6 (day 360) 139
5.1.7 The southward evolution of a shallow current initiated over the continental slope when flowing into a basin with an established frontal structure (run 7) and one with a simple stratified structure (run 8) 140
5.1.8 Spatial evolution of a 300m deep current flowing over realistic topography Model run 9 Day 360 142
5.1.9 Contrasting the differing southward evolution of baroclinic currents of different depths, strengths and starting positions 144
5.1.10 Tracer 1 surface concentration: Model run 14, day 370 146
5.1.11 The impact of fjord runoff of 0.1 Sv, from the two major fjord complexes on a quasi-realistic EGC. Model run 14 – cumulative run time 600 days 148
5.1.12 Detailed cross-sections showing tracer concentrations across the Greenland shelf. Model run 14 - cumulative run time 600 days 149
5.1.13 The impact of increases in fjord runoff on two EGC scenarios 150
5.1.14 The impact of wind stress on the EGC/EGCC system 152
5.1.15 The impact of wind stress on the cross-sectional structure of the EGC 153
6.2.1 North Atlantic model domain 166
6.2.2 Contour map of bottom layer temperature after 720 days. The northern reservoir temperature was set to -2^{o}C and the interface depth set to 500m 167

Tables

3.3.1	Water Mass Characteristics In The EGC and DWBC	31
GRL1	Summary Details Of Hydrographic Sections Employed	70
DSR1	Typical water-mass characteristics for the components of the DWBC	76
DSR2	Source of World Ocean Database historic sections	82
DSR3	Summary results from D298 geostrophic velocity calculations	87
DSR4	Summary of transport and DWBC water characteristics for the historic sections in comparison with D1.	95
DSR5	Sources of 3.5 kHz and 5.1kHz profiler data	99
DSR6	Summary of the echo-character types observed in the Cape Farewell Eirik Drift region.	100
4.4.5	Geostrophic Transports For The D298 Sections Via Different Methodologies	123
5.1.1	Frontal Model Parameters Used To Define Incoming EGC Main characteristics of model runs employed	132
5.1.2	Main characteristics of model runs employed	133
5.1.3	Example plume dimensions after Yankovsky and Chapman (1997)	158

DECLARATION OF AUTHORSHIP

I, David Wilkinson declare that the thesis entitled:

An Investigation Into The Dynamics Of The Ocean Current System Off Southern Greenland

and the work presented in the thesis are both my own, and have been generated by me as the result of my own original research. I confirm that:

- this work was done entirely or mainly whilst in candidature for a research degree at this University;
- where any part of the thesis has previously been submitted for a degree or any other qualification at this University or any other institution, this has been clearly stated;
- where I have consulted the published work of others, the source is always given. With the exception of such quotations, the thesis is entirely my own work;
- I have acknowledged all main sources of help;
- where the thesis is based on the work done by myself jointly with others, I have made clear exactly what was done by the others and what I have contributed myself.
- parts of this work have been published as:

The spatial and temporal variability of the East Greenland Coastal Current from historic data: Wilkinson & Bacon, 2005 – Geophysical Research Lettters Vol.32

Deep western boundary current dynamics and associated sedimentation on the Eirik Drift, Southern Greenland Margin: Hunter et al., 2007 - Deep Sea Research Part I, Vol. 54

Signed:

Date: 30th September 2008

ACKNOWLEDGEMENTS

The author would like to acknowledge the support of the following:

The Master and crew of the R.R.S. Discovery for their role in the role in gathering new data off the SE Greenland coast during cruise D298.

The scientific party aboard cruise D298 for their assistance with the data collection and its subsequent processing.

Dr. Alex Megann for his invaluable assistance in setting up the regional implementation of HYCOM used in the modelling studies.

Prof. Eelco Rohling, who acted as lead supervisor. Prof. Dorrik Stow and Dr. Sheldon Bacon who acted as co-supervisors.

The author's work was funded as part of the NERC Rapid Climate Change Program under Grants NER/T/S/2002/00453 and NER/T/S/2002/00436.

DEFINITIONS & ABBREVIATIONS

AABW – Antarctic Bottom Water

AAW - Arctic Atlantic Water

AIW - Arctic Intermediate Water

CBDW - Canadian Basin Deep Water

CGFZ - see GFZW

DSOW – Denmark Strait Overflow Water

EBDW - Eurasian Basin Deep Water

EGC – East Greenland Current

EGCC – East Greenland Coastal Current

GFZW – Charlie Gibbs Fracture Zone Water

GIS – Greenland-Iceland-Scotland

IAIW - Iceland Sea Arctic Intermediate Water

IC – Irminger Current

KF/T – Kangerlugssuaq Fjord/Trough

ISOW – Iceland Scotland Overflow Water

LSW – Labrador Sea Water

LC – Labrador Current

MEIW - Modified East Icelandic Water

MW - Mediterranean Water

NAC – North Atlantic Current

NADW - North Atlantic Deep Water

NEADW - NE Atlantic Deep Water

NDW - Nordic Deep Water

NWC – Norwegian Atlantic Current

PIW - Polar Intermediate Water (PIW)

PSW - Polar Surface Water

PSWw - Polar Surface Water warm

RAW - Re-circulating Atlantic Water

TF/T – Tasiilaq Fjord/Trough

Upper Polar Deep Water (uPDW)

Upper Labrador Sea Water (ULSW)

WGC – West Greenland Current

WSC – West Spitsbergenn Current

1. INTRODUCTION

The northern North Atlantic is a key component of the Earth's climate system. It exerts a powerful influence on the climate of the surrounding landmasses and local circulation changes in the area can be transmitted to the other ocean basins due to the role the region plays in driving the global thermohaline circulation.

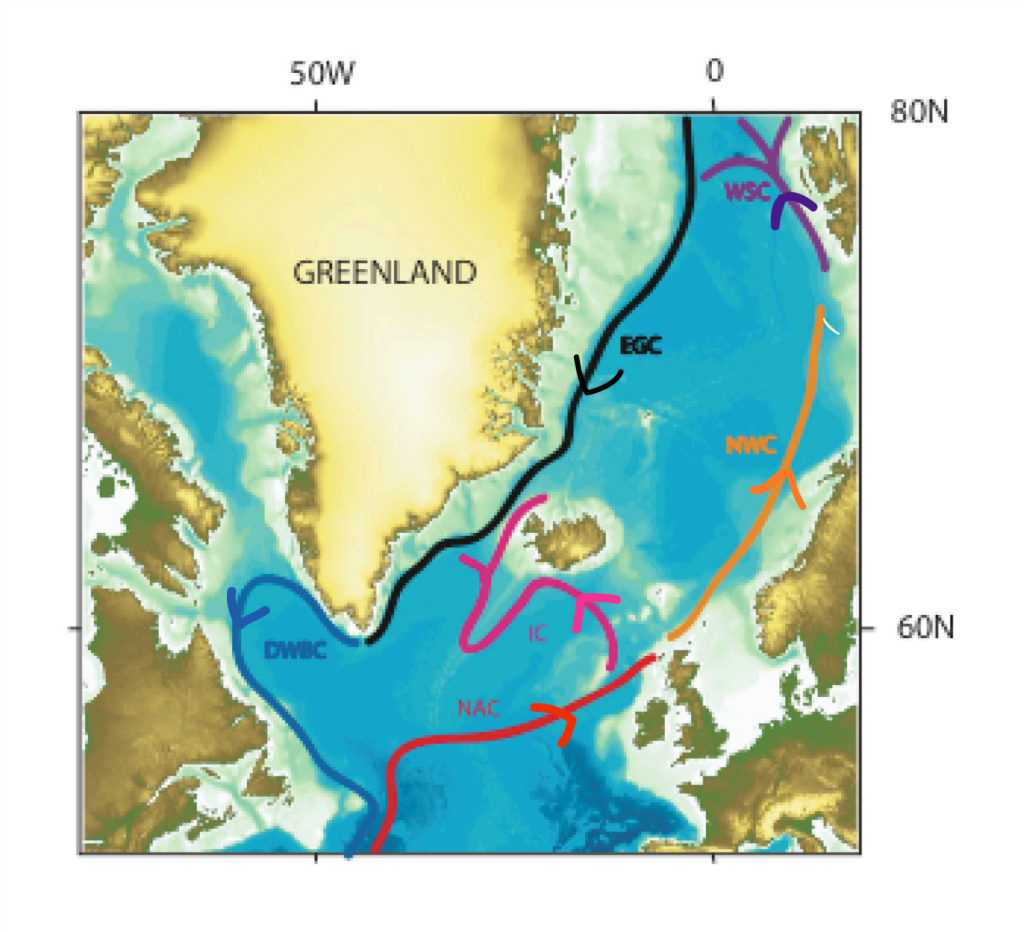

Figure 1.1 Key ocean currents of the northern North Atlantic

WSC- West Spitsbergen Current: EGC – East Greenland Current: NWC – Norwegian Atlantic Current IC – Irminger Current: DWBC – Deep Western Boundary Current (Labrador Sea): NAC – North Atlantic Current

The low frequency circulation of the region is driven by a combination of wind stress and thermohaline forcing. Predominantly cyclonic winds around the Icelandic Low create an upper layer circulation known as the sub-polar gyre consisting of the East Greenland Current (EGC), the North Atlantic Current (NAC), the Norwegian Currents (NWC) and the West Spitsbergen Current (WSC). The Irminger Current (IC) provides an additional westward flow south of Iceland. The buoyancy forces of

the thermohaline circulation drive cold, lower salinity deep water south. There is a corresponding northward return of warm higher salinity surface waters that have been transformed via a combination of upwelling, surface heating and evaporation.

The deep circulation in the region is significantly affected by the local bathymetry [*McCartney*, 1992]. The northern North Atlantic is divided into a series of basins by a network of islands and submarine ridges *[GEBCO charts of the northern North Atlantic & Arctic Oceans]*. The Greenland-Iceland-Scotland (GIS) Ridge and the extension of the Barents Sea shelf, out to Spitsbergen, form latitudinal barriers that prevent the equatorward flow of deep waters and restrict the flow of lower intermediate waters to specific channels. Deep flow between the Arctic and the Nordic Seas (consisting of the Norwegian, Greenland & Iceland Seas) is restricted to the Fram Strait, located between north-east Greenland and the island of Spitsbergen. To the south deeper flow across the GIS is restricted to a series of narrow pathways, of which the most significant are the Denmark Strait and the Faeroe Shetland Channel. Denmark Strait has a maximum depth over the sill of about 600m, the Faeroes-Shetland Channel about 800m *[GEBCO charts of the northern North Atlantic & Arctic Oceans]*. There are also a series of shallower channels along the Iceland-Faeroes Rise that reach depths of about 450m. As a result the GIS ridge only allows waters down to intermediate depths to be exchanged between the Nordic Seas and the main North Atlantic. The densest of these waters spilling south over the ridge are known as the overflow waters.

The basins of the region are also split longitudinally by a combination of the mid-ocean ridge and Greenland itself. The mid-ocean ridge consists of the island of Iceland with the Mohn Ridge to the north and the Reykjanes Ridge to the south. To the west of the ridge the Greenland basin reaches depths in excess of 3,500m and to the east the Norwegian basin has a maximum depth of approximately 3,000m.while the depth on the Mohn Ridge is typically only 2,000m. These dividing ridges have a profound effect on the ocean circulation preventing flow at depth between the basins. This produces strong intra-basin re-circulating gyres that mask the inter-basin transport *[Schmitz & McCartney, 1993]*.

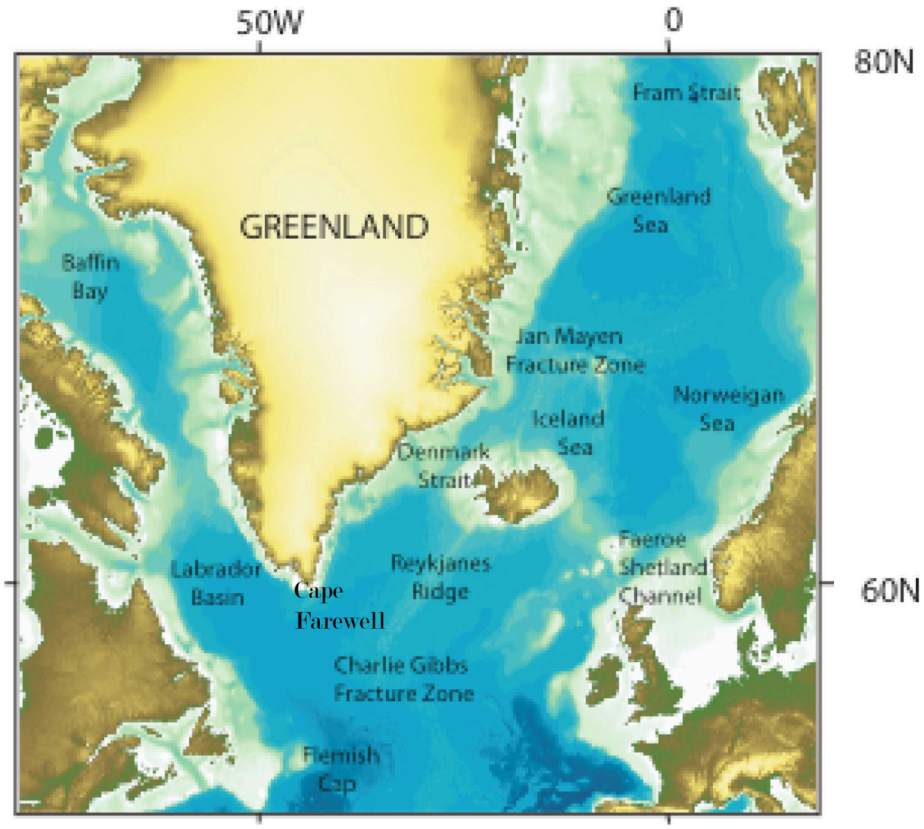

Figure 1.2 Key geographic features of the northern North Atlantic

This thesis focuses on the southward flowing current system off south-east Greenland between Denmark Strait and Cape Farewell (fig. 1.2). Both the near-surface and deep currents of the region play a significant role in the global thermohaline circulation (THC). The THC and its role in shaping the Earth's climate will be discussed in more detail in chapter 2.1.

The main deep current in the region is the Deep Western Boundary Current (DWBC), which flows southward along the foot of the continental slope. This provides the primary input to the flow of North Atlantic Deep Water (NADW), which spreads from the North Atlantic to form the deep limb of the global thermohaline circulation (THC). Therefore the strength of the DWBC off south-east Greenland is intimately linked with the strength of the THC. Contourite sediments deposited by the DWBC on the Eirik Drift off southern Greenland can provide data on current strength over the last 20,000 years *[e.g. Stanford et al., 2006]* making the

region of key importance for the study of the relationship between climate and the THC. Palaeoceanographic investigations allow the pre-historic relationship between current strength, circulation patterns and climate to be established. A more detailed understanding of the present-day dynamics of the region established through observation and numerical modelling allows these historic patterns to be analysed with more confidence.

The main surface currents in the study area are the East Greenland Coastal Current (EGCC) and the southern portion of the East Greenland Current (EGC). The EGCC is a low-salinity baroclinic jet flowing close to the Greenland coast over the continental shelf [*Bacon, et al.*., 2002]. The EGC is found further offshore above the continental slope. The combined flow is responsible for a significant component of the freshwater export from the Arctic Basin [*Aagaard and Carmack*, 1989]. It is important to understand the dynamics of this surface system if we are to accurately predict the impact of global warming on global ocean circulation. Global coupled atmosphere-ocean models, of relatively low resolution, are commonly used to predict the impact of anthropogenic CO_2 emissions on the ocean circulation and climate. Due to the resolution constraints the additional export of freshwater from the Arctic region is commonly seen (or in some scenarios forced) to result in a widespread freshening of the surface waters of the north-west Atlantic. This is of great significance due to its impact on the deep-water formation process in the Labrador and Irminger Basins and the recirculation of fresher waters into the Nordic Seas.

Developing our understanding of the behaviour of the regional current system using modern observational techniques combined with high resolution regional modelling will allow us to assess how well global models simulate the impact of global warming. It will also help to prepare for a more thorough handling of the region in the next generation of adaptive mesh models.

2. THESIS LAYOUT

This thesis looks at both the surface and deep currents of the south-east Greenland region through a combination of observational and modelling studies. The results are presented in chapters 4 and 5 respectively.

The first section of chapter 4 was largely published in Geophysical Research Letters [*Wilkinson and Bacon*, 2005] . This work was initiated by my co-supervisor, Dr Sheldon Bacon, Dr. Bacon also reviewed the manuscript prior to submission.

The second section of chapter 4 has again been largely published, this time in Deep-Sea Research [*Hunter et al.*, 2007]. This paper was a joint piece of work primarily with Ms Sally Hunter and it consequently also forms part of Ms. Hunter's PhD thesis. Ownership of the different parts of the paper is easily established with Ms Hunter's work covering the sedimentological aspects and mine the physical oceanography. The discussions where the two fields are brought together are a joint venture. The remaining authors on the paper were acknowledged for the following reasons. Essylt Louarn was a member of Discovery cruise D298 and was responsible for the silicon analyses included in the paper. Professor McCave provided invaluable advice on the interpretation of transmissivity data. Dr. Bacon was the principal scientist on cruise D298 and acted as a pre-submission reviewer of the paper. Profs. Stow and Rohling were Ms Hunter and my primary supervisors and acted as pre-submission reviewers of the paper.

Chapter 5 on high-resolution regional modelling of the surface and deep currents of the region is currently unpublished but is solely my work. I have been fortunate to benefit from the assistance of Dr Alex Megann in setting up and running the Hycom model [*Bleck*, 2002] employed.

3. BACKGROUND

3.1 The Global Thermohaline Circulation

The global thermohaline circulation (THC) is the component of the ocean circulation driven by spatial variations in the density of sea-water. Surface cooling at high latitudes forms cold, dense water. In regions where the highest density water is produced it sinks to the ocean floor in a process known as deep/bottom water formation. Deep and bottom waters spread, from their point of formation, across the planet's ocean floors. Deep-water formation in the northern North Atlantic gives rise to the deep limb of the THC. The upper limb of the THC is formed by the inflow of warm surface waters to high latitudes.

Stommel (1961) first documented the theory behind thermohaline convection in a single basin but it was not until *Broecker's 1991* paper "The Great Ocean Conveyor" that the global nature of the THC became widely recognised. The transfer of heat energy by this "Global Conveyor" plays a major role in shaping the Earth's climate.

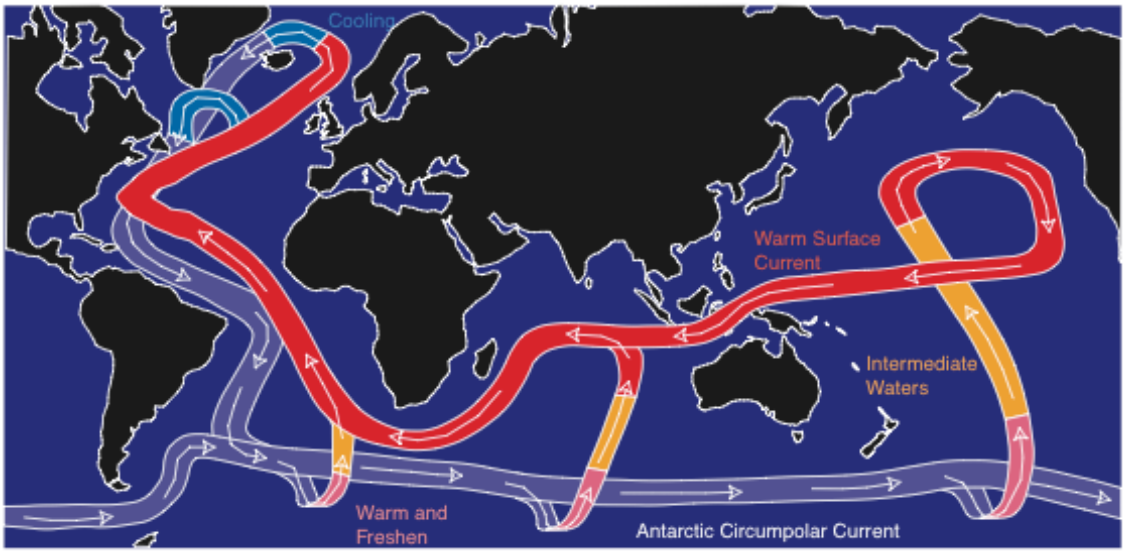

Figure 3.1.1 The global thermohaline circulation after *Broecker (1991)*

With the THC in its current mode deep water is formed in the northern North Atlantic (Greenland, Labrador & Irminger Seas) and the Antarctic (Weddell Sea). Recent estimates for the rate of deep-water formation are 15+/-2 Sv for the North Atlantic and 23+/-3Sv for the Antarctic *[Ganachaud & Wunsch 2000*].

There is no deep-water formation in the Pacific due to its lower surface salinity in comparison with the Atlantic. This difference results from the net export of fresh water from the Atlantic to the Pacific by the atmosphere *[Oort, 1983]*. This export is a function of the combination of prevailing winds, continental geometry and continental topography. The easterly trade winds in the low latitude areas of high evaporation transport water vapour more readily out of the Atlantic across the narrow belt of Central America than back into the Atlantic across the wider African continent. The prevailing westerly winds in the mid-latitudes of the northern hemisphere allow greater transport of water vapour out across Asia than in across the USA. Water vapour leaving the Pacific is largely re-precipitated on the windward side of the Rocky Mountain chain from where it is returned to the Pacific basin *[Seager et al., 2002]*.

The salinity differential, between the Atlantic and Pacific, is kept in dynamic equilibrium by the THC. The warming effect of the THC on the surface waters of the North Atlantic promotes evaporation. This maintains the salinity differential and stabilises the THC in this mode *[Broecker et al., 1985]*. Estimates for the net evaporation from the Atlantic vary between 0.45 Sv *[Manabe & Stouffer, 1988]* and 0.20 Sv *[Maier Reimer and Mikolajewicz, 1989]*. *Oort (1983)* gives an intermediate value of 0.32 Sv.

The asymmetry in water properties between the Atlantic and Pacific basins produces one of the most significant aspects of the present day THC. There is a northward flow of warm surface waters up the full length of the Atlantic (Fig. 3.1.1). The upper limb of the Atlantic THC is comprised of warm surface waters from the Pacific and Indian Oceans carrying about 1PW of heat energy (1.3PW at 27^{o}N, *[Ganachaud and Wunsch, 2000]*) to the northern North Atlantic. This influx of heat significantly warms the continents bordering the northern North Atlantic. *Broecker (1991)* suggested that Western Europe and Greenland are warmed by between 5 and 8^{o}C.

The warming influence of the THC is greatest in NW Europe. This is due to the combination of the northward heat transport in the Atlantic by the THC and the prevailing westerly winds at mid latitudes. *Seager et al. (2002)* also attributed warmer winters in NW Europe, by comparison with NW America, to the northward heat transport by the THC. However they pointed out that the large asymmetry (15-20^{o}C) in winter temperatures between the NW coasts of Europe and the eastern seaboard of the USA is mainly the result of atmospheric circulation patterns. Based upon global circulation models, *Seager et al. (2002)* still attributed a mean 4.5 ^{o}C warming in Western Europe to the THC.

A change in the THC could significantly impact global weather patterns with particular consequences for NW Europe. In the extreme a sudden reduction in the heat transport to the northern North Atlantic could increase northern hemisphere ice cover. The resultant increase in the average planetary albedo would cause net global cooling in addition to the obvious local impact. Comparing estimates of the warming effect of the THC *[Seager et al.. ,2002]* with global warming predictions *[Houghton et al., 2001]* suggests that a weakening of the THC could temporarily mask the effects of global warming on the climate of north-west Europe.

Thermohaline circulation theory [*Stommel 1961, Rooth 1982, Bryan 1986*] suggests that various modes of the THC are possible depending upon the relative levels of thermal and salinity forcing. It is thought that mode changes in the THC and their associated climatic impacts could occur over relatively short time scales in comparison with other climatic events *[Broecker et al. 1985, Broecker 2000]*.

Several periods of rapid climate change observed in the geologic record of the Atlantic region have been associated with changes in ocean circulation. A number of such events, during the past 100,000 years, have been identified from Greenland ice cores [*Dansgaard et al. 1982, Grootes et al. 1993*]. *Gordon et al. (1992)* suggested that some periods of rapid cooling are associated with lower rates of deep-water formation and a weakening of the THC in reaction to a reduction in the salinity of the North Atlantic. For example the Heinrich Event 1 cooling period between 16,000 and 17,000 years ago is associated with a shutdown of the THC *[McManus et al., 2004]*.

Looking to the future concern has risen as to whether another reduction in northern North Atlantic salinity might weaken the THC and produce another cold period. Global warming, due to anthropogenic CO_2 emissions, could paradoxically trigger such a reduction. The rate of increase in global mean temperature and atmospheric CO_2 concentration has escalated rapidly since the beginning of the industrial revolution (Figs. 3.1.2 & 3.1.3).

Global warming could cause a reduction in the salinity of the northern North Atlantic via two mechanisms:

- The melting of land and sea ice (land ice has greater potential due to the much greater existing volume).
- The increased export of fresh water from the tropics to high latitudes due to global warming increasing net evaporation at low latitudes.

There is still some debate as to the significance of either. Recent research has suggested that the ice caps are melting significantly faster than previously thought due to the lubricating effects of the meltwater *[Rignot and Kanagaratnam, 2006]*. However a Utrecht group has recently refuted this work *[van de Wal et al., 2008]*. The impact of the enhanced hydrological cycle could also be offset by the oceanic transport of the resultant more saline tropical surface waters. A generally warmer planet is likely to result in higher atmospheric water vapour concentrations and a corresponding increase in the average salinity of the oceans. We need a more detailed understanding of how the two components of the system affect the particular regions of deep-water formation in the northern North Atlantic.

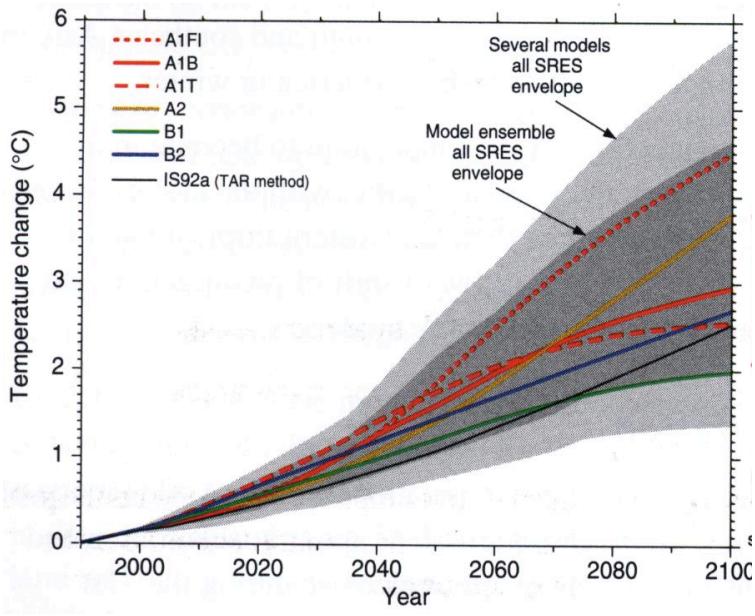

Figure 3.1.2 Temperature Change – Projections for the 6 illustrative SRES scenarios along with IS92a for comparative purposes [*Houghton et al.*, 2001, originally figure 5d - page 14]

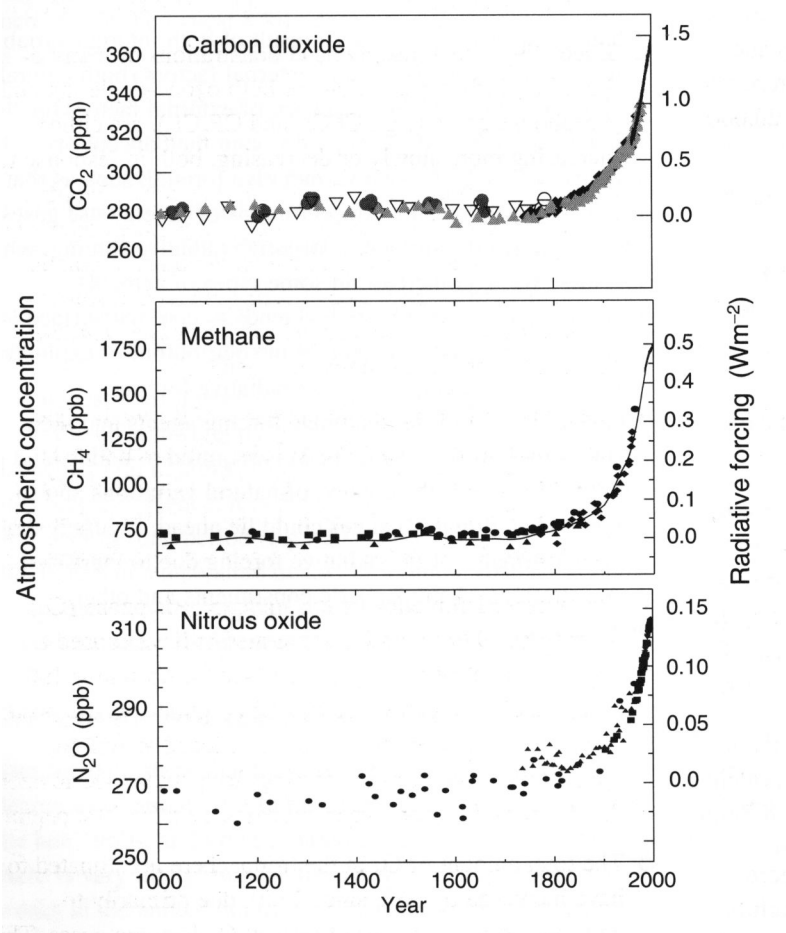

Figure 3.1.3 Global atmospheric concentrations of three well mixed greenhouse gases [*Houghton and al*, 2001, originally figure 2a - page 6]

The most commonly used tools to assess the potential impact of global warming on the THC and climate are coupled climate models. Many researchers have looked at this issue over the past 20 years. Due to the extended run times of more complex models there has always been a trade off between the realism of the model and the number and length of scenarios that can be run. Predictions of the impact of global warming on the ocean circulation vary by model. It is generally accepted that a reduction in salinity in the northern North Atlantic will, at least, weaken the THC *[e.g. Rahmstorf 2000]*. Although global warming does provoke a reduction in northern North Atlantic salinity in the majority of models tested to date there are exceptions *[Sun & Bleck 2001, Latif et al. 2000]*. The work of *Latif et al. (2000)* suggests that many models may lack the resolution to generate an El Nino type response capable of stabilising the THC under the effects of global warming.

The NERC RAPID program has proposed work to monitor the present-day strength of the THC and to build a 20,000 year pre-historic record by combining the modern THC record with palaeoclimate data. This will provide a valuable way of testing coupled climate models that hope to predict future changes in the THC. The present study is part of the RAPID program and specifically aims to provide a more detailed understanding of the current dynamics in the region of SE Greenland to assist with the interpretation of observational data and to identify key areas for future observational studies, making use of, and developing high resolution regional ocean models.

3.2 Modern Physical Oceanography of the Northern North Atlantic

Over the last 30 years the role of the global thermohaline circulation in shaping global climate has become better understood. This has led to increased interest in the circulation of the northern North Atlantic and in particular the formation of North Atlantic Deep Water.

Oceanographers have used always a combination of current measurement and water mass identification to build a picture of ocean circulation. Modern developments have produced instrumentation (such as acoustic doppler current profilers, long term current meter moorings and in situ CTD sensors) capable of making accurate direct current measurements at all depths and with the ability to identify and accurately measure a variety of water mass tracers. The resultant high volume of data can be combined, using inverse modelling techniques, to develop basin scale circulation patterns. However, even with these advances, it is difficult to precisely determine the large-scale ocean circulation from a limited set of data.

Water mass tracers can indicate possible transport routes provided the tracer sources can be precisely defined. More quantitative analysis of tracer concentration data can be highly dependent on the exact definitions of the end member water masses. For example North Atlantic water with a certain combination of temperature, salinity and potential vorticity is considered Labrador Sea Water (LSW). LSW was traditionally considered to be formed by seasonal deep-convection in the Labrador Sea *[e.g. Lazier 1973]* hence providing the name. However recent work by *Pickart el al (2003)* and *Bacon et al. (2003)* has shown that a significant portion of LSW may be formed by winter convection in the Irminger Sea. This discovery changes the inferences we can make about the circulation in the area and demonstrates the problem of missing an end member with similar characteristics to a known water mass. The same problem extends to inverse modelling. For example *Alvarez et al. (2004)* combine a wide array of tracer data to give a mathematical solution for the flow of different water mass components across a section of the North Atlantic. Although mathematically rigorous the results are highly dependent on the assumed number and characteristics of the end members.

The older dynamic method for the calculation of current velocities and transports, uses hydrographic data by assuming geostrophic balance. This approach is still valuable but requires a known level of motion. Where currents are strongly baroclinic (such as the SE Greenland Shelf) assuming a zero current at the bottom may be reasonably accurate but in areas of significant barotropic flow (such as the Labrador Basin) current meter or drifter data are also required.

Direct current measurements from current meters and drifters appear more precise but the results are subject to transient eddies (as well as high frequency signals such as tides that may be systematically removed – *[e.g. [Munchow, 2000]*). Such, relatively random, intermediate timescales signals mask the mean circulation that is typically under investigation. For example *Lavender at al (2000)* used drifters to trace the pathways of LSW from its areas of formation. They were surprised to find no drifters directly flowing south past Flemish Cap despite the chemical tracer evidence that this is the main pathway for uLSW *[*e.g. *Talley and McCartney, 1982]*. The mean signal may be unveiled by recording data over longer time periods or using huge numbers of drifters but these types of survey are expensive and consequently are rarely carried out. This masking of the mean signal becomes an even more significant problem when looking at current variability over years and decades *[Saunders, 1994]*. Even if perfect long-term current records are available, tracer data are still useful in understanding the relationships between current systems and water masses. Transports and fluxes for specific water masses are sometimes calculated based upon accepted density ranges. However, simple density ranges do not always differentiate well between water masses without additional tracer evidence. Comparison between the results of different researchers is often complicated by the use of different water mass definitions. Older papers tend to use simple potential temperature boundaries *[e.g. Swift and Aagard, 1981]* while more precise definitions are now achieved using a combination of potential temperature, potential density, salinity and possibly additional tracers *[e.g. Stramma et al., 2004]*.

By combining these different types of analysis it is possible to more precisely define the circulation than would be the case using a single approach. All the available data and analysis techniques must be combined to produce a model that is consistent with

the observations. The recent Variability of Exchanges In The Northern Seas program *[http://www.awi-bremerhaven.de/Research/IntCoop/Oce/veins/index.html]* has attempted to do just this to determine the circulation of the Nordic Seas and the Irminger Basin. The group, consisting of 18 European research institutions, used a wide variety of analytical techniques and several research ships to determine the flows synchronously around the northern North Atlantic between 1997 and 2000. Their results demonstrated some of the weaknesses of point in time data samples from CTDs. They calculated transports for the EGC and WSC that were generally higher than previously published estimates (e.g. *[Schmitz and McCartney, 1993]*).

The *Schmitz and McCartney (1993)* and *Schmitz (1996)* reviews of the North Atlantic circulation combine the evidence available at the time to suggest possible circulation schematics. Looking at the formation of the DWBC they suggest a contribution of about 6Sv of Overflow Waters split evenly between those exiting the Nordic Seas via the Denmark Strait (DSOW) and the Iceland-Scotland Ridge (ISOW). The addition of Labrador Sea Water (LSW) and possibly some Antarctic Bottom Water produces a DWBC off Cape Farewell of between 14 and 16Sv. With the addition of further LSW and ISOW in the Labrador Basin this grows to 16-17Sv as it exits the sub-polar gyre off the Grand Banks of Newfoundland. *Schmitz & McCartney (1993)* compare this with a net thermohaline circulation of 13Sv as a result of the northward transport of 3Sv of Antarctic Bottom Water (AABW). Although these figures are based on a synthesis of the best work at the time *[e.g. Dickson & Brown 1994, Worthington 1976]* they do not take into account the significant annual variability that more recent detailed studies have revealed [e.g. *Bacon*, 1998]. However combining the variability observed in small parts of the system into a larger-scale picture is difficult, Transit times between different parts of the circulation need to be given careful consideration when interpreting the impact of an event in one area on the circulation in another. Conversely good continuous records from multiple locations can be used to calculate transit times where a particular event creates a signature that is clear enough to act as a tracer. Unfortunately synchronous continuous records from multiple locations are rare.

Before going on to consider the detailed observations that have been made with regard to the circulation of the northern North Atlantic it is worth considering the

water masses involved. As discussed early water mass classifications were based on simple combinations of temperature and salinity. For example *Stefansson (1962)* suggested three main water masses were present in the region north of Iceland; Atlantic Water (S>35), Polar Water (T<0^{o}C, S<34.5), and Arctic Bottom Water (T<0^{o}C, 34.90<S<34.94). The traditional tracers of temperature, salinity and potential density have now been supplemented by naturally occurring geochemical species such as the rare earth elements *[Piepgras & Wasserburg 1987]* and silica. Anthropogenic inputs (e.g. CFCs and atomic bomb tritium) and mathematical concepts such as potential density and potential vorticity *[Talley & McCartney 1982]* also have great value as tracers of water masses. To be effective as a tracer a water property needs to be accurately quantifiable, exhibit reasonably conservative (or predictably non-conservative in the case of nutrients) behaviour and have well defined boundary exchanges. These additional tracers have increased the number of water masses commonly recognised and provided a more reliable link between a given sample and its place of formation. For example the isotopic ratio of the rare earth element neodymium (Nd) in sea-water reflects the age of the rocks over which a water sample has travelled *[Piepgras & Wasserburg 1987].* In the Atlantic Ocean, North Atlantic Deep Water (NADW) has a higher concentration of Nd but a lower percentage of the radiogenic isotope (^{144}Nd) than the surface waters. This is indicative of the fact that the sources waters of NADW have travelled across geologically ancient rocks in which a higher proportion of the radiogenic isotope has decayed. Further analysis of the potential source waters indicates that the constituent of NADW causing the low level of the radio-isotope is Labrador Sea Water (LSW). LSW contains runoff waters that have crossed the Precambrian rocks of the Canadian Shield *[Piepgras & Wasserburg 1987]. Lacan & Jeandel (2004)* performed a more detailed Nd analysis of the waters of the EGC between 77^{o}N and 70^{o}N. North of the Denmark Strait the deep waters that feed Denmark Strait overflow water (DSOW) and subsequently NADW do not contain LSW. Not surprisingly the relative abundance of the radioisotope is higher than is seen by *Piepgras & Wasserburg (1987)* in NADW. A more detailed look at changes in the EGC revealed an increase in the total Nd concentration, the relative abundance of the radiogenic isotope and the heterogeneity of each of these tracers on the approach to Denmark Strait south of 70^{o}N. These data provide a possible solution to the question of how the Iceland Sea contributes to DSOW (see section on the Nordic

Seas) but further follow-up work remains needed. The data of *Piepgras & Wasserburg (1987)* also show that the heterogeneity of the tracers is lost in the DSOW that exits Denmark Strait indicating that turbulent mixing over the sill has a produced a homogeneous water mass. In general the use of different tracers such as advective tracers (e.g. helium/tritium and freon), radioisotope tracers (e.g. Nd,) and short residence time tracers (e.g. Al) has the potential to answer many questions about ocean circulation but the work required has only just begun *[Measures & Edmond, 1992]*.

The water masses discussed in this review are introduced in section 3.3.

3.3 Water Masses

Polar Surface Water (PSW) – [Rudels et al., 2002]

This cold low salinity surface water is formed in the Arctic Ocean and is also known as Arctic Surface Water. The main flow of PSW into the North Atlantic is through the Fram Strait and into the East Greenland Current.

Polar Surface Water warm (PSWw) – [Rudels et al., 2002]

PSWw is the result of sea ice melting on warmer Atlantic Water. This produces a low salinity water mass that is warmer than PSW.

Arctic Atlantic Water (AAW) – [Rudels et al., 2002]

AAW is modified Atlantic Water (aka Modified Atlantic Water) that flows into the Arctic basin via the Norwegian Atlantic Current (see fig. 1.1). Cooling and freshening of the source water produces an intermediate layer lying above uPDW.

Re-circulating Atlantic Water (RAW) – [Rudels et al., 2002]

RAW is the Atlantic Water that is carried to high latitudes by the North Atlantic Current and then re-circulated by the West Spitsbergen Current, without reaching the Arctic Basins to the North of Spitsbergen. This forms the warm, high salinity portion of the EGC in the Greenland Sea although before reaching the EGC the Atlantic Water brought north in the Norwegian Atlantic Current has already been cooled and freshened within the Norwegian Sea.

Polar Intermediate Water (PIW) – [Rudels et al., 2002]

PIW is an intermediate water of Arctic origin.

Upper Polar Deep Water (uPDW) – [Rudels et al., 1996]

uPDW is formed by shelf-slope convection in the Canadian Basin and by an inflow from the Barents Sea into the Eurasian Basin.

Arctic Intermediate Water (AIW) – [Rudels et al., 2002]

AIW is formed by winter cooling with moderate depth convection in the Nordic Seas. It is commonly divided into an upper (uAIW) and lower part (lAIW) *[e.g. Swift & Aagard, 1981].* The upper division contains a temperature minimum and shows increasing temperature and salinity with depth. AIW is a seasonal thermocline water found at the surface in winter but at intermediate depths in summer. The lower division is from the temperature maximum downwards and is formed by winter cooling of saline Re-circulating Atlantic Water (RAW), predominantly in the Greenland Sea. AIW can also be subdivided based upon the basin of formation, e.g. Norwegian Sea Arctic Intermediate Water (NSAIW) which is one of the components of the Iceland-Scotland overflow waters *[Bacon, 2002].*

Modified East Icelandic Water (MEIW) - (Bacon, 2002)

MEIW is an intermediate water mass formed by the interaction of East Icelandic Water with North Atlantic Water and AIW to the east of Iceland close to the Iceland-Scotland Ridge. East Icelandic Water is an intermediate water mass carried by the element of the EGC that does not cross the Denmark Strait sill but turns east to the north of Iceland. MEIW is a component of ISOW.

Eurasian Basin Deep Water (EBDW) – [Rudels et al., 2002]

EBDW is deep water formed in the Eurasian Basin of the Arctic Ocean situated to the north of the area from Scandinavia to Siberia. EBDW has its salinity maximum at the bottom.

Canadian Basin Deep Water (CBDW) – [Rudels et al., 2002].

CBDW is deep water formed in the Canadian Basin of the Arctic Ocean situated to the north of Canada and Alaska. In the Nordic Seas CBDW lies above EBDW and is identifiable by an intermediate salinity maximum

Nordic Deep Water (NDW) – [Rudels et al., 2002].

NDW comprises deep waters formed in each of the Nordic Seas; Norwegian Sea Deep Water (NSDW), Greenland Sea Deep Water (GSDW), and Iceland Sea Deep Water (ISDW). NDW has a similar density range to EBDW and CBDW but is less saline. The bottom waters formed in the Greenland, Norwegian and Iceland Seas are

trapped by the topography and do not contribute to the EGC as it flows between basins.

Iceland Sea Arctic Intermediate Water (IAIW) – [Rudels et al., 2002]

IAIW has two parts. The layer down to the temperature maximum is formed in the Iceland Sea, the lower layer comprises a mixture of AIW and uPDW

Labrador Sea Water (LSW) & Upper Labrador Sea Water (ULSW) [Lazier. 1973 and Stramma et al., 2004]

LSW was traditionally thought to form as the result of winter convection in the Labrador Sea. *[e.g. Pickart et al. 1997].* uLSW is formed in the shallower waters of the shelf break off the Labrador coast, while classical LSW is produced further into the basin above the slope. However *Pickart et al. (2003)* and *Bacon et al. (2003)* show that some LSW is also formed by deep convection in the Irminger Sea (see section 3.4.2d).

Gibbs Fracture Zone Water (GFZW) also known as NE Atlantic Deep Water (NEADW) [Smethie and Swift, 1989]

GFZW is composed of overflow waters that cross the Iceland-Scotland Ridge and join with Mediterranean Water before flowing through the Charlie Gibbs Fracture Zone to join the DWBC in the Irminger and Labrador Basins.

Denmark Strait Overflow Water (DSOW) – [Knudsen, 1899]

DSOW is composed of intermediate Nordic Sea waters that overflow the 550m deep sill of the Denmark Strait. DSOW is formed from a combination of waters of Arctic, Atlantic and Nordic Sea origin. The exact processes involved are the subject of much debate (see section 4.3).

Iceland-Scotland Overflow Water (ISOW) – [Knudsen, 1899]

ISOW is composed of intermediate Nordic Sea water that overflows the Iceland-Scotland ridge at various points. The main conduit is through the Faeroe Shetland Channel followed by the Faeroe Bank Channel but smaller amounts flow just to the east of Iceland and through 4 further smaller channels between Iceland & the Faeroes *[Dickson & Brown, 1994].* ISOW undergoes modification due to mixing with

Atlantic & Mediterranean waters before joining the DWBC.

Antarctic Bottom Water (AABW) – [Wust, 1935]

AABW is formed by winter convection in the Weddel Sea. AABW flow north into the Atlantic. Although modified by mixing with the deep waters of the Atlantic Basin it is still identifiable as it joins the DWBC in the Irminger & Labrador Basins.

Mediterranean Water (MW) – [Wust, 1935]

MW is warm (approx. 13°C), very saline (approx. 38.4) intermediate water formed in the Mediterranean that spreads west from the Straits of Gibralter. It has a similar density to LSW but with high salinity and potential vorticity. Isopycnal mixing of MW with LSW forms upper NADW.

North Atlantic Deep Water (NADW) – [Wust, 1935]

NADW is the name commonly applied to the deep water formed by the combination of the overflow waters spilling over the sills in the GIS ridge and the ambient water masses encountered on their paths around the Irminger and Labrador Basins. The resultant mixture is a combination of LSW, DSOW, ISOW/GFZW and AABW. The NADW signature is seen to spread throughout the length of the Atlantic and beyond into the other ocean basins forming the major component of the deep limb of the THC.

Table 3.3.1 on the following page provides a summary of the identifying characteristics for each of the water masses discussed.

Table 3.3.1 Water Mass Characteristics In The EGC and DWBC
(After Swift & Aagaard 1981,Reid 1994, Rudels et al. 2002, Fischer et al. 2004, Stramma et al. 2004)

Water Mass	Potl. Density Range, σ_θ	Potl.Temp. Range, Θ	Salinity Range	Other Identifiers
AABW	σ_4 ~46			Low in O_2
AAW	a)27.70 to 27.97 b)>27.97 and $\sigma_{0.5}$ <30.444	a)<2 b)>0	If Θ<0 S<34.676 + 0.232Θ	b) –ve slope in Θ-S diagram.
AIW	σ_θ>27.97 $\sigma_{0.5}$ <30.444	<0 (R2002) Upper <2 Lower 0-3 (S&A 81)	Upper 34.7-34.9 Lower >34.9 (S&A 81)	Θ-S slope negative but inc. with depth
CBDW	$\sigma_{0.5}$ >30.444 $\sigma_{1.5}$ <35.142		>34.915	Intermediate salinity max
DSOW	>27.88			High in O_2
EBDW	$\sigma_{1.5}$ >35.142 $\sigma_{2.5}$ <39.738	-0.6 to -0.9	>34.915	Salinity max at bottom
GFZW	27.80-27.88			Intermediate salinity max
GSDW		<0 usually <-1	34.88-34.90	Salinity maximum O_2 minimum
IAIW	a) >27.70 b) >27.70, $\sigma_{0.5}$ <30.444 c) >27.97, $\sigma_{0.5}$ <30.444	a) <0 b) <1 c) <0	a) >34.676 + 0.232Θ b) >34.676 c) <34.676 + 0.232Θ	
ISDW				Salinity maximum O_2 minimum
ISOW				
LSW	27.74-27.80			Low potl. Vorticity
MEIW		<2	In the region of 34.74 (EIW)	Vague definition (Read & Pollard, 1992)
MW		~13	~38.4	Low in O_2
NADW	>27.80			High in O_2
NDW	$\sigma_{0.5}$ >30.444		<34.915	
NSDW		<-0.4	34.90-34.94	Salinity maximum O_2 minimum
PIW	>27.70	>0	S<34.676 + 0.232Θ	
PSW	<27.70	<0	<34.5	
PSWw	<27.70	>0		
RAW	a) 27.70-27.97 b) >27.97 $\sigma_{0.5}$ <30.444	a) >2 b) >0		Stable in temp. but not salinity
ULSW	27.68-27.74			Low potl. Vorticity
uPDW	σ_θ>27.97 $\sigma_{0.5}$ <30.444	<0		Θ-S slope negative and ~ constant

3.4 Spatial Evolution of the East Greenland and Deep Western Boundary Currents

For the purpose of this review the East Greenland Current (EGC) is assumed to consist of the currents, of Polar origin, flowing southwards along the length of the eastern coast of Greenland at all depths. Some authors apply the name EGC to the surface flow with the deeper flow being termed the Deep Western Boundary Current (DWBC). The Atlantic DWBC extends the full length of the Atlantic basin. This section will cover its extension beyond the EGC as far south as the Grand Banks of Newfoundland, as this is the point at which the formation of NADW is commonly considered to be complete.

The evolution of the EGC and DWBC is significantly influenced by the bathymetry of the region and the associated basin re-circulations. For the purposes of discussion it is convenient to split the area under consideration into three sections divided by Denmark Strait and Cape Farewell.

3.4.1 Fram Strait To Denmark Strait (The Nordic Basins)

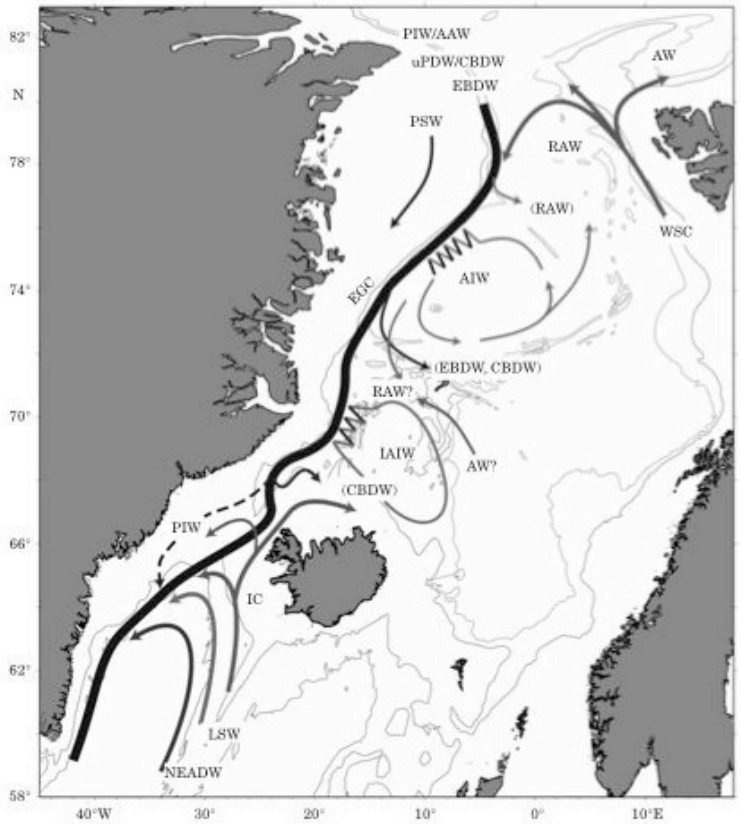

Figure 3.4.1 The East Greenland Current: its interaction with the waters of the Nordic Seas and its contribution to the Denmark Strait overflow *(reproduced from Rudels et al., 2002).*

3.4.1a Main Features

The Fram Strait lies at approximately 79°N, between the islands of Greenland and Spitsbergen, and marks the beginning of the EGC. With a maximum depth of about 2500m at the sill the Strait provides the main conduit for the exchange of waters between the Arctic Ocean and the Atlantic Ocean via the Nordic Seas *[Rudels et al., 2002].* To the east of Spitsbergen, water crossing the Barents Sea on its way to the Atlantic must cross a shelf with only around 200-300m depth of water.

The EGC consists of a variety of cold waters exiting the Arctic Ocean that combine with warmer higher salinity re-circulating Atlantic Water carried by the West Spitsbergen Current. Polar waters carry a high tritium signal in comparison with waters of Atlantic origin which allows them to be traced beyond the point where mixing has removed their characteristic temperature-salinity signal *[Swift and Aagaard, 1981]. Swift and Aagaard (1981)* suggest that low tritium concentrations in the Iceland Sea are indicative of little Polar Water influence. Somewhat confusingly *Swift et al. (1980)* suggest high tritium concentrations in DSOW (in comparison with GSDW) result from the inclusion of AIW from the Iceland Sea. They do not seem to consider AIW of Greenland Sea origin (see theory 1 for DSOW production discussed later in this section).

The EGC mixes with waters formed during winter cooling in the Greenland and Iceland Sea gyres (see fig. 1.2) on route through the Arctic Mediterranean. Although deep-water formation has largely been absent from the region since the 1980's *[Schlosser et al., 1991]*, winter cooling in both gyres regularly produces intermediate water (AIW). AIW is a potential constituent of DSOW and ISOW. The more saline waters of the Greenland gyre do intermittently produce denser waters by winter deep convection. The exact mechanisms involved are beyond the scope of this review but theories referred to by *Swift and Aagaard (1981)* include localised small-scale "chimneys" *[Kilworth, 1979]* and the influence of double diffusion on lAIW formed by moderate depth convection *[Carmack, 1972].*

The EGC is also the main conduit for the export of ice out of the Arctic Ocean (90% - *Rudels et al., 1999*). The transport of freshwater (ice and liquid) has a crucial impact on the hydrographic structure and circulation of the region due to the high impact of salinity, in comparison with temperature, on density at low temperatures *[Aagard and Carmack, 1989].* Continental run-off and land ice calving provide an input of freshwater that is released, in the case of land-ice, at the point of melting. Sea ice has a

typical salinity of 4, so has a distilling effect on the local water at the time of formation and a freshening effect in the area of melting. The EGC exports about 2,800 km^3 of ice per annum through the Fram Strait *[Aagard and Carmack, 1989]*. This is comparable with the total runoff into the Arctic Ocean of 3,300 km^3 per annum. About 80% of this sea-ice volume melts in the EGC during passage through the Nordic Sea, leaving about 560 km^3 of sea-ice per annum to pass through Denmark Strait *[Aagard and Carmack, 1989]*. This balance is significant as an increase in the net import sea-ice into the Nordic Seas may have the potential to inhibit the convective overturning process (that contributes to the formation of DSOW) due to the formation of a stabilising low salinity surface cap *[e.g. Rahmstotf, 2000]*.

Intermediate waters carried and altered by the EGC between Fram Strait and Denmark Strait feed the overflows (DSOW and ISOW) that are major contributors to the production of NADW. Four main theories for the formation of DSOW have been identified in the literature *[Bacon, 2002]* and combination with other work yields the following:

- An early theory proposed that the main source region of DSOW is the Iceland Sea. *Swift (1986)* suggests that the main component is uAIW, formed by deep winter mixing in the Iceland Gyre.

- *Mauritzen (1996)* suggests that DSOW is primarily formed from Atlantic Water that has undergone winter cooling and freshening due to the inclusion of runoff (primarily via the Norwegian Coastal Current) during its transport around the Nordic Seas. The two key components would be AAW that has passed through the Arctic Basin and RAW that bypasses the Arctic Basin circulation by joining the EGC directly via Fram Strait. *Mauritzen's (1996)* opposition to the view that intermediate water masses of Nordic Sea origin are a major input to DSOW stems from two ideas. The first is that estimates of total intermediate water production in the gyres are low (e.g. 0.84Sv of uAIW, *Swift & Aagaard (1981)* in comparison to the total overflows over the Greenland-Iceland-Scotland Ridge (ca 6Sv, *Dickson & Brown,1994*). The second is that the overflows show little seasonal or longer-term variability (*Ross, 1984, Dickson & Brown, 1994*) while seasonal and inter-annual variations in ice cover in the gyres would imply significant variability *[e.g. Clarke et al., 1990]*. However *Bacon (1998)* has challenged the concept that the there is little long-term variability in the production of overflow waters by comparing data collected over decadal periods. Also it should be noted that *Swift & Aagard (1981)* only quoted 0.84Sv as a minimum production rate of

uAIW and argued that their data did not cover the winter time production of AIW in the Greenland and North Iceland Seas which could be much higher.

- *Rudels et al. (1999)* suggests that half the DSOW is supplied by RAW and the other half by a series of water mass formation processes that occur along the path of the sub-polar gyre through the Atlantic and Arctic.

.

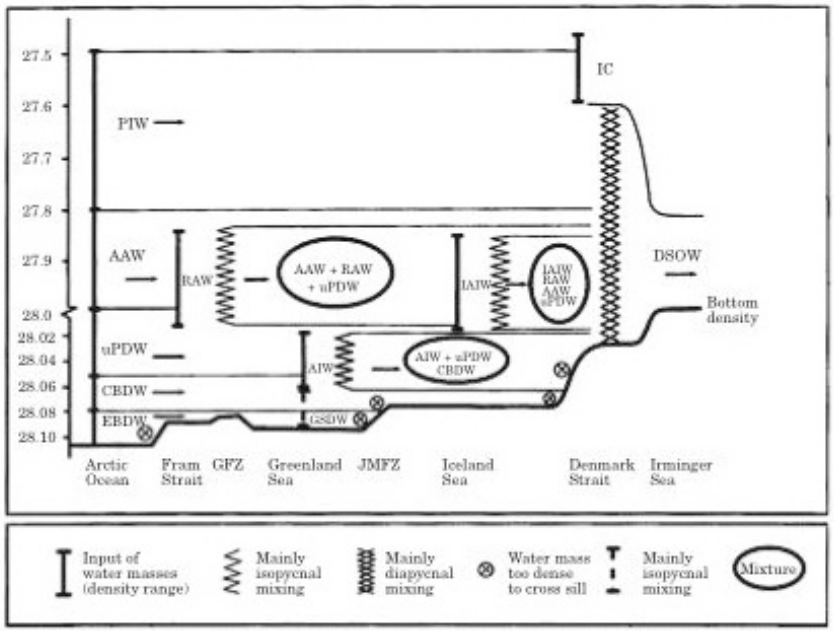

Figure 3.4.2 The different water masses as they flow along the Greenland slope shown on a density axis. The East Greenland Current loses its densest components progressively as the waters lying to deep to cross the sills are deflected into the interior of the basins. The loss is compensated by an input of and mixing with less dense gyre waters, the AIW and IAIW. The mixing between the gyre waters and the East Greenland Current is mainly isopycnal, while the mixing taking place at the sill in the Denmark Strait is strongly diapycnal. *(reproduced from Rudels et al., 2002).*

- *Rudels et al. (2002)* developed his earlier theories to suggest that DSOW is primarily the result of isopycnal mixing in the EGC between intermediate Arctic Waters (AAW & uPDW) and intermediate waters from the Nordic Seas (RAW & AIW), the AIW in question being formed by winter deep convection within the Greenland gyre. This is similar to the theory of *Strass et al. (1993)* who suggested that DSOW results from isopycnal mixing in the EGC between RAC and AIW. Figure 3.4.2 provides a more thorough representation of the theory.

It is highly likely that all the processes discussed in the four theories play a part in the formation of DSOW. *Bacon's (2002)* review concludes that ISOW is formed from a

combination of three intermediate water masses of eastern Nordic Sea origin; NSDW, NSAIW and MEIW. *Mauritzen (1996)* proposes that ISOW is formed mainly from Atlantic Water that has been circulated around the Barents Sea before passing in to the Arctic and down through Fram Strait. This is a similar theory to that mentioned earlier in relation to DSOW with similar reasoning.

3.4.1b *Transports & Variability*

Fram Strait:

Foldvik et al. (1988) employed current meter arrays (mid. June 1984 to mid. July 1985) to measure transports in the EGC between 1 and 8°W at 79°N just south of Fram Strait. They calculated 3Sv for the upper 700m and 0.5Sv between 700 and 1000m. However the dataset was quite sparse (a mooring spacing of 20km) and they admitted that it was not capable of resolving all the lateral variations in the current. They did manage to observe that the transport was about 50% barotropic with significant short-term variability but no clear seasonal pattern.

Rudels et al. (1999) calculated somewhat smaller transports for Fram Strait inferred from an analysis of the transport budget for the Arctic Ocean (a combination of data sources was used for the other imports and exports to leave Fram Strait as the residual). This gave 2.8Sv for the full water column consisting of 0.5Sv PSW, 1 Sv AAW and 1.3Sv intermediate and deep water. Given the different approaches and depth levels these numbers are reasonably consistent with *Foldvik et al. (1988)*.

Rudels et al. (2002) looked in more detail at the water masses flowing through Fram Strait. PSW was observed flowing over the Greenland Shelf, AAW, uPDW and Arctic Deep Waters were found over the Greenland slope. Further to the east is found RAW with some isolated lenses penetrating nearer to the slope. Surface, low salinity PSWw was also found to the east of the Greenland slope as a result of sea ice melt. Unfortunately *Rudels et al. (2002)* do not include any new transport calculations

The Greenland & Iceland Seas:

South of the Greenland Fracture Zone the EGC passes through the Greenland Sea before reaching the next topographic rise at the Jan Mayen Fracture Zone (JMFZ). The Greenland Sea has its own surface recirculation that combines with the EGC on

its western boundary. Estimates of the strength of the Greenland gyre vary (2 to 35Sv [*Mosby, 1962 and Aagaard & Coachman, 1968*]).

Woodgate et al. (1999) provides a more detailed transport analysis from mooring data (15 current meters) placed over the continental slope at 75°N between summer 1994 and summer 1995. They found a strongly barotropic current with surface and bottom intensification. Maximum velocities were recorded over the slope near the surface; 33cm s^{-1} in January and 14 cm s^{-1} in August. The width of the EGC (ca 100km) was consistent with a boundary current limited by horizontal friction (25-100km *Gill, 1982*). The annual mean transport from 14W to 9W (140km section) was calculated as 21+/-3Sv. *Woodgate et al. (1999)* compared this with much lower hydrographic estimates such as 7Sv (*Aagard & Grerisman, 1975*) and reconciled the difference by identifying a 5cm/s near-bottom current. Using this as the reference level adds an additional 13 Sv to the hydrographic estimate and demonstrates the significance of apparently small barotropic currents.

Woodgate et al. (1999) also found a strong seasonal cycle in the EGC data for 1994-1995, with a maximum transport of 37+/-5 Sv in January and March compared with summer values of approximately 11+/-5Sv. Further analysis of 7 years of data (1987-1994) for a shorter Greenland Sea section (111km long, approx. 80% of transport) gave consistent results of 9+/-3Sv in summer and 27+/-3Sv in winter. This contrasts with the lack of a seasonal cycle in Fram Strait, as inferred by *Foldvik et al., (1988),* and Denmark Strait [*Dickson & Brown, 1994*]. *Dickson and Brown (1994)* suggest that this seasonality is a function of the gyre recirculation and must therefore be significantly wind driven, while interbasin transport is mainly thermohaline. The limited data suggest that the interannual variability is small in comparison with the seasonal variation.

The JMFZ is not deep enough to allow the bottom layer (>1600m, *Rudels et al. 1999*) to leave the Greenland Basin. The bottom layer in the Greenland Basin consists of Arctic Ocean deep waters that are cooled and freshened to form GSDW *(Aagard et al. 1985, Swift and Koltermann, 1988)*. The densest waters capable of crossing the JMFZ flow south to feed the Denmark Strait overflow. The degree of stratification seen in the intermediate to deep layers varies as a result of the depth of recent winter convection. *Rudels et al. (1999)* found an almost homogeneous layer, indicative of deep convection, down to below 2000m. Although deep convection can contribute to the formation of deep water it is thought that recently it has only formed AIW in significant quantities. The combined production of AIW and GSDW by deep convection is estimated at 2Sv with 1Sv of AIW flowing south in the EGC and 1Sv of

AIW and GSDW flowing east into the Norwegian Sea *[Rudels et al. 1999]*. In addition to the 1Sv of AIW *Rudels et al. (1999)* estimate that the EGC, crossing the JMFZ, carries approximately 1Sv of surface waters, 0.5Sv of RAW, 1Sv of AAW and 1.3 Sv of Arctic deep waters totaling 4.8Sv.

A combination of CBDW, uPDW and AIW also cross the JMFZ in the EGC to form the deep waters of the western Iceland Sea. These waters mix isopycnally to form Iceland Sea Deep Water but are prevented from flowing south by the rise of the Denmark Strait and re-circulate to the east in the Iceland Sea.

3.4.2 Denmark Strait To Cape Farewell (The Irminger Basin)

3.4.2a *Main Features*

The EGC carries surface and intermediate waters southward over the sill of the Denmark Strait. The surface waters of the EGC are found over the Greenland shelf and the main channel. The northward flowing branch of the Irminger Current (IC) is found on the eastern side of the Strait over the Iceland shelf. The IC carries warm, saline water from the North Atlantic Current west around the Reykjanes Ridge before passing through the Strait into the Iceland Sea. The contrast between the IC waters and the cold, low salinity polar surface waters of the EGC forms a sharp front over the eastern edge of the main channel *[e.g. Blindheim, 1968]*. The front is also characterised by a drop in subsurface concentrations of oxygen and phosphate *[e.g. Dietrich, 1957]*.

DSOW is contained in the lower part of the main channel and on crossing the sill follows the bathymetry south to form a cold, low salinity bottom layer. The densest water is trapped low down on the Greenland Slope and flows south in the DWBC where it is slowed as it entrains ambient waters. DSOW is the youngest, in terms of age since ventilation, of the overflow waters found in the DWBC. *Swift et al., (1980)* estimate the age of DSOW to be 3-4 years after crossing the sill, while *Strass et al. (1993)* suggest 1.5 to 2 years. DSOW therefore provides the fastest transmission of atmospheric changes to the deep ocean.

Between Denmark Strait and Cape Farewell the EGC is joined by LSW that has been circulating in the northern North Atlantic, GFZW carrying modified ISOW and modified deep water of Antarctic origin (AABW) [*McCartney*, 1992]. The southward

flowing branch of the IC also joins the EGC in this region. IC water has a narrow potential density range between that of the EGC surface waters and LSW. IC water is therefore found splitting these water masses in the EGC as well as forming a front at the surface on the eastern side of the EGC *[McCartney, 1992]*.

Bruce (1995) found increased eddy activity south of Denmark Strait that he attributed to stretching of the overflow water column as it follows the bathymetry having crossed the sill. *Bruce (1995)* suggested that eddy formation was linked with intermittent bursts of DSOW flowing over the Denmark Strait sill. The eddies, with a mean diameter of 34km, were seen to travel as far south as 62°50'N following their formation. They were predominantly on the eastern side of the East Greenland Front where they promoted vigorous mixing between the IC waters and the Polar Waters. The presence of eddies is consistent with the increased variability in current speed and direction going east across the EGC identified by *Malmberg et al. (1972)*.

3.4.2b Transports & Variability

Surface Waters

Malmberg et al. (1972) used a combination of current meter and hydrographic data collected off Cape Nordenskjold, near Angmagssalik (between 65°N and 66°N) in August to September 1965 to measure the EGC over the shelf. They calculated a transport of 2.75Sv for a section extending about 130km offshore. Repeating the calculation using geostrophic currents, based on a 300m reference level, gave similar results for the inshore half of the section (1.4Sv) but gave no net transport over the outer half. Maximum currents of just over 30cm/s were seen at the surface about 20 km from shore. Although they considered this current to be the EGC more recent work suggests that the main EGC is found over the slope with much higher transports *(e.g. Dickson & Brown, 1994)*. The majority of *Malmberg et al.'s (1972)* transport may be more consistent with the EGCC identified by *Bacon et al. (2002)* near Cape Farewell.

Blindheim (1968) analysed Norwegian data collected between 1954 and 1963 covering 5 sections from Denmark Strait to Price Christians Sound, just north of Cape Farewell. He found that Polar Water (defined as S<34.5) extended between 36 and 72km offshore. Near surface cores of cold water were found in Denmark Strait close to the Greenland shore (within 54km of the coast) over the middle of the shelf (108km

to 198 km offshore) and over the western edge of the main channel (250km to 290km offshore).

To the south, in the vicinity of Cape Farewell, *Bacon et al. (2002)* identified a distinct low salinity jet flowing south over the shelf with a transport of ca 0.8 Sv in August. This current, which *Bacon et al. (2002)* named the East Greenland Coastal Current (EGCC) to distinguish it from the main EGC, was estimated to carry 0.06Sv in August with an annual average of 0.02Sv. *Bacon et al. (2002)* suggest that these transports are consistent with the precipitation in SE Greenland. However the relationship between the EGCC and the low salinity currents, such as the three cores identified by *Blindheim (1968)* traditionally considered part of the EGC, requires further investigation.

Estimates of the total transport of the EGC from Cape Farewell to the centre of the Irminger gyre vary from 26-36Sv. E.g. *Bacon (1997)* – 26-27 Sv, *Schmitz & McCartney (1993)* 36Sv, *Reid (1994)* 30Sv and *Clarke (1984)* 33.5 Sv. *Bacon's (1997)* estimate is made up of 18Sv surface waters, 3Sv intermediate LSW and 5.5Sv DSOW. The lower value of *Bacon (1997)* is mainly attributable to the low estimate of the DSOW component and is perhaps indicative of the interannual variability in the production of overflow waters.

Deep Waters (DSOW And The DWBC)

The overflow waters just south of the Denmark Strait show an average transport of 2.9Sv *[Dickson & Brown 1994, Ross 1984]. Dickson and Brown (1994)* found significant daily variation in this flow but no seasonal or longer-term signal. *Worthington (1969)* had already used current meters placed just south of the Denmark Strait to show that the overflow waters crossed the sill in sudden bursts lasting about 24 hours every 4 days. However *Bacon (1998)* found significant decadal variability in the DWBC off Cape Farewell between the 1950's and the 1990's using geostrophic analysis of historic data. He attributed the variation in transport from 6 to 13Sv to changes in the contribution of the overflow waters.

Progressing south the transport of deep water (defined as σ_θ<27.80) is seen to grow based on analysis of current meter data from a series of sections. The increase in transport is attributed to the addition of GFZW, LSW and modified AABW. *Dickson & Brown's (1994)* mooring data give transports of 5.2Sv and 5.1Sv 160km and 320km south of the Strait. 160km south, the Angmagssalik arrays show this to have

grown to 10.7 Sv *[Dickson et al. 1990]* and by Cape Farewell, a further 740km south, to 13.3 Sv *[Dickson & Brown 1994, Clarke 1984]. Bacon (1997)* calculated a lower flow of between 3 and 7 Sv for DSOW off Cape Farewell using geostrophic current shears combined with a range of plausible reference currents.

GFZW is modified ISOW that has flowed through the Charlie Gibbs Fracture Zone and then north into the Irminger Basin. Overflow waters passing over the Iceland-Scotland Ridge through the Faroe Bank Channel average 1.7Sv with a further 1Sv passing through channels to the east of Iceland *[Dickson & Brown,1994]. Bacon's (2002)* review concludes that these Iceland-Scotland Ridge overflows are similar to the Denmark Strait overflows in that they occur in short bursts but show little seasonal variability. These overflows entrain warmer water and grow to 5Sv. However only 2.4+/-0.5Sv is observed to flow through the Bight and Charlie Gibbs Fracture Zones at the southern end of the Reykjanes Ridge *[Saunders 1994]*. This leaves 3.2Sv of the 10.7Sv seen in the EGC off Angmagssalik unaccounted for which *Dickson & Brown (1994)* assume to be LSW. They also attribute the growth in the EGC of 2.6Sv between Angmagssalik and Cape Farewell to the addition of modified AABW (which they term Lower Deep Water). *Alvarez et al. (2004)* used an inverse model to deduce that 12Sv of LSW flows south in the EGC off Cape Farewell but this seems exceptionally high in comparison to other studies and may be the result of the end member definitions employed.

3.4.2c Labrador Sea Water Formation In The Irminger Sea

LSW, formed by deep convection in the Labrador Basin, has long been recognized as a significant mode water that spreads across the North Atlantic and is a key ingredient in the formation of NADW *[e.g. Talley & McCartney, 1982]*. Although historical data had suggested the presence of deep-water formation in the Irminger Sea more recently it has been assumed that LSW is solely formed in the Labrador Basin. *Pickart et al. (2003)* showed tracer data from the mid-1990's to be inconsistent with this theory. The age of recently ventilated LSW in the Irminger Sea implied unrealistically high spreading rates if formation had occurred solely in the Labrador Basin. They then used models to show that the atmospheric conditions in the Irminger Sea were capable of producing deep convection to depths of 1500-2000m. The combination of weak stratification in the Irminger Sea, the cyclonic Irminger Gyre (which raises the thermocline) and the Greenland Tip Jet (whose strong winds enhance surface heat loss) is capable of promoting wintertime deep convection. Conditions are at their best with the higher wind stresses associated with a high North Atlantic Oscillation (NAO)

index. *Pickart et al. (2003)* suggest that formation of LSW in the Irminger Sea can be as strong as in the Labrador Sea during extended periods of high NAO index.

Bacon et al. (2003) subsequently demonstrated that deep convection had occurred in the Irminger Sea to the SE of Cape Farewell during the winter of 1996/97. Profiling float data showed the presence of 700m and 1000m low salinity deep convection plumes. They further noted that years of high NAO index coincided with accepted periods of high LSW formation.

3.4.3 Cape Farewell To The Grand Banks (The Labrador Basin)

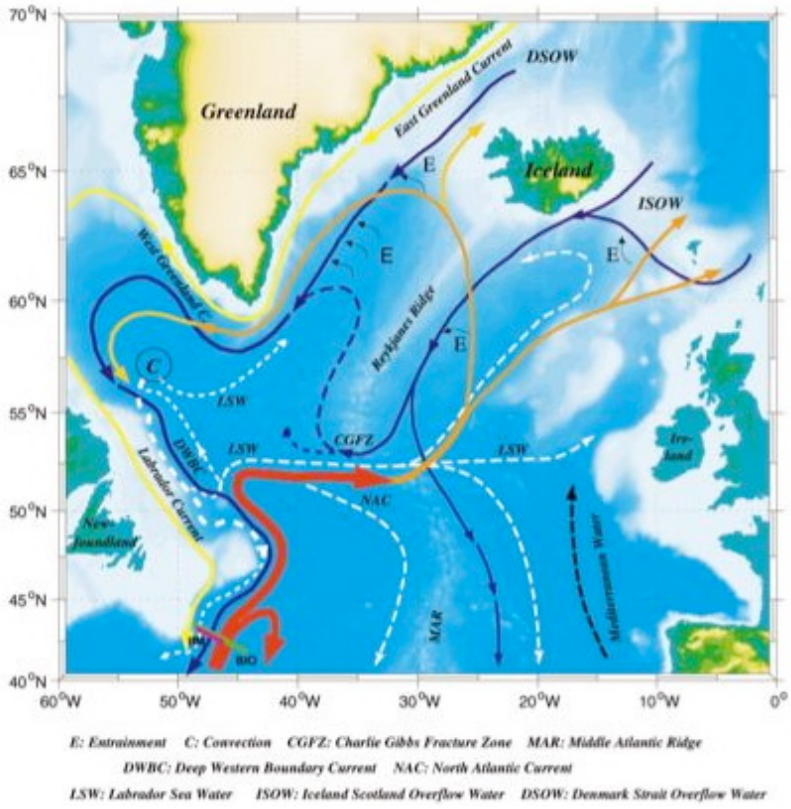

Figure 3.4.3 The major current systems of the northern North Atlantic between Denmark Strait and the Grand Banks (reproduced from *Schott et al., 2004*)

3.4.3a Main Features

The DWBC follows the contours around the Labrador Basin first in the West Greenland Current (WGC) and subsequently the Labrador Current (LC). Once again we shall consider the DWBC to be the downward continuation of the surface currents and use their names to identify the location of the DWBC under discussion. The near surface currents flow cyclonically around the edge of the basin and are driven by a combination of wind stress and thermohaline forces due to the prevailing cyclonic wind curl and the cross-shelf density gradient *[Fischer et al., 2004]*. The deep part of the current (the DWBC) follows a similar cyclonic path but is thermohaline driven. A large proportion of the surface current exits the basin over the Flemish Pass (depth 1100m) whilst the deeper currents are forced outside Flemish Cap. There is a counter-circulation in the interior of the basin that plays a significant role in the direct transport of newly formed LSW to the Irminger Sea *[Lavender et al., 2000]*.

The surface waters in the current are similar to those to the east of Greenland with a cold low salinity upper layer fed by freshwater and ice from the coast overlying warmer saltier water of Irminger Sea origin. The intermediate depths contain LSW formed by winter convection within the basin. At depth the DWBC is fed by the EGC with its combination of DSOW and modified LSW. This combines with overflow waters from the Iceland Scotland Ridge that have mixed with Mediterranean Water (MW) and have passed through the Charlie Gibbs Fracture zone, hence named Gibbs Fracture Zone Water (GFZW).

3.4.3b Transports & Variability

The LC is primarily barotropic with a mean inter-basin transport of ca 30Sv *[Pickart et al. 2002, Lohmann 1999]*. Due to its barotropic nature transport measurement requires the use of current meters and drifters. Additional transport can be seen in the LC due to basin recirculation. This is highly seasonal, *Pickart et al. (2002)* measuring ca 10Sv in wintertime falling to 2.5Sv in spring. The DWBC is responsible for about half of the 30Sv throughflow. *Schmitz (1996)* and *Dickson &*

Brown (1994) estimate the DWBC to be about 14Sv on entering the Labrador Sea at Cape Farewell growing to 17Sv on exiting off Flemish Cap. This increase may, in part, be due to the direct entrainment of newly formed LSW on the western edge of the basin. *Pickart (1992)* further subdivides the DWBC as it exits the Labrador Basin into three based upon the contributing water masses. The lower layer, from 2500-4000m, is composed of modified overflow waters (DSOW & ISOW). The middle layer, from 1300-2500m is classical LSW and the upper layer, from 700-1300m is uLSW. *Watts (1991)* calculated the transports for the three layers as; 2-6Sv for the 4-6^{o}C layer (approximating to uLSW), 1-3Sv for LSW and 1.7-5Sv for the Nordic overflow waters. His measurements were based on data collected further south in the mid-Atlantic Bight but his upper estimates are reasonably consistent with the overall transport estimates mentioned earlier. More recent work by *Fischer et al. (2004)* looked at the boundary current as it exits the Labrador Basin in the region of 53^{o}N. *Fischer et al. (2004)* used a combination of moorings, profile floats and geostrophic calculations to measure transports and current speeds over a two year period from July 1997. They calculated a total transport of ca 37Sv of which about 12Sv they attributed to surface waters. 9Sv of the 25Sv deep-water transport was due to recirculation leaving a net export of 16Sv. The deep flow consisted of GFZW, LSW and DSOW with an upper cut-off of σ_{θ}=27.74 and respective transports of approximately 11Sv, 9Sv, 4Sv. The surface layer showed seasonal variability in line with the wind flux. The DSOW also showed annual variability but with a 180^{o} phase shift compared with the surface. The LSW and GFZW components showed low annual variability.

Mooring arrays south of Flemish Cap off the Grand Banks at ca 43^{o}N recorded an average transport for the DWBC of 12Sv using the same density cut-off *[Schott et al., 2004]*. The stronger NAC passes further offshore with an average transport of 51Sv (see fig. 3.4.4 for cross-section with water mass breakdown). These averages are taken from two periods of current meter readings; 1993-1995 and 1999-2001. The transport was seen to vary significantly in the two week to two month period and also interannually, but without a significant seasonal signal. The figure of 12Sv is a little lower than the estimates of the export from the Labrador Sea but again it is hard to say whether this is indicative of interannual variation or inaccuracies in the analyses of the different data sets.

The Grand Banks is commonly regarded as the point at which NADW is fully formed and only minor additions are made as it travels the length of the Atlantic Basin.

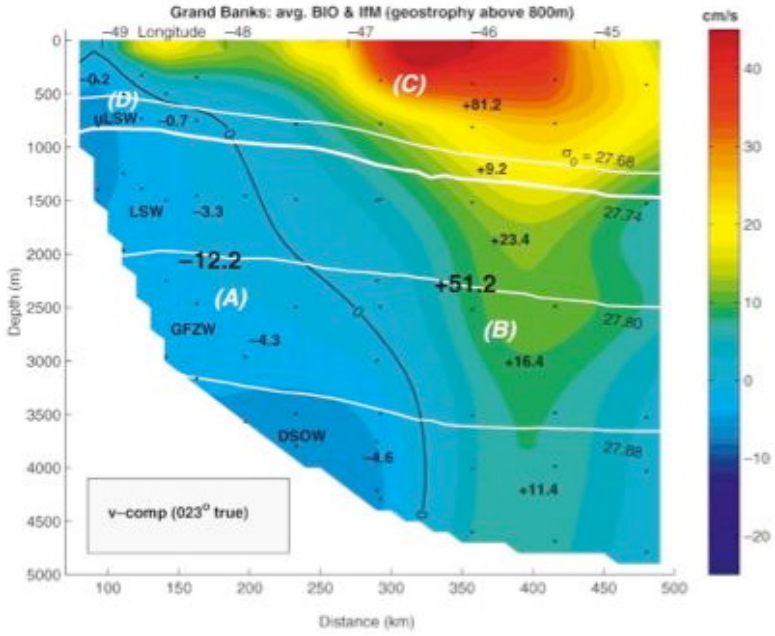

Figure 3.4.4 Cross section of DWBC and NAC off the Grand Banks (reproduced from *Schott et al., 2004)*

Comparing the deep transport at the exit of the Labrador Sea with that at Cape Farewell suggests that about 3Sv of entrainment occurs during the circulation of the basin. This can be attributed to the direct entrainment of LSW and possibly the addition of some deep water of Antarctic origin *[Schmitz, 1996]*. However the accuracy and variability of the two sets of results create a high degree of imprecision in this number. Clearly the variability in the rate of formation (discussed below) of LSW suggests that rate of direct entrainment may also display significant seasonal and inter-annual variability.

The transports recorded off the Grand Banks are a little lower than the estimates of the export from the Labrador Sea but it is impossible to say whether the difference is

indicative of interannual variability (as the data are not synchronous) or inaccuracies in the different analyses. The data collected around the path of the DWBC is sufficiently consistent to suggest an average transport in the region of 15Sv, even if it is difficult to be precise about where the smaller components join and the longer-term variability.

3.4.3c Labrador Sea Water Formation

The formation of LSW is a key process affecting the boundary currents in the Labrador Basin, the ocean currents of the North Atlantic and possibly the global thermohaline circulation. LSW was first identified by its low salinity and high oxygen concentration in comparison to neighbouring water masses *[e.g. Wust 1935]*. The high oxygen content is the result of recent atmospheric contact indicative of the fact that LSW has recently formed by deep winter convection in the Labrador Sea. Similarly, recent atmospheric contact makes atomic bomb tritium *[Jenkins & Clarke 1976]* and CFCs *[Stramma et al., 2004]* suitable tracers of LSW. Deep convection produces a thick mixed layer, the resulting low vertical density gradient giving rise to a low potential vorticity. As potential vorticity is a conservative property it has become a commonly used tracer for LSW *[Talley & McCartney 1982]*. LSW is commonly divided into an upper (ULSW) and a lower (or classical) LSW division. The lower density upper layer was thought to be produced on the shelf break *(Pickart et al., 1997)* to the west of the Labrador Basin and the lower layer by deeper convection in the west of the main basin and on the continental slope. More recent work by *Stramma et al. (2004)* has suggested that ULSW formation occurs in the central and northern Labrador Sea based on CTD and CFC data.

Talley & McCartney (1982) made use of potential vorticity to identify three principal routes for the spreading of LSW from its area of formation. The least modified LSW immediately joins the DWBC and flows south along the North American coast. The second pathway takes the LSW east into the North Atlantic Current and the third north-east into the Irminger Sea. LSW becomes widely spread across the North Atlantic at depths of between 500 and 2000m, its high density

preventing it from crossing the Greenland-Iceland-Scotland ridge. Modification during its travels in the North Atlantic means that the branch of LSW joining the EGC is of higher salinity and potential vorticity than that immediately joining the DWBC in the Labrador Basin. LSW has a lower tritium concentration than both uLSW and the Nordic overflow waters *[Pickart, 1992]*. This supports the idea that the LSW follows a slower route to the DWBC than either of the other two water masses. Drifter data *[Lavender et al., 2000]* illustrate two of the three suggested pathways for newly formed LSW. Floats were seen to pass directly into the Irminger Sea via an anticyclonic counter-current in the centre of the Labrador Basin. The travel time for this route to the Rockall trough was 2.8 years (4.9cm s^{-1}) for a 1,500m float. Floats leaving the LC between 51 and 54^{o}N travelled east with a 700m float taking between 1.6 and 2.6 years to reach the Iceland basin (average 8.7 cm s^{-1}) and a 1500m float 3.8 years (average 6.6 cm s^{-1}) for the same journey.

The studies of *Pickart et al. (2003)* and *Bacon et al. (2003)* raise the question of what proportion of LSW seen joining the EGC is of Labrador Sea origin as opposed to Irminger Sea origin (see section 3.4.2).

Winter atmospheric conditions control the depth to which deep convection takes place controlling the volume and temperature of the LSW produced each year. The maximum depth of convection is estimated to be 2000m but in some years there can be a total absence of deep convection *[Pickart et al., 2002]*. *Pickart et al. (2002)* cite atmospheric changes associated with the North Atlantic Oscillation (NAO) as the most obvious source of this variability. The NAO refers to the variation in the winter time sea-level pressure difference between Iceland and the Azores *[Hurrel, 1995]*. Intense regions of low pressure over the Labrador Sea during periods of high NAO produce strong, cold, dry winds that promote deep convection. *Pickart et al. (2002)* also recognise changes in surface water composition as a key influence on LSW productivity. For example a reduction in surface salinity, such as that observed during the Great Salinity Anomaly, produces a stable stratification that inhibits deep convection *(Dickson et al., 1996)*. The characteristics of LSW therefore change recognisably with its year of formation. Rates of production show considerable variation and these translate to changes in the overall reservoir of LSW seen in the Labrador Sea. *Lazier et al. (2002)* and *Stramma et al. (2004)* observe a reduction in

the volume of LSW in the late 1990s as a result of low formation rates. *Stramma et al. (2004)* go on to link the reduction in the formation of LSW to the shift of the ULSW formation zone from the western boundary to the central basin. *Stramma et al. (2004)* also observed a reduction in the temperature and salinity of GFZW and bottom water (DSOW) between 1996 and 2001. The changes in DSOW characteristics act as a marker for the flow of DSOW and enabled them to calculate a time of 2 years for it to flow from the Labrador Sea to the Grand Banks.

Pickart et al. (2002), reporting on the Labrador Sea Deep Convection Experiment of February-March 1997, made a number of observations about deep convection and LSW formation during a period of moderate level NAO index. Deep convection was found in the commonly accepted location on the western side of the Labrador Basin and also further west on the continental slope. They suggested that this second source contributed LSW directly to the DWBC as it flows south out of the Labrador Sea. Deep convection was absent in the northern and eastern regions due to the stable stratification of the water column in these locations.

3.5 Palaeoclimate And Palaeocirculation Records From North Atlantic Contourite Sediments

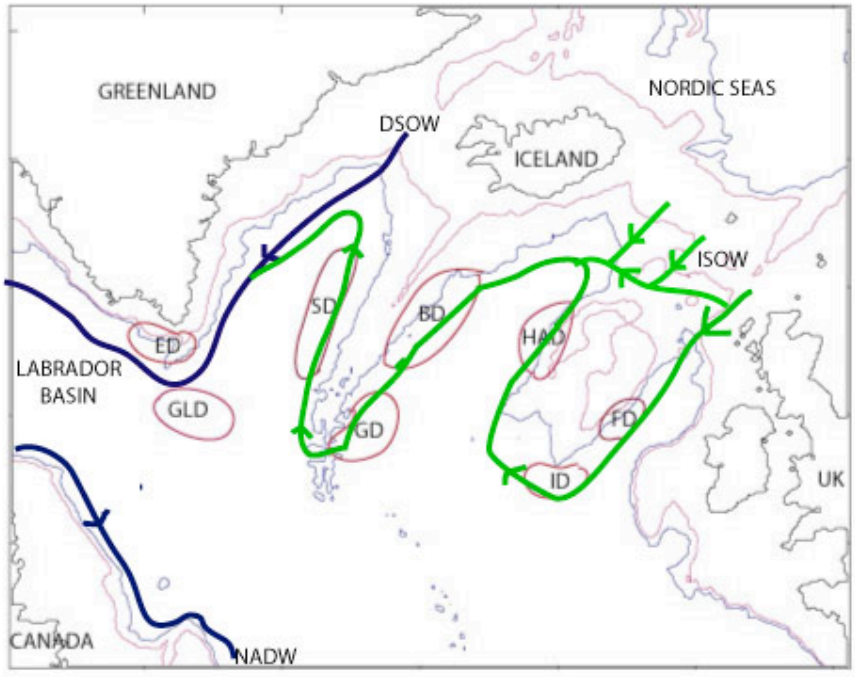

BD-Bjorn Drift, ED-Eirik Drift, FD-Feni Drift, GD-Gardar Drift, GLD-Gloria Drift, HAD-Hatton Drift, ID-Irminger Drift, SD-Snorri Drift

Figure 3.5.1 Sediment drifts in the northern North Atlantic – drifts in red – overflow pathways in heavy blue and green -500m and 1000m isobaths in purple and blue *(after Wold, 1994)*

Wold (1994) identifies seven sediment drifts in the northern North Atlantic south of the Greenland-Scotland Ridge (see fig. 3.5.1 above). The largest of these occur on the western side of basins as a result of intensified deep western boundary currents (e.g. the Bjorn & Gardar Drifts on the eastern side of the Reykjanes Ridge and Eirik Ridge off the southern tip of Greenland). The sediments making up these large drifts have been deposited by contour following, geostrophic bottom currents. Such deposits were first termed contourites by *Heezen et al. (1966)*. A number of analytical techniques can be applied to cores taken from these drifts to yield information about prehistoric climate, circulation and bottom current strength.

These techniques require the relationship between time of deposition and core depth to be reliably established. The starting point is typically accelerator mass spectrometer radiocarbon dating (AMS ^{14}C). AMS ^{14}C dating requires rapid sedimentation to minimize the effects of bioturbation *[Manighetti et al., 1995]*. The reliability of the dating can be improved by tying the record with climatic events of known age. X-radiography, bulk magnetic susceptibility and water content can be used to identify features consistent with ice rafting during cold periods. The presence of ash can also be identified which can be linked to known volcanic events. By tying the record to such specific events the effect of bioturbation can be quantified.

Carbon 14 dating of sediment layers combined with mass determination can give deposition rates in kg m^{-2} yr^{-1} *[Wold, 1994]*. Sediment depth accumulation per year can also be obtained but compaction rates must be taken into account. This approach can provide the age of drifts and the variation in sedimentation rates over their lives. Unfortunately the technique does not allow for the effect of sediment cycling.

Sediment analysis can provide information about the climate at the time of deposition. The measurement of stable isotope ratios (^{18}O to ^{16}O and ^{13}C to ^{12}C) in foraminiferal carbonates is a key technique. Planktonic abundances, nutrient proxy concentrations and physical sediment characteristics also provide evidence of shifts in climate and ocean circulation.

- The ratio of oxygen 18 to oxygen 16 ($\delta^{18}O$) found in foraminiferal shells is a measure of ice volume and therefore temperature *[Cooke & Rohling, 1999]*. ^{16}O is preferentially stored in land ice leaving the oceans enriched in ^{18}O during glacial periods. The $\delta^{18}O$ ratio is therefore linked with temperature and sea level.

- Carbon 12 is preferentially taken up during photosynthesis enriching the carbon 13 to carbon 12 ratio ($\delta^{13}C$) in surface waters and depleting it in deep waters by remineralisation of the organic matter *[Cooke & Rohling, 1999]*. $\delta^{13}C$ ratios can therefore be used to "age" deep water with the more recently formed water masses showing the least depletion. $\delta^{13}C$ ratios taken from sediments can be used to track deep-water pathways and changes in circulation strength.

- The calcium/cadmium and $\delta^{13}C$ ratios can be used as a nutrient proxy *[Boyle & Keigwin, 1987]*. For example nutrient poor NADW is enriched in

$\delta^{13}C$ and depleted in cadmium in comparison with Antarctic waters. Cadmium is found in calcium carbonate shells replacing calcium based upon the concentration of cadmium in the water. Based upon the assumption that the cadmium/phosphate ratio is constant the cadmium/calcium ratio is a proxy for phosphate concentration.

- The relative abundance of the planktonic formanifera *N. pachyderma* is an indication of water temperature *[Manighetti et al., 1995]*. *N. pachyderma* is the only planktonic foramnifera with a preference for polar water.

- A combination of X-radiography, magnetic susceptibility and water content analysis can be used to identify layers in the sediment record corresponding to cold periods.

- Grain size can be used to infer current speeds as stronger bottom currents give rise to a larger mean grain size *[McCave et al., 1995]*.

Keigwin & Lehman (1994) used a combination of planktonic abundance, N. pachyderma abundance, the planktonic $\delta^{18}O$ ratio and the benthic formaniferal $\delta^{13}C$ ratio to identify the Heinrich I and Younger Dryas events in cores taken from the Mid-Atlantic Ridge at 43°N. They also linked these events with reduced NADW production based upon reduced $\delta^{13}C$ ratios at the appropriate depths in the cores. *Sarnthein et al. (1994)* used $\delta^{13}C$ ratios taken from 95 cores throughout the eastern Atlantic to track the pathways of NADW over the past 30,000 years. *Boyle & Keigwin (1987)* used $\delta^{13}C$ and Cd/Ca nutrient proxies to link a reduction in nutrient poor NADW content of bottom water with the Younger Dryas cold period. This is consistent with the contemporary theory that the Younger Dryas resulted from a weakening in the THC due to a salinity reduction in the North Atlantic areas of deep-water formation.

Changes in circulation and current strength can also be related to climatic variations more indirectly. *Faugeres & Stow (1993)* suggest that major increases in bottom circulation correspond to periods of climatic instability. They also comment on the role of sea level. High stands increase the exchange of surface and bottom waters between the marginal and main ocean basins giving rise to increased bottom circulation. Low stands produce more turbidity current activity that can mask bottom current sedimentation.

Bacon et al. (2003) identify Eirik Ridge as the only location capable of providing a "continuous calibrated record of the THC from the present day back to the Last Glacial Maximum". Eirik Ridge marks the point where the East Greenland Current is slowed as it turns west and then north to become the West Greenland Current. The drift began to accumulate in the late Miocene between 7 and 8 Ma. *Wold (1994)* suggests that this was initiated by an uplift of the Greenland-Iceland Ridge reducing the flow of DSOW and weakening the strength of the deep western boundary current as it makes the turn to a point where deposition occurred. The drift is probably composed largely of material eroded from the East Greenland margin and Denmark Strait *[Wold, 1994]*. The sediment load of the fjords of East Greenland may also contribute to the drift. Unfortunately the sediments are severely affected by bioturbation removing any surface structures in the vast majority of cores *[Chough & Hesse, 1985]*.

4 OBSERVATIONAL STUDIES

This chapter of the thesis covers new research into the dynamics of the ocean currents off south-east Greenland using observational data. The first section (published in Geophysical Research Letters, 2005) explores the hydrography of the East Greenland Coastal Current and its relationship with the East Greenland Current by making use of all the available historic data that is publicly available. The second section (first published in Deep Sea Research I, 2007) concentrates on the deeper flows of the Deep Western Boundary Current. This paper is cross-disciplinary and was written in partnership with Sally Hunter, a post-graduate sedimentologist. The analysis is primarily based upon new data collected on Discovery Cruise D298 but this is combined with the use of historic data in order to look at temporal variations.

Both papers are reproduced in their original journal form except that their references have been moved into the overall list at the end of the thesis and the page, table and figure numbers have been adjusted by use of a prefix. Each paper is followed by an appendix presenting unpublished material relating to the research. The appendix to the GRL paper is more extensive as the four page limit for this publication ensured that some of the detail had to be excluded from the original manuscript. The appendix to the DSR I paper presents an analysis of how to estimate transport along a sloping bottom using the geostrophic method.

4.1 Geophysical Research Letters Paper

THE SPATIAL AND TEMPORAL VARIABILITY OF THE EAST GREENLAND COASTAL CURRENT FROM HISTORIC DATA

by

David Wilkinson and Sheldon Bacon

National Oceanography Centre, Southampton
University of Southampton Waterfront Campus
European Way
Southampton SO14 3ZH, UK

Published in Geophysical Research Letters, 28/10/05

GRL Abstract

[1] Analysis of historic hydrographic data collected between 1932 & 1997 show a freshwater jet flowing southward along the East Greenland Shelf between Denmark Strait & Cape Farewell with a typical baroclinic transport of between 0.5 & 2 Sv. This jet has been labelled the East Greenland Coastal Current (EGCC). The depth of the jet is a function of transport but the lateral extent of the jet is mainly defined by the position of the shelf break. Comparing section transports from different times & locations it is seen that significant short-term variability masks both longer-term variability & latitudinal variations. The data suggest an increase in EGCC transport during the early 1930s Greenland warm period followed by reduced average fluxes thereafter but there is insufficient data for this result to be considered statistically significant. In addition there is no evidence of significant growth in the transport as the jet progresses south as might be expected with the addition of run-off from the SE Greenland fjords.

GRL 1 Introduction

[2] The southward flowing surface currents off the east coast of Greenland are of global climatic significance as they are major exporters of freshwater from the Arctic Basin [*Aagaard and Carmack*, 1989; *Bacon et al.*, 2002 hereafter B2002] . The interaction between the freshwater circulation in the northern North Atlantic & the thermohaline circulation (THC) has received increasing attention over recent years with the acceptance that changes in surface salinity in the areas of deep water formation could alter the strength & form of the THC impacting global climate [*Rahmstorf*, 2000]. Increased melt-water runoff from the Greenland ice cap, due to global warming (eg [*van de Wal*, 2003]) , is a potential trigger for such a change. The shrinking of the ice cap would also cause an increase in sea-level. It is estimated that complete melting of the Greenland ice cap would lead to a 6.7m rise in global average sea level [*Ohmura and Reeh*, 1991].

[3] The southward flowing near surface currents have historically been grouped together under the title of the East Greenland Current (EGC). The term EGC is typically now reserved for the western boundary current situated in the region of the continental slope. Many early studies recognised a low-salinity surface layer over the Greenland Shelf (e.g. [*Malmberg et al.*, 1972],[*Blindheim*, 1968]) but during this period the calculation of salinity & freshwater fluxes was uncommon. As a result the significant role played by the jet in the freshwater budget of the Arctic was not appreciated & it was not investigated further until the late 1990s. This on-shelf freshwater jet was given its own name, the East Greenland Coastal Current (EGCC), when the results of a 1997 cruise on RRS Discovery were published [*B*2002]. The B2002 spot value of 0.06Sv calculated for the EGCC freshwater transport would equate to 30% of the net Arctic freshwater gain if seen throughout the year. This work was based primarily on a single 1997 section running out across the shelf from Cape Farewell with support from historical hydrographic & drifter data. From this combination they hypothesised that the EGCC was primarily driven by seasonal melt-water from the SE Greenland coast.

[4] We have performed a more extensive analysis of all the historic hydrographic data available in an attempt to characterise the spatial & temporal variability of the freshwater jet between Denmark Strait in the north & Cape Farewell in the south. The term “total transport” is used below to refer to the flux of seawater in the EGCC, & the term “freshwater transport” to refer to the flux of fresh water based upon a reference salinity of 34.956, as derived in [*Bacon*, 1997]) & used in B2002.

GRL 2 Data & Methodology

[5] A hydrographic dataset for the SE Greenland shelf region was compiled from the World Ocean Database (WOD) [*Conkright et al.*, 2002] & the International Council for the Exploration of the Seas database (www.ices.dk/ocean/). This was supplemented with additional Icelandic data provided by the Marine Research Institute, Reykjavik. The full dataset provides a valuable picture of average temperature & salinity patterns but for the calculation of geostrophic velocities the data had to be carefully filtered. Stations not forming synoptic sections across the majority of the width of the East Greenland shelf with good vertical resolution of the full water column were eliminated leaving 147 suitable stations forming 40 sections. They dated from 1933 to 1997 with observations mainly concentrated in the summer months (60% in August). Details of the dataset are available on request.

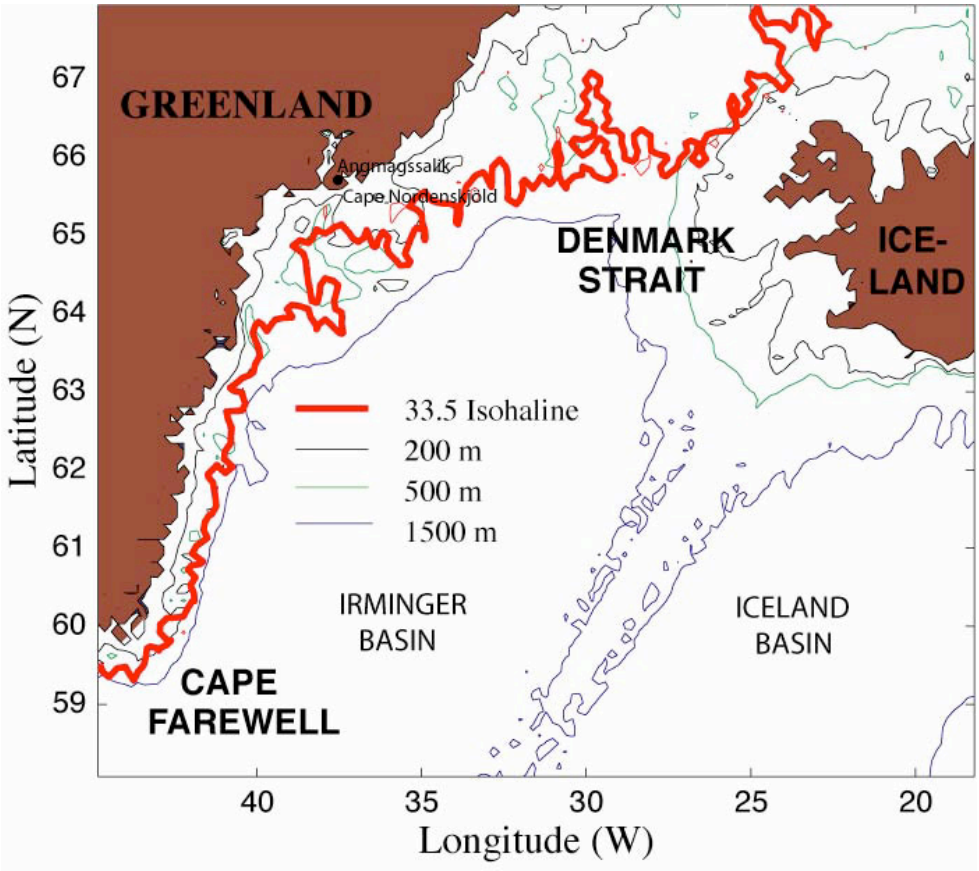

Figure GRL1 Map of the SE Greenland region showing the relationship between the eastern edge of the EGCC (as marked by the 33.5 surface isohaline) and the shelf break.

[6] In the vicinity of Cape Farewell the shelf is narrowest at about 40km wide, & is around 200m deep (Figure 1). The shelf break is abrupt with the depth increasing rapidly to over 2000m. North of Cape Farewell to 63˚N the shelf widens slowly out to about 60km & there are a number of submarine holes & trenches with on-shelf depths exceeding 500m. Between 63˚N & 65˚N the shelf widens more rapidly to about 250km with a submarine trench running out from Angmagssalik. The shelf reaches a maximum width of about 350km in the region of Denmark Strait.

[7] The section data were first processed to calculate geostrophic, baroclinic velocities & transports (i.e. geostrophic flow with a level of no motion at the seafloor) for the sections of the flow encompassed by the stations. The resultant transport data were still difficult to compare directly as the sections did not cover equal proportions of the jet. The 1997 section [B2002] had the advantage of two stations specifically sited to capture the transport in the EGCC with the near shore station only ca.4km from the coast & the outer station close to the shelf break. The

inshore stations on the selected sections averaged ca. 16km from the coast therefore omitting a proportion of the jet. A more limited problem was the offshore edge of the jet falling between two stations although more typically there was an area of low baroclinic velocities separating the jet from the main EGC containing at least one station. In order to address these problems & to provide continuous salinity profiles for the estimation of freshwater fluxes a simple analytical frontal model of potential density [*Webb*, 1995] was fitted to each section dataset following B2002. This was achieved by varying six parameters; the position of the ccntre of the front, the width of the front, the density difference across the picnocline, the mean picnocline depth, the picnocline thickness & the vertical position of the centre of the front. The reader is referred to B2002 for a more complete discussion of the model as the approach employed here only differs in that there were no surface data & all the parameters were fixed by the minimisation routine. The analytical model allowed the sections to be extended in either direction to provide full coverage of the EGCC into the coast. High resolution (1km by 10m grid) salinity data was extracted from the model potential density function by using two-dimensional linear interpolation of the observed potential temperature data & then reversing out the salinity from the equation of state for seawater [*Millero and Poisson*, 1981]. Where it was necessary to extend the sections beyond the observations the temperature profile was assumed to match the nearest station. The less rigorous approach to temperature is justified as salinity is the dominant driver of density variations in the region [*B*2002]. Interpolation of the observed temperature data for use in the model provides a more realistic profile than that employed in B2002 & the linear relationship between the total transport derived mainly from observational data & the fresh water transport derived from model data (figure 2) demonstrates that salinity is still the dominant driver of density variations & the implied geostrophic flow.

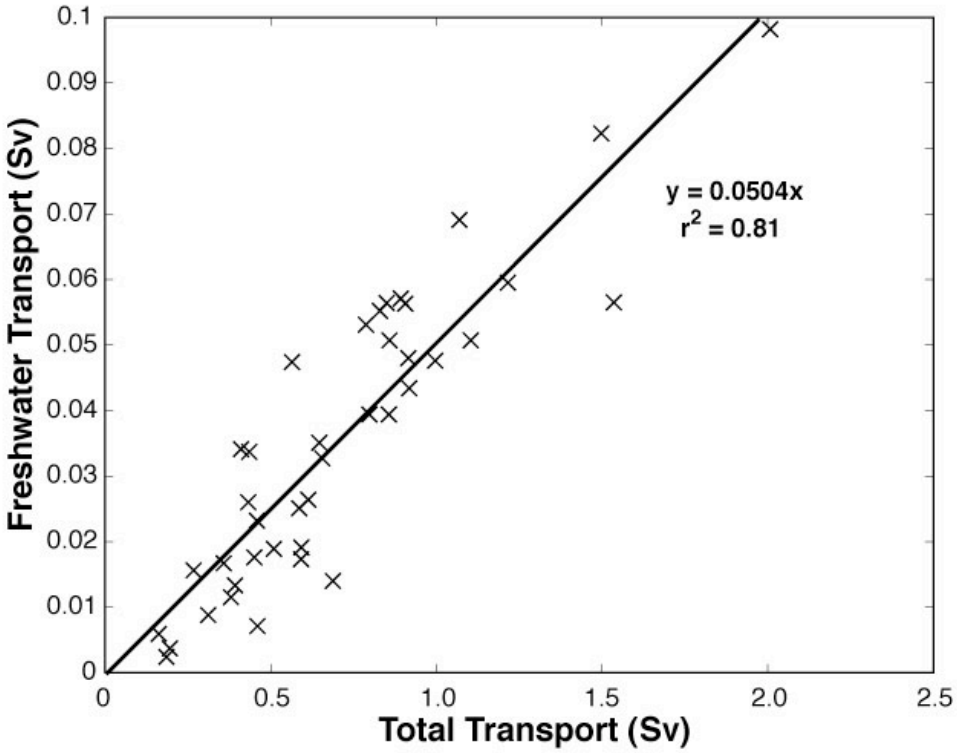

Figure GRL2 Plot of model derived freshwater transport against total transport calculated from combined observations and model data.

[8] While B2002 achieved a good fit between the 1997 hydrographic data & the model, initial results fitting the model to sections in deeper water than found off Cape Farewell produced disappointing results. Significant errors were found in the transport across the sections implied by the model in comparison to the geostrophic transports calculated from the hydrographic observations. It was found that the model fit was generally good in the upper 200m of the water column. However errors resulted from deeper velocities inconsistent with a simple near-surface front. Where the shelf was significantly deeper than 200m the jet was being advected by the deeper circulation. Therefore the model was only fitted to the upper 200m of observations. Where the water depth exceeded this, reference velocities at 200m were applied by calculating the geostrophic velocity profile referenced to zero at the bottom. A comparison of transports calculated directly from observations with those taken from the model showed good agreement (figure 3). The model error shown was calculated as follows where the model total transport is for the section covered by the observations:

$$\text{Model error} = \frac{\left(\text{Model Total Transport} - \text{Observed Total Transport}\right)}{\text{Observed Total Transport}} \times 100\%$$

There were only 5 outliers where the model error was greater than 33% & the r.m.s. error for all sections was 20.5%. For comparison the 1997 *Discovery* section validated by comparison with acoustic Doppler current profiler (ADCP) currents shows a slightly better than average error of 13%.

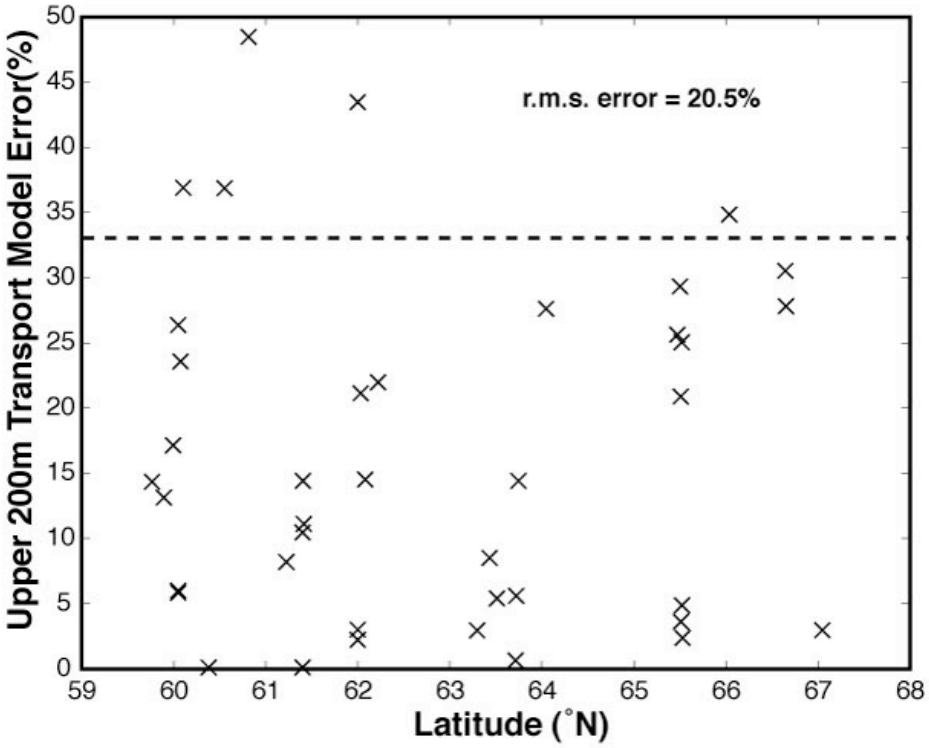

Figure GRL 3 Plot of percentage error in model derived transport in comparison with the equivalent transport calculated directly from observational hydrographic data.

[9] Total & freshwater transports calculated here are for the upper 200m of the water column, which is typically responsible for more than 95% of the total southward transport & a larger proportion of the freshwater export. Total transports are calculated from a combination of observed geostrophic transports & model transports to extend the section outside the observations. Fresh water transports are produced from model data based on a reference salinity of 34.956.

GRL 3. Accuracy Of Model Fitting & Results

[10] The use of geostrophic velocity shears to determine transports assumes that the flow is in geostrophic equilibrium & that there is no significant barotropic flow. These assumptions have been shown to be reasonable for the freshwater jet off Cape Farewell in 1997 [*B*2002] & off Cape Nordenskjold (ca. 66˚N) in 1965 [*Malmberg et al.*, 1972] by comparison with current meter data. The zero velocity reference level has been assumed to coincide with the deepest data point at each station with interpolation between stations. Only stations with the deepest readings close to the sea bottom have been chosen excepting two stations in separate sections that required extrapolation of the data to the bottom based upon the model.

[11] The use of the analytical model also introduces uncertainty. However the sections were selected such that the contribution to the total transport in the model extensions is typically only around 10% & so does not significantly impact the overall conclusions. An additional section that met the earlier selection criteria but relied upon the model extensions for the majority of its transport was omitted from the final results. The derived continuous salinity data is reasonable given the low significance of temperature on density in the area but does not resolve features smaller than the station spacing. B2002 showed that for the 1997 sections these were not significant. The 200m reference velocities were only available at the resolution of the stations & the inter-station average was applied to all intermediate model points. Although this does not affect total transport it introduces some uncertainty in the calculation of fresh water fluxes. To test the significance of this a 1933 section at 62˚N with unusually high reference velocities was selected & the fresh water flux was recalculated using linearly varying reference velocity adjustments with the same inter-station averages. This only resulted in an increase in the freshwater transport from 0.0823Sv to 0.0826Sv.

[12] In the majority of sections the EGCC & EGC could be identified as separate entities with an area of near zero baroclinic transport between them. This allowed the offshore extent of the transport calculation to be set by selecting the appropriate number of stations. Where the two currents were not easily separated within the resolution provided by the stations the offshore extent was set approximately at the

position of the 33.5 surface isohaline using the model to extend out from the nearest station.

GRL 4. The East Greenland Coastal Current – Position

[13] ADCP data for a section off Cape Farewell [B2002] shows the jet velocity falling close to zero by a depth of 120m coinciding approximately with the depth of the 33.5 isohaline at the inshore station. Although the surface velocity does not fall to zero over the section the main core is also contained within the 33.5 surface isohaline making this a good indicator of the extent of the EGCC. Time averaging all the available hydrographic data & plotting the position of the surface 33.5 isohaline shows that the eastern edge of the EGCC closely follows the edge of the continental shelf marked by the 500m isobath (figure 1). There are two regions where this is not true. In the vicinity of Denmark Strait the low salinity water is seen to extend over the deep channel. In the area between 66˚N & 63˚N, where the shelf narrows considerably, the low salinity water is often confined to the inner portion of the shelf. This confinement to the inner-shelf coincides with the presence of the submarine trench extending out from Angmagssalik.

[14] Although there is some temporal variability the width of the EGCC is mainly a function of shelf width & hence latitude. However the depth of the current (again based upon the 33.5 isohaline in the observational data) shows no relationship with latitude. Instead there is a clear linear relationship between the depth & the observed geostrophic transport (figure 4). Choosing an isohaline of ca. 33.5 provides the strongest relationship with transport (square of the correlation coefficient, $r^2 = 0.79$), but there is a good correlation ($r^2 > 0.6$) for choices of isohaline between 33.25 & 34. This correlation weakens for salinities lower than 33.25. This can be explained with reference to the relationship between salinity & ADCP velocity seen in B2002 & the fact that the 33.5 isohaline is about the highest value that does not intersect with the shelf seabed in the majority of sections. The robustness of this relationship makes the depth of the 33.5 isohaline, at a suitable cross-shelf location, a potential proxy for measuring the transport in the EGCC.

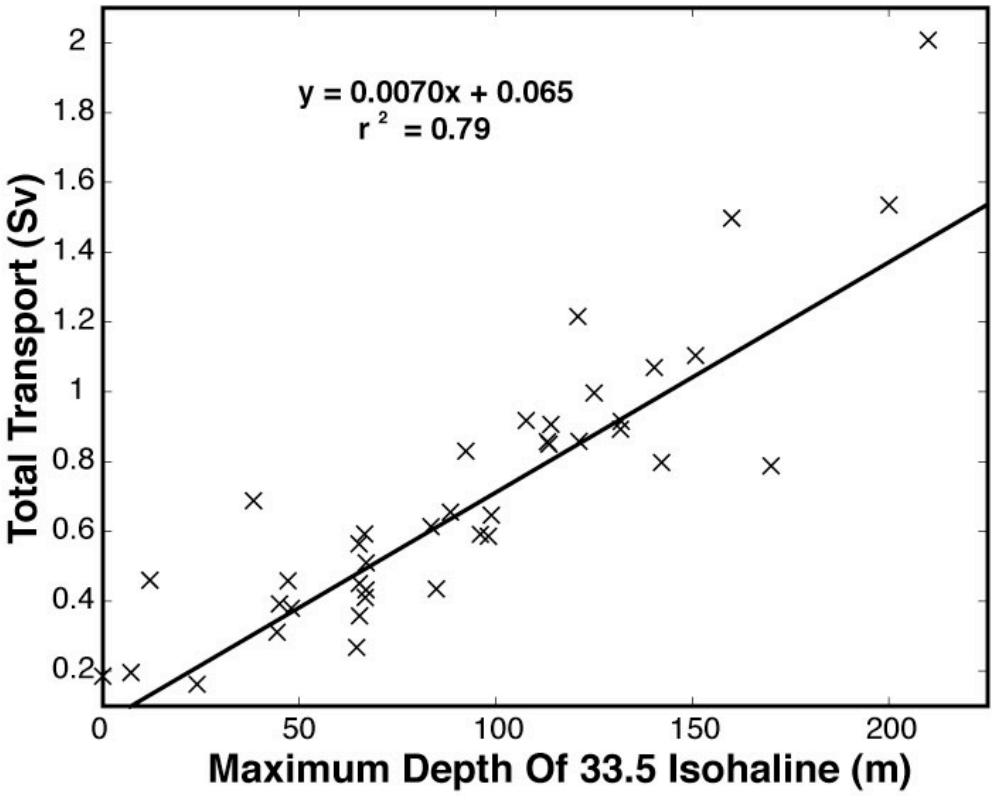

Figure GRL 4 Plot of total transport versus depth of EGCC as defined by the maximum observed depth of the 33.5 isohaline.

[15] A comparison of EGCC transport with latitude surprisingly showed no clear relationship. If the flux of summer melt-water from the fjords of SE Greenland is the dominant driver of the EGCC (as hypothesised in B2002) a growth in summertime transport moving southwards would be expected. The absence of this feature may be due to the limited dataset & requires further investigation. The collection of year-round data to establish whether the current is seasonal would help considerably. Unfortunately the historic dataset is almost entirely concentrated in the summer months.

GRL 5 Temporal Variability & Fresh Water Flux

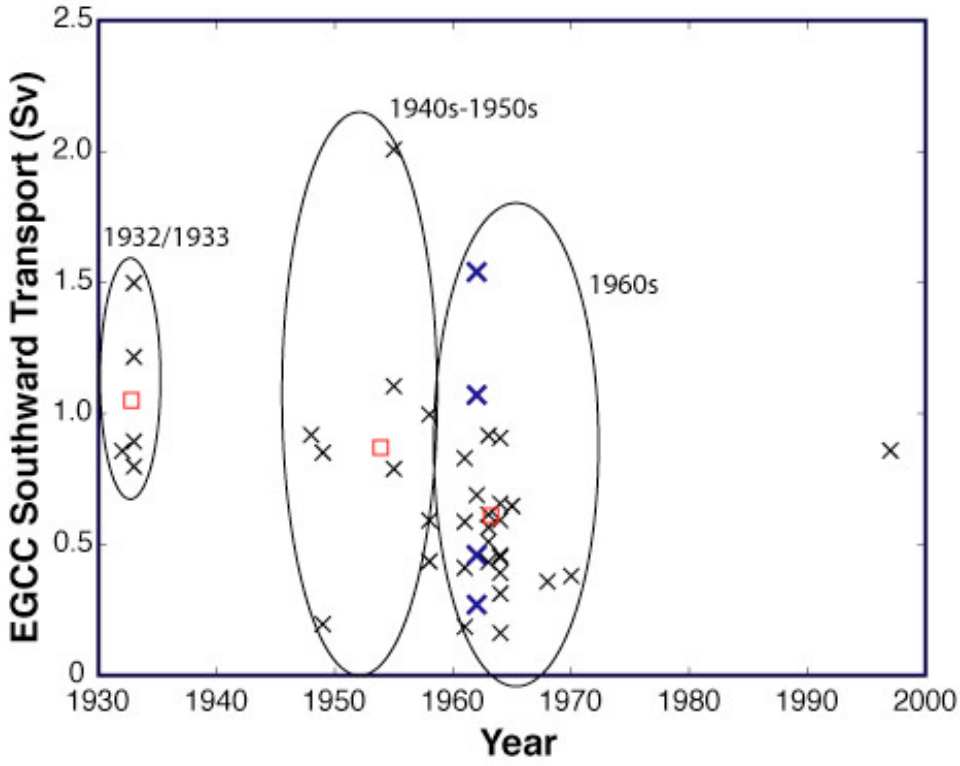

Figure GRL 5 Plot of total transport versus year with period means (red squares). August 1962 data shown in blue.

[16] The large scatter in the total transport in the EGCC (upper 200m of the water column) is clear in a plot of transport against year (figure 5). Four sections from a two week period in August 1962 demonstrate how rapidly the transport varies. The calculated transports of 0.27, 0.46, 1.07 & 1.54 Sv cover almost the whole range observed over the 65 year period (blue crosses on figure 5). These transports correspond to latitudes of 65.5^{o}N, 63.7 ^{o}N, 60.1 ^{o}N & 61.4 ^{o}N respectively.

[17] Comparison of the mean transports for the 1930's, the 1940's-1950's & the 1960's (figure 5) suggests a weakening in EGCC transport moving from the 1930's to the 1960's. It is tempting to link this with the observed Greenland warm period during the early 1930's [*Box*, 2002] based on the B2002 hypothesis that the transport is driven by seasonal meltwater runoff from Greenland. However the limited volume of data combined with the significant short-term variability renders the weakening trend in the transport statistically insignificant. The relationship identified between the transport & the maximum depth of the 33.5 isohaline does

suggest the possibility of expanding the dataset by looking for single hydrographic stations close to the shore. Unfortunately this does not produce a significantly larger dataset as it is the lack of inshore stations that reduced the number of suitable sections in the initial search.

[18] The fresh water transport is approximately 5% of the total transport & shows similar short-term variability ranging from 0.002 to 0.1 Sv (figure 2). The value of 0.06Sv observed by B2002 represents an average summer flux over the entire record.

GRL 6 Conclusions

[19] Historic data from throughout the 20th century shows the presence of an on-shelf freshwater jet flowing south between Denmark Strait & Cape Farewell confirming the permanence of the feature during the summer months. The eastern edge of the jet closely follows the shelf edge for most of this distance but its depth varies significantly with the instantaneous transport. Short-term variability masks longer-term trends & further observation is required to draw confident conclusions about seasonal & longer-term variability. The limited evidence of a correlation between EGCC transport & Greenland surface summer air temperature requires verification with new data.

[20] Further study combining hydrographic measurements with geochemical analysis (e.g stable isotope studies) will shed more light on the source of the freshwater in the jet. Planned measurements from moored instruments will determine the extent to which the jet is a seasonal feature & whether it is present at all in winter. This additional information will allow conclusions to be drawn as to the extent to which the jet is driven by freshwater run-off from SE Greenland as opposed to other sources. The relationship between EGCC transport & maximum isohaline depths also presents possibilities for monitoring the current transport. Monitoring would need to take place in the region of 10km from the shore where the freshwater wedge is close to its maximum thickness. Sensitivity testing the strength of the current depth to transport relationship for varying distances from shore

revealed that the correlation falls off rapidly approaching 20km. Monitoring the hydrographic profile close inshore is difficult as the passage of ice makes the use of moorings problematic. However a similar approach may be possible using a bottom mounted ADCP to identify the depth of penetration of the EGCC by measuring the vertical velocity profile & assuming a relationship between the depth of the 33.5 isohaline & (e.g.) the depth of the maximum velocity shear.

GRL Acknowledgements

The authors are grateful to Hedinn Valdimarsson of the Marine Research Institute, Reykjavik for the provision of 4 hydrographic sections not available at the time in the main databases. The authors' work was funded by the U.K. Natural Research Council's Rapid Climate Change program under grant NER/T/S/2002/00453.

4.2 Appendices To GRL Paper

4.2.1 Details Of Analytical Model Employed

The frontal model employed to provide a continuous potential density function through the EGCC is a simple hyperbolic tangent function. The model is that of [*Webb*, 1995] and fits a shape to the typical nature of a density front rather than attempting to deduce the form from primitive physical equations. This model was shown to imply geostrophic currents consistent with those measured by ADCP off Cape Farewell on the 1997 Discovery cruise [Bacon*, et al.*, 2002].

The mathematical details of the model are laid out in equations 1 to 4 below:

$$\rho(x,z) = \rho_0 - \rho_1 f(x,z) \quad (1)$$

$$f(x,z) = 0.5 \{1+\tanh[(z-z_c(x))/z_2]\} \quad (2)$$

$$z_c(x) = z_1 - z_3 \tanh(x/x_1) \quad (3)$$

$$x = x' - x_0 \quad (4)$$

Where ρ is the potential density as a function of depth, z, and horizontal distance, x. x is defined by equation 4 where x_0 is the position of the centre of the front with respect to the inshore CTD station and x' is the horizontal coordinate also with respect to the inshore CTD station. ρ_0 is a reference density and was set to 1028 kg m^{-3} as in *Bacon et al (2002)*. z_c is the vertical position of the centre of the front as a function of horizontal position defined by equation 3.

x_0 is one of the six parameters that were varied to achieve the best fit between the observed potential densities and the model values at the same points. The other five are; x_1 - the width of the front, z_1 - the mean depth of the pycnocline, z_2 - the pycnocline thickness, z_3 - the change in pycnocline depth across front and ρ_1 - the density difference across the pycnocline. The fitting of the model was achieved using the Matlab least squares non-linear fitting algorithm ("lsqnonlin").

4.2.2 Table Of Hydrographic Section Data Used In The Paper

Summary details of the hydrographic data employed are shown in table 4.2.1 on the following page. Cruise ids. prefixed with WOD are from the World Ocean Database and the data can be obtained via the US National Oceanographic Data Center web page *[Conkwright et al, 2002]* . Those prefixed with an "I" have been supplied directly by Hedinn Valdimarrson of the Marine Research Institute, Reykjavik.

Table 4.2.1: Summary Details Of Hydrographic Sections Employed

Cruise	Int. Ref.	Country	Ship	Start Date	Inshore Station Latitude	Stations Used	Seawater Flux (Sv)
WOD01_06000083	2	W.GERMANY	HERWIG, W.	12/8/1968	59.76	4	0.3581
WOD01_06000847	4	W.GERMANY	A. DOHRN	18/9/1955	62.08	3	0.7879
WOD01_06000847	5.1	W.GERMANY	A, DOHRN	18/9/1955	63.51	3	2.0075
WOD01_06000847	6	W.GERMANY	A. DOHRN	16/9/1955	65.53	3	1.1038
WOD01_06002175	9	W.GERMANY	A. DOHRN	5/9/1958	65.51	3	0.4352
WOD01_06002175	10	W.GERMANY	A. DOHRN	9/9/1958	63.43	3	0.9963
WOD01_06002175	11	WGERMANY	A. DOHRN	10/9/1958	61.23	3	0.5918
WOD01_26001146	23	DENMARK	DANA	11/8/1933	63.75	3	1.2158
WOD01_26001146	24	DENMARK	DANA	12/8/1933	62.22	4	1.4976
WOD01_26001146	25	DENMARK	DANA	13/8/1933	60.82	3	0.7978
WOD01_58000065	35	NORWAY	JOHAN HJORT	21/8/1963	60.05	3	0.9155
WOD01_58000065	37	NORWAY	JOHAN HJORT	26/8/1963	65.50	5	0.4326
WOD01_74010083	40	UK	RRS DISCOVERY	31/8/1997	59.89	2	0.8584
WOD01_90008016	44	USSR	TOPSEDA	6/5/1961	62.00	3	0.1855
WOD01_90008023	45	USSR	SEVASTOPOL	26/9/1964	59.99	2	0.1620
WOD01_90008023	47	USSR	SEVASTOPOL	30/9/1964	62.03	3	0.4586
WOD01_90008023	48	USSR	SEVASTOPOL	24/7/1964	64.05	4	0.5927
WOD01_90008020	48	USSR	TOPSEDA	11/5/1962	62.00	3	0.6880
WOD01_90008024	49	USSR	TOPSEDA	22/7/1964	62.00	3	0.3117
WOD01_58000066	55	NORWAY	JOHAN HJORT	21/8/1964	61.40	3	0.9064
WOD01_58000066	56	NORWAY	JOHAN HJORT	21/8/1964	60.05	3	0.3921
WOD01_58000066	57	NORWAY	JOHAN HJORT	27/8/1964	63.72	3	0.4508
WOD01_58000066	58	NORWAY	JOHAN HJORT	30/8/1964	65.52	4	0.6554
WOD01_58000093	60	NORWAY	JOHAN HJORT	24/8/1961	60.07	3	0.5862
WOD01_58000093	61	NORWAY	JOHAN HJORT	27/8/1961	61.40	3	0.8296
WOD01_58000093	62	NORWAY	JOHAN HJORT	4/9/1961	65.51	3	0.4106
WOD01_58000094	63	NORWAY	JOHAN HJORT	15/8/1962	61.41	3	1.5353
WOD01_58000094	64	NORWAY	JOHAN HJORT	16/8/1962	60.05	3	1.0696
WOD01_58000094	65	NORWAY	JOHAN HJORT	23/8/1962	65.52	4	0.2676
WOD01_58000094	66	NORWAY	JOHAN HJORT	29/8/1962	63.72	3	0.4602
WOD01_58001078	67	NORWAY	POLARIS	14/8/1932	63.30	4	0.8566
WOD01_58001414	68	NORWAY	HEIMLAND I	6/8/1933	60.10	4	0.8926
WOD01_58001466	72	NORWAY	URAN	19/8/1948	60.55	3	0.9177
WOD01_58001480	75	NORWAY	VARDHOLMEN	13/8/1949	60.38	3	0.8503
WOD01_58001480	76	NORWAY	VARDHOLMEN	14/8/1949	61.41	4	0.1956
WOD01_58001727	82	NORWAY	G.O. SARS (LLZG)	8/8/1970	65.47	3	0.3801
I1	0.1	ICELAND	UNKNOWN REF LEID	3/9/1963	67.05	6	0.5101
I2	0.2	ICELAND	UNKNOWN REF LEID	3/9/1963	66.65	5	0.5645
I3	0.3	ICELAND	UNKNOWN REF LEID	11/9/1963	66.66	8	0.6135
I4	0.4	ICELAND	UNKNOWN REF LEID	29/8/1965	66.04	12	0.6469

4.3 Deep Sea Research Paper

DEEP WESTERN BOUNDARY CURRENT DYNAMICS AND ASSOCIATED SEDIMENTATION ON THE EIRIK DRIFT SOUTHERN GREENLAND MARGIN

Sally Hunter [a] (sallyh@noc.soton.ac.uk), David Wilkinson [a], Essyllt Louarn [b], I. Nick McCave [c], Eelco Rohling [a], Dorrik A.V. Stow [a] and Sheldon Bacon [a]

[a] National Oceanography Centre, Southampton, University of Southampton Waterfront Campus, European Way, Southampton SO14 3ZH, UK

[b] Laboratoire de Chimie Marine, UMR CNRS 7144 Roscoff & Institut Universitaire Europeén de la Mer/UBO, Place Nicolas Copernie, 29280 Plouzane, France

[c] Department of Earth Sciences, University of Cambridge, Downing Street, Cambridge, CB2 3EQ, UK

Published in Deep Sea Research Part 1, 11/09/07

Deep Sea Research I 54 (2007) 2036-2066

DSR Abstract

Growing interest in the dynamics and temporal variability of the deep western boundary current (DWBC) in the northern North Atlantic has led to numerous studies of the modern hydrography and palaeoceanography of this current system. The DWBC is fed by the two dense water-masses that spill over the Greenland-Iceland-Scotland Ridge; Denmark Strait Overflow Water (DSOW) and Iceland Scotland Overflow Water (ISOW). These overflows entrain ambient water masses, primarily Labrador Sea Water (LSW), as they cross the Iceland and Irminger Basins before merging in the vicinity of south-east Greenland. A number of studies have been performed around the Eirik Drift, located off the southern Greenland margin, downstream of this main merging point. However, the relationship between the DWBC and the associated sedimentation at this location has yet to be fully elucidated. New hydrographic data show that the current's main sediment load is carried by only one of its components, the DSOW. Seismic surveys and sediment cores confirm that Holocene sedimentation is limited to areas underlying the most offshore part of the current, where the hydrographic data show the highest concentration of DSOW. Active sedimentation through the Holocene therefore appears to have been controlled by proximity to the sediment-laden DSOW.

Our interpretation of new and historic geostrophic transport and tracer data from transects around the southern Greenland margin also suggests that the DWBC undergoes significant growth through entrainment as it flows around the Eirik Drift. We attribute this to multiple strands of ISOW following different depth-dependent pathways between exiting the Charlie Gibbs Fracture Zone and joining the DWBC. Comparison of our new data with other modern hydrographic datasets reveals significant temporal variability in the DWBC, associated with variations in the position, structure and age since ventilation of the current in the vicinity of Eirik Drift. The complexity of the current dynamics in this area has implications for the interpretation of hydrographic and palaeoceanographic data.

DSR 1. Introduction

The North Atlantic is separated from the Nordic Seas by the Greenland-Iceland-Scotland (GIS) Ridge. The ridge plays a prominent role in shaping the ocean circulation of the region as it only allows waters down to intermediate depths to be exchanged between the two areas. The densest of these waters spilling south over the ridge are known as the overflow waters. Two key overflow waters, with distinctly different temperature and salinity characteristics cross the GIS Ridge to the west and east of Iceland; the Denmark Strait Overflow Water (DSOW) and Iceland Scotland Overflow Water (ISOW). Having crossed the GIS Ridge the overflow waters descend rapidly, following bathymetrically controlled pathways on route to their primary meeting point in the deep western boundary current (DWBC) off southeast Greenland, where this current is commonly referred to in the geological literature as the Western Boundary Undercurrent (see Figure DSR1).

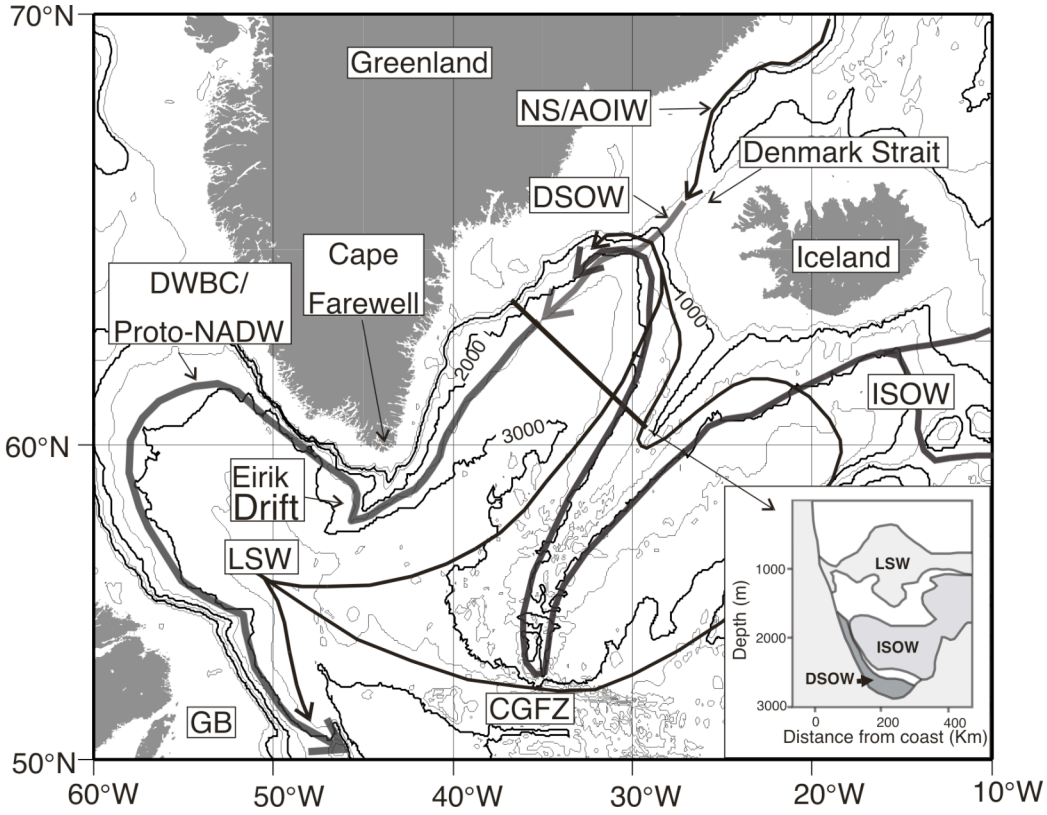

Figure DSR1. Pathways of the main deep and intermediate water masses contributing to the DWBC. NS/AOIW – Norwegian Sea/Arctic Ocean Intermediate Water; DSOW – Denmark Strait Overflow Water; ISOW – Iceland Scotland Overflow Water; LDW – Labrador Sea Water. GB – Grand Banks; CGFZ – Charile Gibbs Fracture Zone. Inset from *Dickson and Brown (1994)*.

During their journey through the Iceland and Irminger Basins the overflow waters entrain a combination of Labrador Sea Water (LSW) and modified Antarctic Bottom Water (known as Lower Deep Water - LDW). On reaching the Eirik Drift off the southern Greenland margin, the DWBC carries a combination of DSOW, ISOW, LSW and LDW that represents nearly mature (or proto) North Atlantic Deep Water (NADW). NADW is normally considered fully formed when the DWBC reaches the Grand Banks of Newfoundland after further additions of LSW, LDW and ISOW in the Labrador Basin. The DWBC off Cape Farewell, however, constitutes the major input to NADW. This input has been referred to as lower North Atlantic Deep Water (lNADW) in a growing number of modern physical oceanographic texts *(e.g. Tanhua et al. 2005)*.

NADW spreads across the world's ocean floors forming one of the dominant constituents of the lower limb of the global thermohaline circulation system (THC). The associated, density driven, component of the near-surface flow in the North Atlantic is responsible for significant poleward transport of heat, which helps to maintain the relatively moderate European climate *[Ganachaud and Wunsch 2000; Seager et al. 2002]*.

As research over the last few decades has increasingly focused on the role of the THC in shaping global climate *[e.g. Broecker 1991; 2000; Rahmstorf 2000; Millwood et al. 2002]* , there has been a growing interest in the mechanisms governing the rate of NADW formation and hence DWBC flux. The flux of the DWBC is known to have varied on time scales ranging from days *[Clarke 1984]* to millennia *[Bianchi and McCave 1999]* , with the longer term variations thought to be intimately linked to climate-change events *[e.g. Chamberlin 1906; Broecker et al. 1985; Broecker 2000; Rahmstorf 2002]* .

The Eirik Ridge was first recognised as being constructed by deep currents, i.e. a sediment drift, by the group at Lamont Observatory in the late 1960s *[Johnson and Schneider 1969; Jones et al. 1970]* . The Eirik Drift contains an expanded sedimentary section, with sedimentation rates over 30 cm ka^{-1} in places *[e.g. Hillaire-Marcel et al. 1994]* making it suitable for high-resolution (decadal to millennial scale) studies of the current's variability. However, despite its importance

as a record of DWBC variability, relatively little is known about the detailed relationship between current activity and sedimentation on the drift.

The aim of this investigation is to use a combination of geological and hydrographic techniques to determine the detailed water mass and velocity structure of the DWBC at the Eirik Drift and to determine the relationship between these features and the patterns of Holocene sedimentation. The results improve our understanding of DWBC activity at this important location, and so allow more informed interpretation of its sedimentary record.

DSR 2. Present Day Oceanographic Setting

Clarke (1984) identified the DWBC in the Cape Farewell-Eirik Drift region as a bottom-intensified current that resides between the 1900 m and 3000 m isobaths towards the foot of the continental slope. The DWBC transport is commonly accepted to be about 13-14 Sv (1 Sv = 1 x 10^6 m^3/s); for example, *Dickson and Brown (1994)* quote 13.3 Sv for the flow below the σ_0 = 27.80 kg m^{-3} isopycnal. Although this figure is often cited, it is based largely on a single dataset collected in 1978 by the *RV Hudson [Clarke, 1984]*. *Bacon (1997)* calculates a much lower value of 6 Sv from data collected in 1991 by the *RRS Charles Darwin,* and *Bacon (1998)* argues that a comparison of data collected between 1958 and 1997 illustrates a significant decadal variability of the DWBC due to changes in the output from the Nordic Seas.

Dickson et al. (1999) found that the relative warming of the subsurface waters of the West Spitsbergen Current during the winter of 1996-1997 resulted in a thinning and slowing of the DWBC in its lower reaches. They demonstrated that the extreme warmth of the overflow causing it to run higher on the continental slope off east Greenland could be reproduced in a numerical model that gave an upslope movement of the current core of between 15 and 20 km. Combining this result with the decadal variability inferred by *Bacon (1998)*, it is clear that there is a high probability of significant inter-annual changes in the structure and position of the axis of maximum velocity of the DWBC.

DSR 2.1 Deep Western Boundary Current Water Masses

Currently accepted values for DWBC water mass characteristics in the vicinity of southern Greenland are summarised in Table DSR1.

	Potential Temperature	**Salinity**	**Potential Density***	**Other**
DSOW	<1.5	~34.9	>27. 88	High O_2
ISOW – Irminger Basin	1.8 – 3.5	~34.96 – 35.05	σ_2 36.95 – 37.05	Low O_2
ISOW – Near overflows	~ -0.5	~34.92	~28.07	High O_2
LSW	~3 - 4	34.85	27.74-27.80	Low potl. vorticity
AABW	~2		σ_4 46	Low O_2 - High Si
NADW	2 – 3.5	34.88 – 34.98	>27.80	

Table DSR1. Typical water-mass characteristics for the components of the DWBC. (Swift 1984; McCartney 1992; Dickson and Brown 1994).
* Referenced to surface (σ_0) unless otherwise stated.
σ_2 = referenced to a depth of 2000 m and σ_4 = referenced to a depth of 4000 m.

Denmark Strait Overflow Water (DSOW)

Denmark Strait Overflow Water is composed of Nordic Sea intermediate waters that cross the Denmark Strait sill and then descend rapidly, entraining ambient waters, primarily LSW *[Rudels et al., 2002]* . The resultant modified DSOW is identifiable as the lower layer of the DWBC off Cape Farewell. The transport of DSOW across the sill and into the DWBC is estimated to be 2.9 Sv *[Dickson and Brown, 1994]* , growing to around 10 Sv through entrainment along its route to Cape Farewell.

Iceland Scotland Overflow Water (ISOW)

Iceland Scotland Overflow Water is also composed of Nordic Sea intermediate waters, but with a significant component of Norwegian Sea Deep Water due to the deeper sills in the Iceland-Scotland Ridge to the east of Iceland. *Dickson and Brown (1994)* estimate the total overflow of ISOW to be about 2.7 Sv, of which 1.7 Sv flows through the Faeroe Bank Channel. The remainder of the overflow occurs via a series of five smaller channels between Iceland and the Faeroe Islands. The density of ISOW is reduced by entrainment of ambient waters as it travels around the Reykjanes Ridge and into the Irminger Sea via the Charlie Gibbs Fracture Zone

(CGFZ), such that it forms the upper layer of the DWBC at a depth of around 2000 m. The contribution of this modified ISOW to the DWBC off Cape Farewell is estimated at between 2 and 3 Sv *[Dickson and Brown, 1994; Schmitz, 1996]* .

Labrador Sea Water (LSW)

Labrador Sea Water is formed by wintertime deep convection in the Labrador and Irminger Seas. As the name suggests, it was originally thought to be formed solely in the Labrador Sea, but more recent work has concluded that a second formation site exists in the Irminger Sea *[Bacon et al. 2003; Pickart et al. 2003]* . LSW spreads across the North Atlantic and populates the low velocity layer between about 700 m and 1500 m off the east coast of Greenland. LSW contributes a significant proportion of the DWBC because of entrainment with the two types of overflow water. *Dickson and Brown (1994)* estimate the contribution of LSW to the DWBC at around 4 Sv off Cape Farewell, though inverse modeling has produced a figure as high as 8 Sv *[Alvarez et al., 2004]* . This difference could be due to the high inter-annual variability in the production of LSW *[Lazier et al., 2002)*, which model studies suggest may influence DWBC strength with a lag of 2 to 3 years [Eden and Willebrand, 2001] .

Lower Deep Water (LDW)/Antarctic Bottom Water (AABW)

Antarctic Bottom Water spreads north from its point of formation in the Antarctic and after modification joins the southward flowing DWBC at various points in the North Atlantic. In its modified North Atlantic form, it is nowadays properly referred to as Lower Deep Water (LDW) *[McCartney, 1992]*. It is estimated that 1-2 Sv of LDW joins the DWBC off Greenland *[Schmitz and McCartney 1993; Schmitz 1996]*, with a further 2 Sv thought to be entrained along the path of the DWBC around Newfoundland and Florida.

DSR 3. Geological Setting and Drift Morphology

Significant drift building began off the southern Greenland Margin in the Early Pliocene (~4.5Ma) linked to intensification in the flow of northern sourced bottom waters, which had begun overflowing from the Denmark Strait in the Late Miocene *[Arthur et al., 1989]* . Active drift construction during the Pliocene was followed by more aggradational sedimentation in the Pleistocene as bottom currents weakened *[Arthur et al., 1989]*. The drift is now generally considered to largely be a relict feature *[Hiscott et al., 1989]* , but thick Holocene sediments do occur at the drift toe *[Hillaire-Marcel et al., 1994]* .

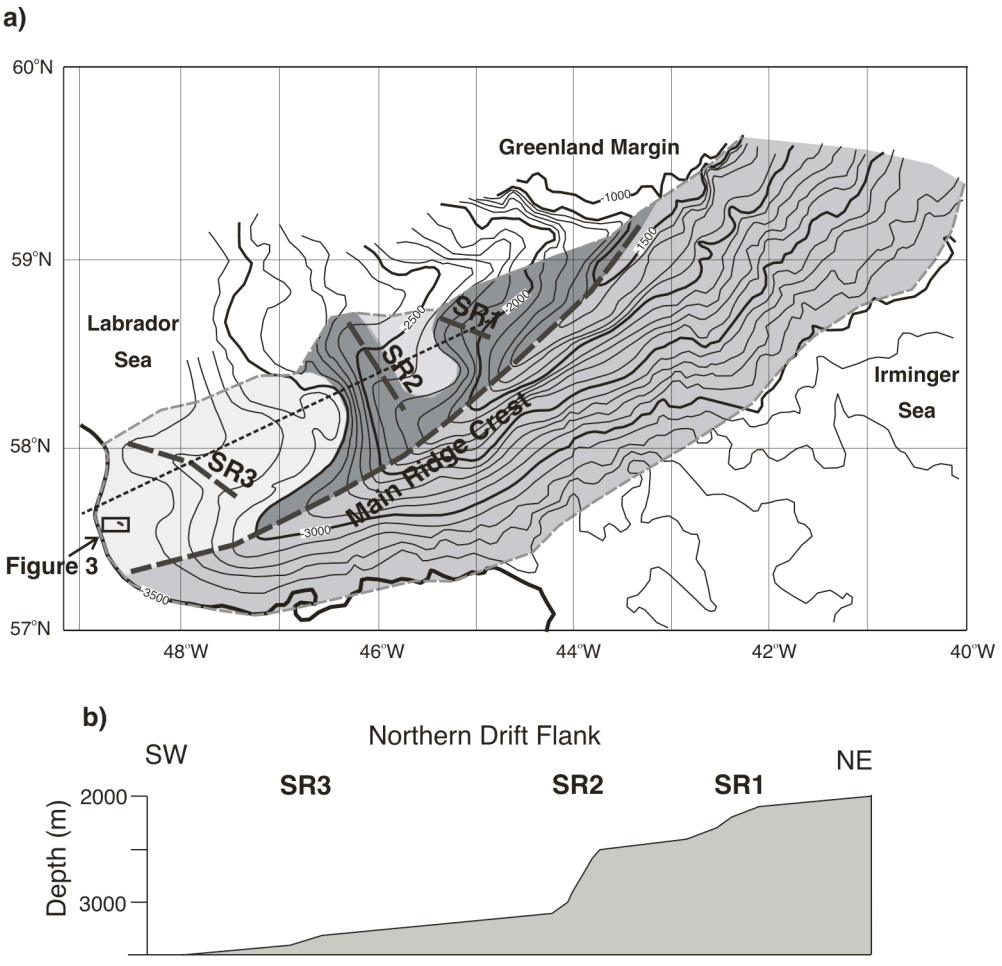

Figure DSR2 (a) Bathymetric map of the Eirik Drift with the main ridge crest and secondary ridge crests (numbered SR1-3) indicated (Modified from Hunter *et al.* 2007). For the northern drift flank, darker shading indicates areas of steeper slope. (b) Schematic cross-section of the northern drift flank (section line indicated on 2a) showing the relative magnitudes of the secondary ridges.

The morphology of the drift is strongly influenced by basement structure *[Hillaire-Marcel et al., 1994; Hunter et al., 2007]*. The drift extends obliquely from the Greenland margin with the crest deepening from 1500 m in the north, adjacent to the margin, to around 3400 m at the drift toe, some 360 km to the southwest (Figure 2a). The southern flank of the drift lies below the southwest-flowing limb of the DWBC in the Irminger Sea and is characterised by a relatively steep and regular slope of around 1.3° that follows basement topography. The northern drift flank and drift crest display marked changes in slope, with variations between 0.3° and 1.5° defining three secondary ridges (Figure 2a and b), which extend to the northwest from the main drift crest and underlie the DWBC as it flows northwest into the Labrador Sea. These secondary ridges approximately overlie basement highs, which are postulated to have controlled their original development *[Hunter et al. 2007]* .

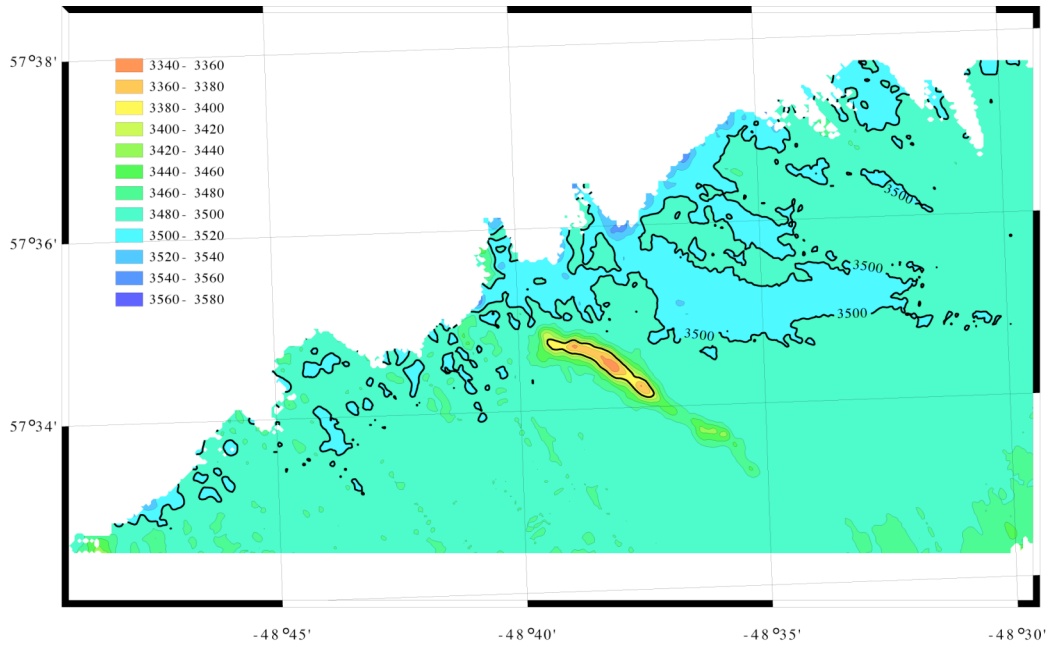

Figure DSR3. Swath bathymetric map of the southern of the two newly discovered seamounts. Location shown on Figure 2.

The deepwater drift toe between around 3000 m and 3500 m displays a marked decrease in the angle of slope from the southern to northern drift flank (shown by the increase in bathymetric contour spacing from south to north in Figure 2a). A number of local topographic variations occur within this area including two newly discovered seamounts (located at 57°34.5`N 48°38`W and 58°31.5`N

48°27`W). Swath bathymetry shows the southern seamount to be an elongate feature trending NW-SE with steep sides and a maximum elevation of around 140 m above the surrounding sea floor (Figure 3). The seamounts are associated with shallow moats, presumably related to local current intensification, and are assumed to represent basement highs similar to those seen in regional seismic sections *[e.g. Srivastava et al. 1989]*.

DSR 4. Hydrography of the Cape Farewell-Eirik Drift Region

DSR 4.1 Hydrographic Data

Our interpretation of the present-day physical oceanography of the Cape Farewell region is based upon two hydrographic datasets. The primary dataset is a series of new data collected between the 1st and 17th of September 2005 by *RRS Discovery* cruise D298 *[Bacon, 2006]* . The D298 data provide five hydrographic sections around and over the Eirik Drift (Figure 4a). These sections (referred to as D1-D5 throughout this text) provide high resolution temperature and salinity data, allowing the construction of detailed geostrophic current cross-sections. In combination with oxygen concentration (to give an indication of age since ventilation), light transmittance (providing an estimate of fine grained sediment load) and silicate concentration (to track the pathways and admixtures of LDW), the geostrophic velocity cross-sections offer a deeper understanding of the current dynamics in the region.

The second data set consists of historical data from the World Ocean Database (WOD) [*Conkright et al. 2002*] . Thirteen sections (referred to as H1-H13 throughout this text) were selected from the WOD that could provide high-resolution temperature and salinity sections in the vicinity of Cape Farwell. Some of these sections also provided oxygen concentration data, but unfortunately there are no transmittance data and only limited silicate concentration data on the WOD. The cruises that provided the historical data are listed in Table 2, and the locations of the transects are shown on Figure 4a.

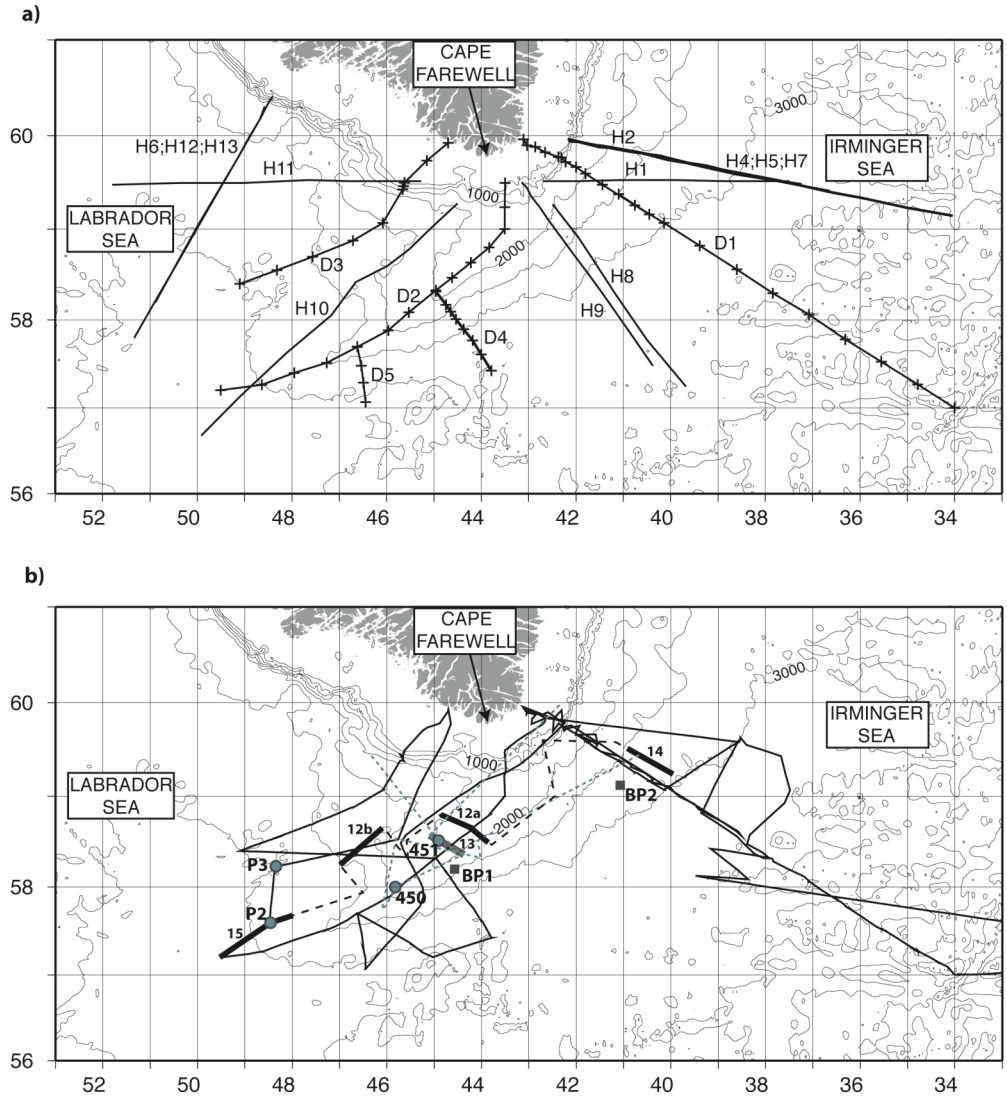

Figure DSR4. a) Location of hydrographic data. The D298 and WOD hydrographic sections are numbered as outlined in the text. For the D298 sections, the crosses indicate the positions of the CTD stations. b) Location of geological and geophysical data. Profiler lines from cruise D298 are shown by the solid black lines, from CD159 by the dashed black lines and from TTR-13 by the dashed grey lines. The position of sidescan sonar line makat-86 (Figure 13) is indicated by the solid grey line. Cores TTR13-450 and TTR13-451, D298-P2 and D298-P3 are labelled 450, 451, P2 and P3 respectively. The locations of Figures 12, 14 and 15 are indicated in black along with the positions of the bottom photographs (BP1 and BP2) shown in these figures (from *Rabinowitz and Eittreim, 1974*).

Reference	Date	Country	Ship	WOD Cruise ID
H1	Mar/Apr 1962	USA	Erika Dan	WOD01_31000170
H2	Nov 1994	UK	Charles Darwin	WOD01_74009777
H3	Sep 1991	Germany	Meteor	WOD01_06009866
H4	Sep 1992	Germany	Valdivia	WOD01_06009201
H5	Nov 1994	Germany	Meteor	WOD01_06009630
H6	Jun 1995	Germany	Valdivia	WOD01_06009881
H7	Aug 1996	Germany	Valdivia	WOD01_06009883
H8	Nov 1994	UK	Charles Darwin	WOD01_74009777
H9	Nov 1996	USA	Knorr	WOD01_31014521
H10	Feb 1962	USA	Erika Dan	WOD01_31000170
H11	Mar 1962	USA	Erika Dan	WOD01_31000170
H12	May 1994	Canada	Hudson	WOD01_18012901
H13	May 1997	Canada	Hudson	WOD01_18012902

Table DSR2 Source of World Ocean Database historic sections

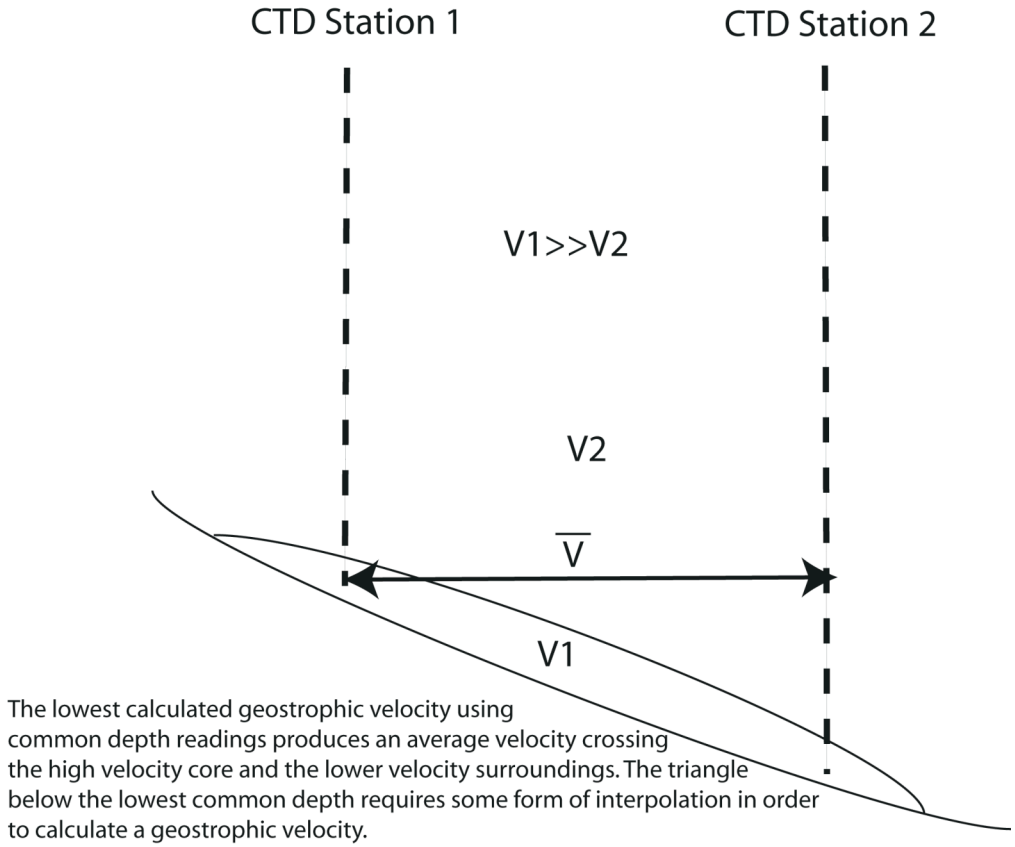

Figure DSR5. Schematic demonstration of the problems associated with the calculation of geostrophic current velocities for a bottom-intensified current on a sloping bottom.

DSR 4.2 Hydrographic Methods

To understand the relationship between the DWBC and sedimentation patterns requires a detailed understanding of the current's velocity structure both in cross-section and as it travels around the Eirik Drift. However, the use of CTD data to calculate geostrophic velocities in the DWBC presents a number of challenges. Firstly, there are the standard problems of determining a reference velocity and the absence of information on the component of the current parallel to the section. The fact that the DWBC is a bottom-following current of around 500 m in thickness *[Clarke, 1984]* lying above a sloping sea floor creates additional problems. The standard geostrophic calculation produces an inter-station average along a level surface and the typical station separation (~10 km) will result in this averaging effect covering sections of the water column that are both inside and outside the main current (Figure 5).

Despite the above drawbacks, the calculation of geostrophic velocity shears still provides the best method for determining the structure of the DWBC from the available data in this region. The geostrophic approach also has the advantage over direct current measurement that there is an inherent degree of spatial and temporal averaging.

Within the area of the DWBC, water temperature, salinity and velocity typically vary as a function of distance above the bottom rather than depth. *Clarke (1984)* used this feature to calculate velocities and transports in the bottom triangle between two stations created by the sloping bottom. We have employed the same technique to calculate bottom triangle velocities and to improve the horizontal interpolation of the data. All water-mass tracers were linearly interpolated onto a 2 km grid along lines of equal height above the seabed for the lower 600 m of the water column. This seafloor following grid was then spliced to a standard horizontally interpolated grid for the upper section of the water column. This simulates high-resolution data to create more realistic contour plots as well as temperature and salinity grids for the calculation of geostrophic velocities.

The method chosen to extrapolate data into the bottom triangles has been shown to be of significance when calculating transports for bottom intensified currents flowing across a sloping bottom *[e.g. Fiadeiro and Veronis 1983]* . In the case of the D298 sections, the bottom triangles contribute between 25% and 30% of the total cross-section transport. Our methodology produces values that are intermediate to those produced by taking a constant velocity and a constant vertical shear from the lowest common depth between station pairs. In line with the observations of *Fiadeiro and Veronis (1983)* our values lie much closer to those using a constant velocity, being 0.2 to 0.5 Sv higher. For the purposes of this paper we are primarily interested in spatial transport patterns employing a consistent and reasonable approach to the transport calculation. We therefore believe that, in this case, the uncertainties due to the extrapolation methodology are immaterial.

In order to calculate DWBC transports it is first necessary to select a reference velocity. In the absence of any direct current measurement data it is usual to set a level of no motion somewhere between 1000 m *[e.g. Bacon, 1998]* and 1500 m *[e.g. Clarke, 1984]*. Although historical current meter data from the region suggest that the mid-depth velocity minimum is not zero *[Clarke, 1984]*, the accepted range of values for the DWBC transport constrains the velocity to be no more than a few cm sec^{-1}. The maximum potential reference level offset is small in comparison with the near bottom velocities, of around 20 cm sec^{-1}, obtained by depth integration of the baroroclinic shears. Therefore the uncertainty in the reference level does not significantly impact on our use of this method to determine the location and structure of the current. In the absence of direct current measurement data we have selected 1500 m as a level of no motion based upon the shear structure seen in the data.

The second decision required in the calculation of DWBC transports concerns the proportion of the water column we attribute to the DWBC. Other authors have typically taken the transport below a particular potential density surface (e.g. σ_0=27.8 kg m^{-3} - *Bacon, 1998*). The work by *Dickson et al. (1999)*, which demonstrates the inter-annual variability in the temperature and density of the current, raises questions over this approach when results from different years are compared. We have therefore chosen the simpler approach of attributing all

transport below the level of no motion to the DWBC. Again the inferences we make are not particularly sensitive to this decision, and our aim is to combine reasonable transport estimates with tracer and sedimentation data in order to develop a coherent picture of current and sedimentation dynamics in the region.

Light transmittance data acquired during *RRS Discovery* cruise D298 have been used to identify variations in turbidity within the water column in order to assess the distribution of sediment load. The principles behind the formation and identification of turbid bottom nepheloid layers are not discussed in detail here, but see *McCave (2003)* for a review.

The transmittance (T) data were converted to beam attenuation coefficient (c) using the equation:

$$c = (\ln(1/T))/l$$

with path length (l) = 0.25 m

Drift in the transmissometer calibration between stations has been corrected by setting the minimum recorded beam attenuation to 0.37 for each station profile. This approach is reasonable for identifying the signals seen in the DWBC as the magnitude of the variation seen across the current far outweighs the spatial variation that can be expected in the clear water minimum over the area of the survey. The beam attenuation data are not interpreted as a quantitative proxy for suspended particulate matter (SPM) concentrations because of a lack of actual SPM measurements for calibration and the necessity to prescribe the minimum beam attenuation value of 0.37 at each station. The transmittance data do, however, provide an adequate basis for the assessment of the location and structure of nepheloid layers, and for process-based interpretations of their development *[Spinrad and Zaneveld 1982; McCave 1983; Gardner et al. 1985; McCave 2001]* .

Oxygen concentrations measured on cruise D298 and obtained from the WOD were converted to saturations with reference to solubilities calculated according to the temperature and salinity relationships of *Weiss (1970)*.

Samples for silicate analysis were taken at each of the D298 CTD stations at a sub-set of depths chosen to characterize the different water masses. The samples were frozen for the transfer to the Laboratoire de Chimie Marine (Roscoff), where they were analyzed on a Bran & Luebbe AutoAnalyzer II.

DSR 4.3 Interpretation Of D298 Water Mass Tracers & Current Profiles

The DWBC is marked in all five D298 sections by a near-bottom reduction in temperature and salinity. The relatively young DSOW is further differentiated by an increase in oxygen saturation in comparison with the ISOW and LSW above. The current extends out slightly beyond the centre of the Irminger Basin in section D1 (ca. 270 km along the section) and then deepens with the bathymetry as it passes around the Eirik Drift. The current was seen to reach further into the basin than expected on sections D2 to D5, extending beyond the most offshore station in each case. Closer inspection reveals a number of more detailed features.

The velocity plots (Figure 6a) show the core of the current to be situated towards the bottom of the slope with a lower velocity tail extending out into the abyssal plains. Sections D1 and D2 show the possible presence of a separate current strand at a bottom depth of around 2000 m. This is a feature that is more prevalent in the historic sections and could be indicative of a separate ISOW pathway. This is discussed further in section 5.2.

The quantitative interpretation of the calculated geostrophic velocities and transports (Table 3) requires some care, as they do not represent total transports or actual maximum velocities. Subject to the normal caveats on geostrophic equilibrium and reference level, the transports represent the total baroclinic flow provided that the sections cross the entire width of the current. The calculated

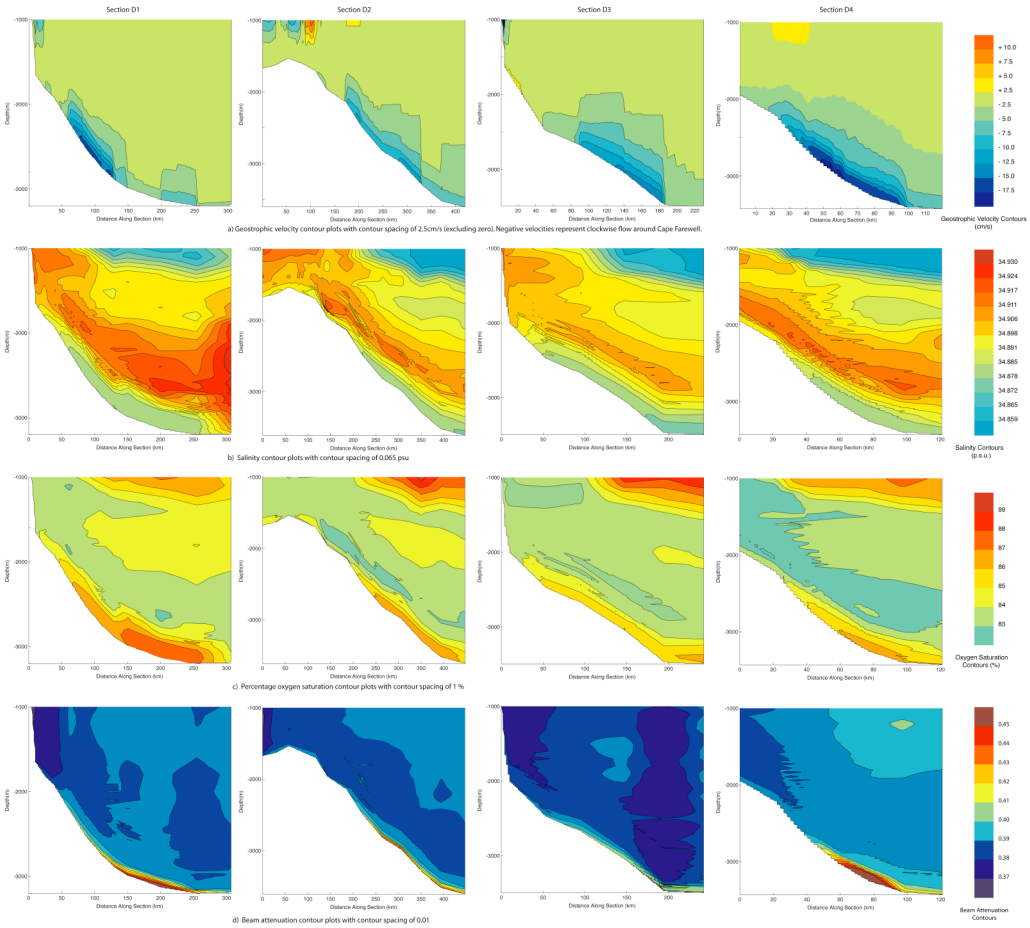

Figure DSR6 Geostrophic velocity and water property contour plots for the D298 sections. a) Geostrophic velocity contour plots with contour spacing of 2.5 cm s^{-1} (excluding zero). Negative velocities represent clockwise flow around Cape Farewell. b) Salinity contour plots with contour spacing of 0.065 c) Percentage oxygen saturation contour plots with contour spacing of 1%. d) Beam attenuation contour plots with contour spacing of 0.01 m^{-1}.

Section	Baroclinic Transport Below 1500m (Sv)	Maximum Velocity Below 1500m (cm/s)	Maximum Station Depth (m)
D1	5.7	17	3202
D2	10.0	12	3614
D3	8.3	14	3498
D4	6.8*	23	3435
D5	9.0*	22	3563

Table DSR3 Summary results from D298 geostrophic velocity calculations

maximum current speed, however, is affected by the angle at which the section crosses the current and will be underestimated by a factor of the sine of this angle. This in particular affects the maximum velocity seen in section D2 (12 cm s^{-1}). Maximum current velocities in the perpendicular sections D4 and D5 (23 and 22 cm s^{-1} respectively) are greater than those in D2 by a factor of at least 2. This suggests that section D2 is at a low angle to the current relative to sections D4 and D5.

The D298 data, collected over a period of less than three weeks, show significant variability in the transport. This variability could be due to short-term temporal variability in the actual DWBC transport, geographic or temporal variability in the reference level current (resulting in a baroclinic variability that is higher than the variability in the true transport) or flow into or out of the current zone between sections. It is likely that all three mechanisms play some role. It is also worth noting that the variation in transports seen between the sections varies in line with the maximum depth to which each section extends. In some cases this is a function of bathymetry (i.e. D1 extends to the maximum depth of the Irminger Basin at this latitude), but in others (D4 and D5) it is in part due to the length of the section being a little short. The latter could explain the relatively low transport calculated for D4 (i.e. the transport is actually higher, but the section was not long enough to capture it all).

The limited direct current measurement data that are available do show high short-term temporal variability at a single location. For example, mooring data for the DWBC off Cape Farewell collected in early 1978 *[Clarke, 1984]* show 100% variability in mean current speeds for consecutive seven-day periods. It is therefore possible that the variability we have observed in baroclinic transport (Table 3) is due entirely to temporal variations in the actual DWBC transport. We should also consider that the very location-specific nature of current meters could produce temporal variability in their records that is removed by the spatial averaging effect of the geostrophic calculation. The interannual movements in the current position observed by *Dickson et al. (1999)*, if repeated over much shorter time periods, could produce much greater variability in current-meter records than is actually present in the DWBC transport. This type of variability may be a common feature of the

DWBC as it was demonstrated farther downstream in HEBBLE by *Hollister and McCave (1984)* and *Gross and Williams (1991)*.

Alternatively, small variations in the reference level velocity could offset the observed baroclinic transport variability. The low baroclinic transport calculated for section D1 (Table 3) could suggest a higher reference velocity at 1500 m on the entry to the drift, whereas the 10 Sv calculated for section D2 may suggest little or no barotropic component. The *Dickson and Brown (1994)* DWBC transport of 13.3 Sv is relatively high in comparison to the baroclinic transports we have calculated and those of *Bacon (1998)*; however, to bring the transport in section D1 to a similar level only requires a reference level velocity of 3.8 cm s^{-1} (assuming the DWBC is 200 km wide and on average 1000 m in vertical extent).

More interestingly water-mass tracer data suggest that at least part of the observed geographic variation in baroclinic transport results from the entrainment of additional water masses on the entry to the Eirik Drift (between sections D1 and D2/D4/D5). This is discussed in more detail in the following paragraphs.

The water-property contour plots show a clear relationship between high oxygen saturation, low salinity and high beam attenuation within the core of the DWBC in all five D298 sections (Figure 6b-d). The beam attenuation data define a distinct bottom nepheloid layer that is around 300 m thick and most strongly developed where the sea floor drops below 2800 m (Figure 6d). Cross-plotting the salinity and oxygen saturation data for the interval of the DWBC with the beam attenuation shown by colour (Figure 7a) confirms this relationship without any influence from the interpolation and contouring routines employed in creating Figure 6. The oxygen saturation high within the DWBC, seen near the base of the continental slope in each section, can be interpreted as the zone of purest or youngest DSOW, as this has a shorter travel time from the point of surface contact than ISOW *[e.g. Smith et al. 2005]* . This is supported by the lower salinity, consistent with DSOW. The higher beam attenuation values in waters of high oxygen saturation and low salinity imply that DSOW is carrying a higher load of the fine sediment (to which the transmissometer is sensitive) than the other water masses within the DWBC. Comparing beam attenuation and velocity sections (Figure 6d and a) it appears that

the area of highest sediment load does not coincide with the area of highest current speeds. This would agree with the earlier observation that sediments along the deep-water eastern margin of Greenland can be traced to sources in east Greenland and are therefore linked to transport by the DSOW *[Innocent et al., 1997]* .

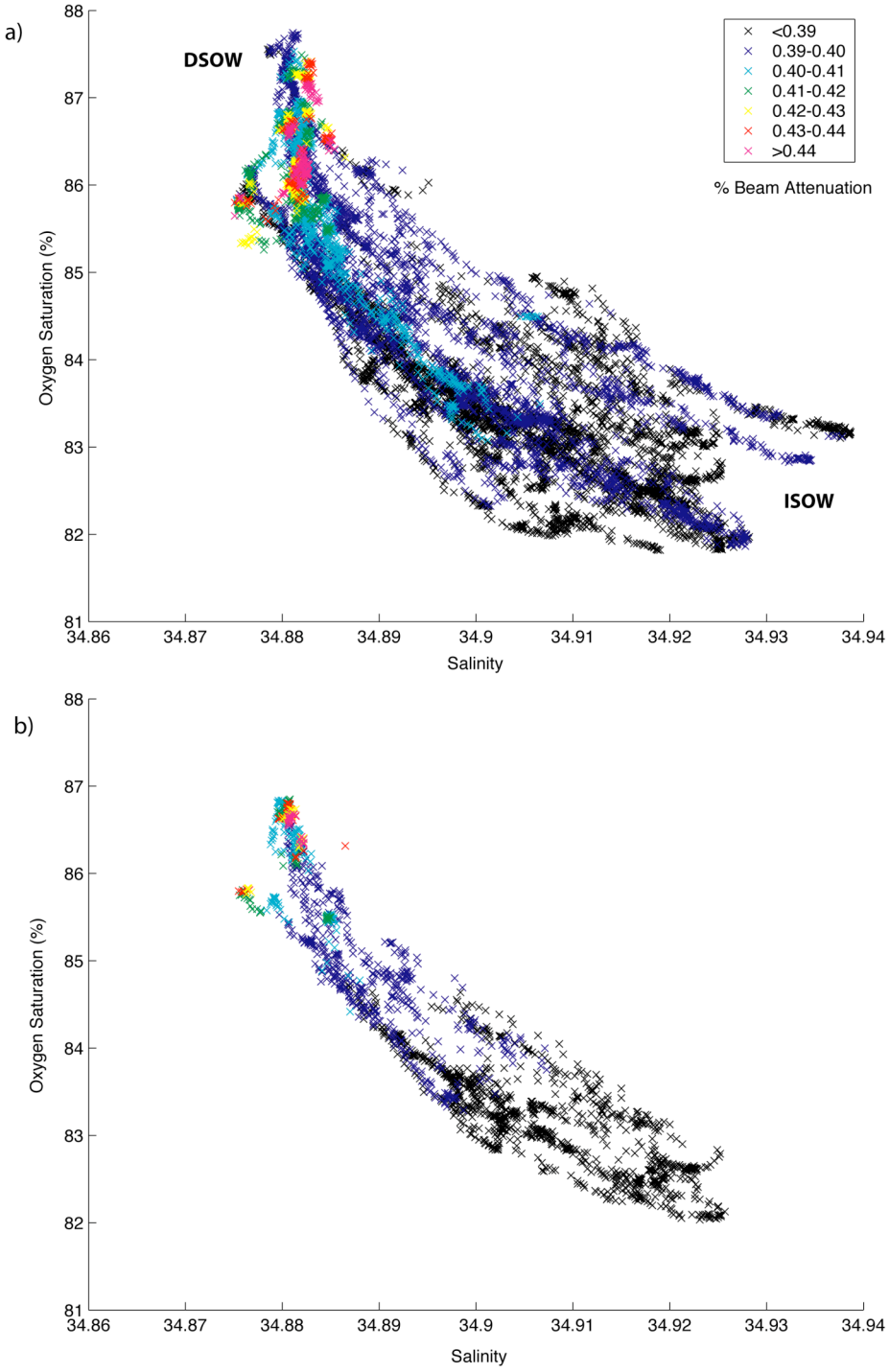

Figure DSR7. Cross-plots of salinity versus oxygen saturation for a) all D298 sections and b) section D2

Our comparison of sections D1 and D2 suggests the addition of new components to the DWBC between these sections. The offshore extent of the DWBC in section D1 is marked by a decrease in oxygen saturation combined with an increase in salinity (Figures 6b and c), which is consistent with the transition from majority DSOW to a higher percentage of older, high-salinity ISOW. Conversely, the offshore end of the DWBC in section D2 shows a decrease in oxygen saturation combined with a decrease in salinity (Figures 6b,c and 7b). Although short-term variability in the salinity of the current cannot be excluded, the appearance, in section D2, of salinities lower than those seen anywhere in section D1 does strongly suggest the addition of a new component.

Two "candidate" water masses of low salinity and reduced oxygen saturation have been previously identified in this area. *Smith et al. (2005)* suggest that there is a component of re-circulating DSOW in the Irminger Basin. This could add a different vintage of DSOW with reduced oxygen saturation and a slightly different salinity to the DWBC in the vicinity of section D2. A re-circulating stream of DSOW lying to the south of section D1, but crossing D2, could also enhance the transport seen at section D2 if the outer arm of the recirculation was in the middle of the Labrador Basin beyond the offshore end of section D2. The second potential low salinity and oxygen saturation source is LDW, which has a substantial AABW component *[McCartney 1992; Dickson et al. 2002; Smith et al. 2005]* . The addition of LDW to the DWBC between sections D1 and D2 could result from the entrainment of LDW that has travelled directly up the western basin of the Atlantic or from a deeper component of ISOW, below about 3200m, that has taken a more direct route across the Irminger Basin, omitting section D1 from its path. *McCartney (1992)* has shown that the proportion of LDW in ISOW increases with depth as shown by increasing silicate concentration in data collected from either side of the Reykjanes Ridge. The elevated silicate concentration signature in LDW, due to its AABW component, provides a good way of tracking its flow.

A cross plot of silicate concentration versus salinity (Figure 8), combined with silicate concentration depth profiles (Figure 9), for the D298 data provides some interesting insights into the movement of AABW in the region. The pattern of data

seen in Figure 8 is consistent with mixing between 3 end members: DSOW with low salinity and low silicate (ca 33.88 and 8 µmol/l), ISOW with high salinity and low silicate concentration (>34.95 and ca 10 µmol/l) and LDW with an intermediate level of salinity but high silicate concentration (ca 34.92 and 17 µmol/l). The lines M1, M2 and M3 are suggested mixing results for combinations of ISOW and DSOW, DSOW and LDW, and ISOW and LDW, respectively.

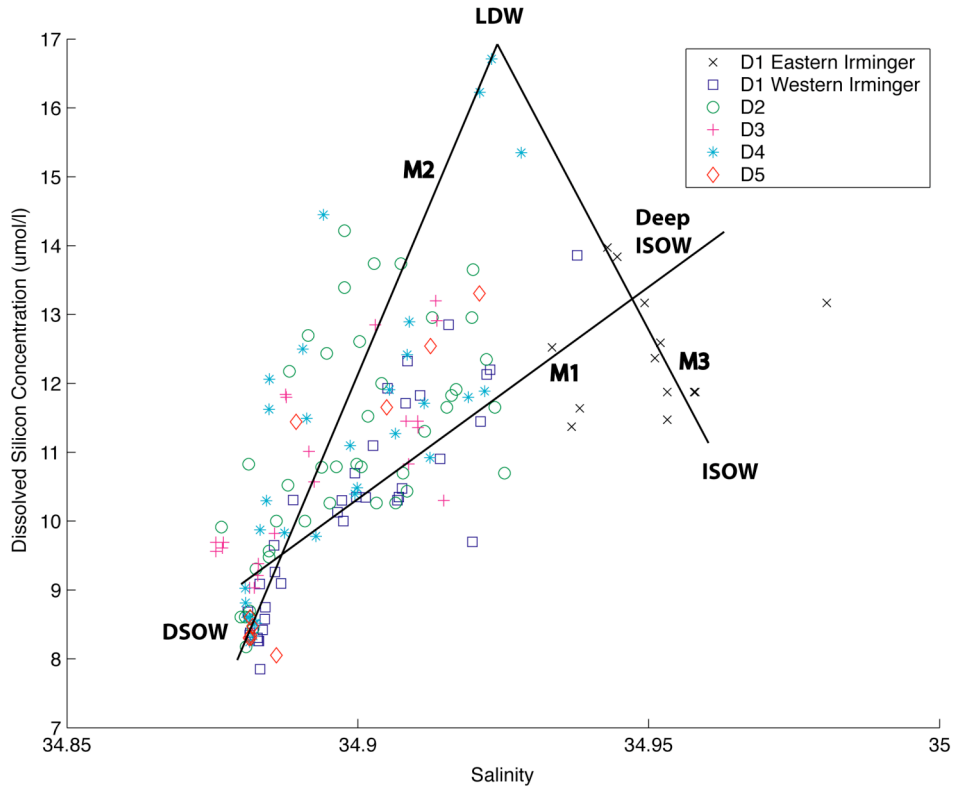

Figure DSR8 Plots of salinity versus silicate concentration for all D298 samples taken within 600 m of the bottom and in water depths of over 1500 m. M1 and M2 represent suggested mixing lines between DSOW and ISOW and between DSOW and Western Basin LDW. M3 represents mixing between ISOW and LDW in the eastern basin of the North Atlantic.

In the eastern Irminger Basin (stations 3 to 5) silicate rich ISOW flows northwards with its proportion of LDW increasing with depth as indicated by the downward increase in silicate concentration and fall in salinity (Figures 8 and 9). The data from these stations define mixing line M3. In the western Irminger Basin, the silicate maximum is displaced upwards by the southward flowing

DSOW (stations 6 to 17 along section D1), and in the region of the main current it is typically 500 to 600 m above the bottom near the upper surface of the main DWBC. Data from stations 6 to 17 lie broadly along mixing line M1 and would therefore suggest mixing between DSOW and the deeper elements of the Irminger current flowing around the Reykjanes Ridge.

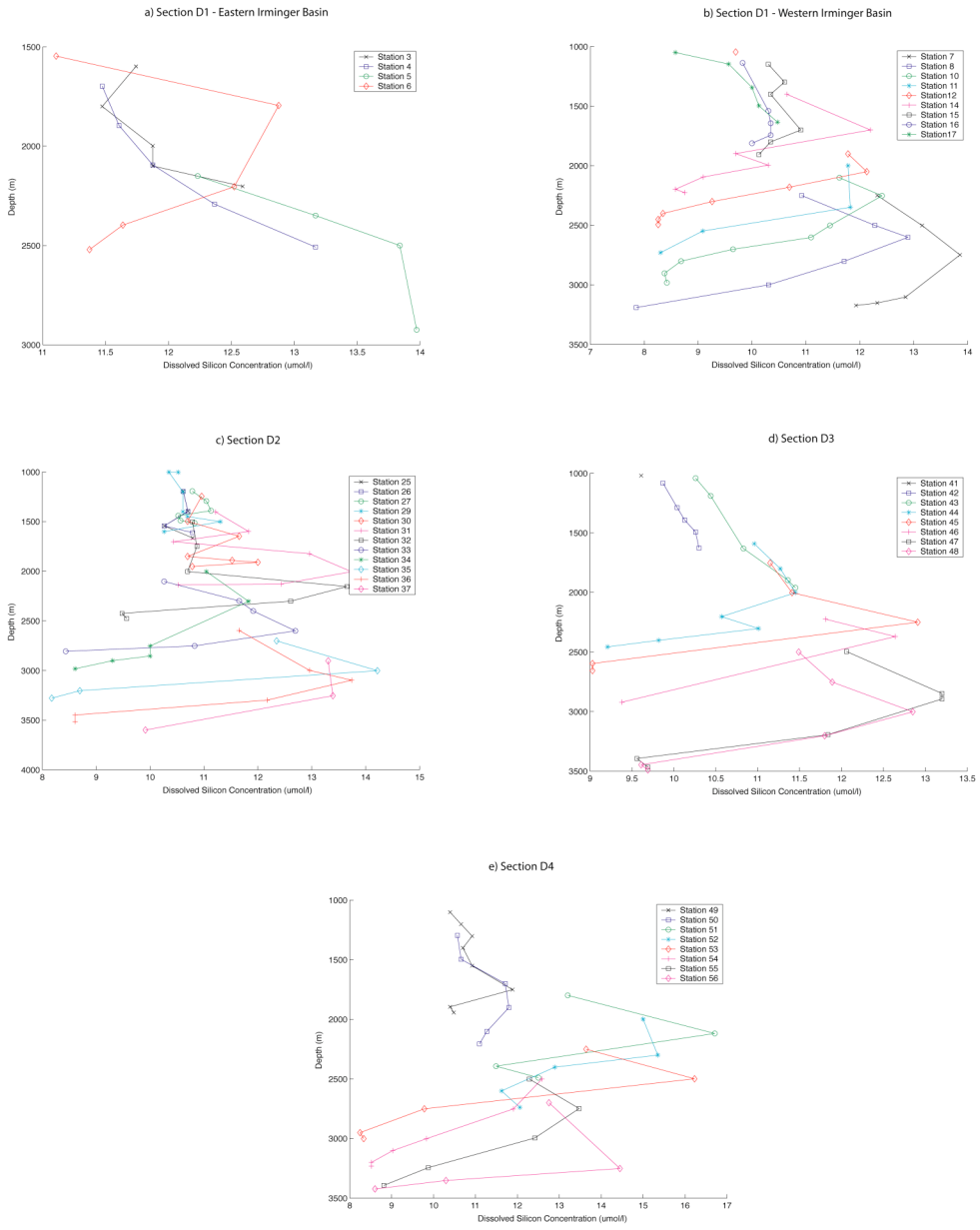

Figure DSR9. Depth profiles of silicate concentration for D298 sections D1 to D4 with section D1 split approximately in the centre of the Irminger Basin. Data are plotted for samples taken within 1000 m of the bottom in depths of over 1000 m.

Following the path of the DWBC around Cape Farewell, the majority of data from sections D2 to D5 appear above mixing line M1, which would support the addition of silicate rich water that was not present anywhere along section D1. Silicate concentrations towards the offshore end of the DWBC in sections D2 and D4 are slightly elevated in comparison with the same part of the current in section D1, whereas a reduction ought to have been expected if there were no additions and continued mixing. Instead, the highest silicate concentrations in the dataset are found in section D4 at the upper edge of the current in water depths of between 2000 and 2500 m. This high silicate concentration zone is seen to continue around Cape Farewell with a slight reduction in values from section D1 to sections D2 and D3.

The silicate data therefore support the concept of entrainment of new water masses between sections D1 and D2 in two areas along the upper surface of the current; one at the foot of the DWBC in water depths of between 3000 and 3500 m, and the other near the upslope end of the current in water depths between 2000 and 2500 m. The first addition would be consistent with the flow of the deepest, most silicate rich component of the ISOW through the CGFZ and across the Irminger Basin at depths greater than 3200 m *[McCartney, 1992]*. However, the intersection of lines M2 and M3 in Figure 8 suggest that, while this may explain the increase in silicate concentration it cannot alone explain the observed reduction in salinity. The second addition, where the highest silicate concentrations were observed, is too high in the water column to be consistent with ISOW exiting the Gibbs Fracture Zone. This agrees with the observations of *McCartney (1992)*, who shows that silicate concentrations of greater than 16 µmol/l carried by ISOW fail to penetrate north-westward through the Irminger Basin. We therefore infer that the second, shallower, region of silicate addition observed in section D2 results from mid-depth spreading in the western basin of an intermediate water mass with a component of Antarctic origin.

4.4 Comparison With Historic Sections From The World Ocean Database

Although the 13 historical sections extracted from the WOD are too few to comment with authority on inter-annual variability in the transport of the DWBC, some interesting comparisons can be made with the calculated D298 transports. Sections

H1, H10 and H11 (1962 bottle data) lie in a similar geographic configuration to sections D1 to D3 (Figure 4a) and were collected over a similarly short period of time. The 1962 results repeat the D298 pattern of low transport at section D1 in the Irminger Basin, with increased transport in the Labrador Basin, and with highest transport over the Eirik Drift (Tables 3 and 4).

Section	*Baroclinic Transport (Sv)*	*DWBC Salinity Minimum*	*Bottom Depth @ DWBC Salinity Minimum (m)*	*DWBC Salinity Maximum*	*Bottom Depth @ DWBC Salinity Maximum (m)*
D1	5.7	34.879	3202	34.939	3190
H1	5.1	34.881	2897	34.954	3106
H2	5.1	34.876	2715	34.939	3185
H3	4.8	34.880	3129	34.945	2861
H4	5.5	34.873	2606	34.943	3114
H5	4.6	34.859	2955	34.936	3130
H6	4.1	34.849	2787	34.934	2985
H7	3.3	34.892	2989	34.928	3097
H8	4.7	34.877	2928	34.934	3239
H9	3.5	34.884	3045	34.929	2765
H10	8.6	34.896	3603	34.950	2213
H11	7.7	34.895	3133	34.938	3354
H12	5.5	34.874	3647	34.911	3419
H13	5.6	34.886	3594	34.911	3511

DSR4 Summary of transport and DWBC water characteristics for the historic sections in comparison with D1.

Although the similarity between these two regional surveys is insufficient to conclusively characterise the spatial and temporal variability, the repeat of the spatial pattern between 1962 and 2005 does hint that temporal variability may not fully explain the increase in transport between the Irminger Basin and the Eirik Drift. It could also lend credence to the suggestion that some of the variability seen in current-meter-based data results from short-term movements in the position of the current. To resolve this issue ideally requires detailed analysis of synchronous, high-resolution mooring, bottom mounted ADCP and CTD data. However, we shall consider the hypothesis that the observed pattern is, to some extent, a regular feature. This would leave an unknown combination of additional entrainment on the entry to the drift area and geographical variation in reference level velocity to explain the increase in transport. Similarly, the reduction in transport between the drift and the Labrador Basin (between transects D2 & D3 and between H10 & H11)

could be due to a combination of reference-level variability and deeper elements of the current crossing the Labrador Basin to the south of sections D3/H11. The drift sections (D2 – 3614 m and H10 – 3750 m) extend to greater depths than their Labrador Sea equivalents (D3 – 3498 m and H11 – 3442 m). As the current is seen to extend beyond the 3500 m isobath on the drift sections, a fall in actual DWBC transport at the Labrador Basin sections is to be expected.

Of the other historical sections, H2 to H7 lie very close to D1 while H8 and H9 reside only slightly further to the south (Figure 4a). These historical sections show baroclinic transports that are similar to that of D1 (3.3 – 5.1 Sv). The two historic Labrador Basin sections (H12 & 13) show slightly higher than average transports but not to the extent of the 1962 and 2005 sections, even though they extend to slightly greater depths (3573 m and 3594 m). These two sections were taken in May 1994 and May 1997, and the closest Irminger Basin section is H5, occupied in November 1994. Therefore, it is not possible to assess how these transports compare with the DWBC transport in the Irminger Basin at the same time.

Moving on to the internal structure of the current, we can see clearer evidence of multiple cores in the historical data than was present in the Discovery data (Figure 10). The presence of multiple cores could be explained by variable isopycnal gradients, eddy formation, topographic Rossby waves, or the propagation of multiple strands from the overflows.

The magnitude and position of the maximum and minimum salinities observed within the current (typically in the lower 500 m of the water column for bottom depths greater than 2000 m but with some adjustment on a case by case basis) offer some insight into the relative contributions of ISOW and DSOW (Table 4). The local salinity maximum within the current is typically found near the top of the flow, close to the 500 m height mark corresponding to the highest concentration of ISOW. The local minimum is typically found within 100 m of

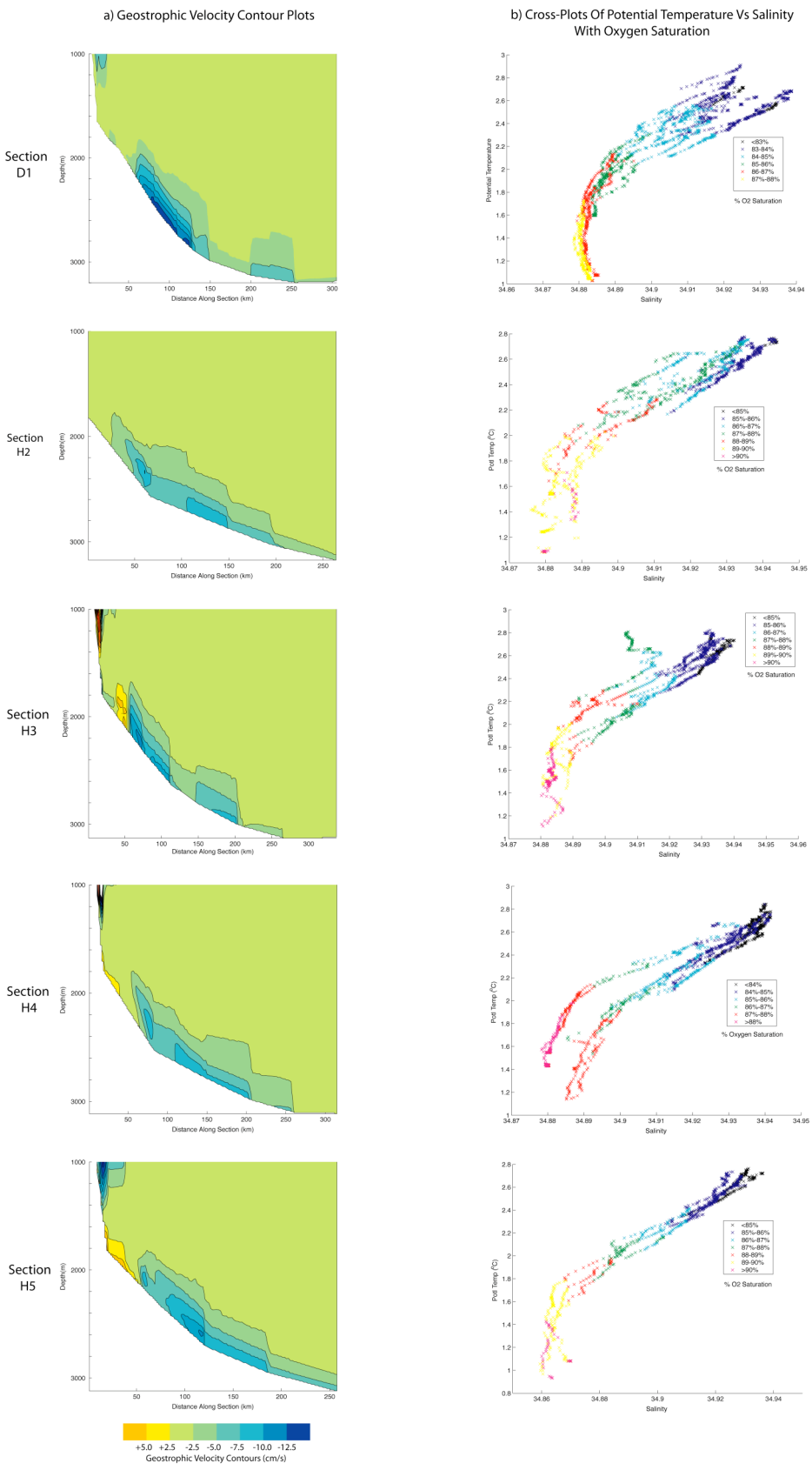

Figure DSR10 Comparison of velocity cross-sections and water-mass characteristics between new and historic sections from the same location in the Irminger Sea.

the bottom in the area of purest DSOW. The position of the salinity minimum on the slope, however, shows some distinct variation.

In the D298 sections, both the salinity minimum and oxygen saturation maximum were found in the slower moving, outer reaches of the current below 3000 m. This appears to be the more typical structure (see Table 4), but section H4 from 1962 provides a distinct contrast, with the salinity minimum much higher up the slope at a bottom depth of 2606 m. A cross-plot of potential temperature versus salinity for this section (Figure 10 – H4) reveals the presence of two mixing lines indicating two distinctly different DSOW end members. The slightly lower salinity branch corresponds to the upper portion of the current with a clearly identifiable separate core. This branch shows higher oxygen saturations, which implies that it has either exited the Denmark Strait more recently, or undergone less mixing with water masses of lower oxygen saturations. The difference in oxygen saturation of about 0.7% between the two branches is similar in magnitude to the range in maximum saturation values between sections D1 and D2 that are separated by about 500 km along the 3000 m isobath, equating to a travel time of about 29 days (with a typical current velocity of 20 cm/s). Even if we allow for some mixing, the observed difference in oxygen saturation between the two strands of the current in section H4 suggests that the age difference between them is of the order of a few months.

The positioning of the younger strand higher up the slope (Figure 10 – H4 b) is the result of its higher temperature and suggests that, in at least this case, the multi-core appearance of the current is the result of strand separation at the overflow. Such a temperature-driven shift across the slope would be consistent with the observations of *Dickson et al. (1999)* but suggests that such variation can occur over much shorter time periods than they may have considered. Figure 10 (H2, H3 and H5) shows cross-plots and velocity sections for the other historic sections for which oxygen saturation data were available on the WOD. Viewed together these present a range of possible scenarios from primarily single-core currents with single ISOW and DSOW end members (D1 & H5), through two DSOW or ISOW end members with only narrow separation resulting in some mixing (H2 & H3), to the clearly separate current strands with two end DSOW end members (H4). These observations support the hypothesis that high short-term velocity variability seen in current meter

records could be driven, in part, by lateral current core movements that do not necessarily have the same impact on overall transport variability.

DSR 5. Holocene Sedimentation on the Eirik Drift

5.1 Geological Data and Methods

The main geological resource used in this study is a collection of 3.5 kHz and 5.1 kHz profiler lines acquired in 2003, 2004 and 2005 (Table 5) along with a sidescan sonar line acquired in 2003. The acoustic character, or echo-character types, observed within the profiler sections have been described following the work of *Damuth (1975; 1980)* and *Jacobi and Hayes (1982)* in order to assess the different sedimentary regimes within the study area.

Cruise	Year	Vessel	Data Type
TTR-13	2003	RV Professor Logachev	5.1 kHz
CD-159	2004	RRS Charles Darwin	3.5 kHz
D298	2005	RRS Discovery	3.5 kHz

DSR5 Sources of 3.5 kHz and 5.1kHz profiler data.

Four main echo-character types were identified based on the characteristics of the seabed echo and on the presence or absence and character of any sub-bottom echoes (Table 6). As discussed by *Bianchi and McCave (2000)*, the temporal resolution of echo-character data is constrained by the vertical resolution of 3.5 kHz data (around 40 cm) and sedimentation rate, with the time interval that can be resolved of the order of 1-10 ka. Profiler data therefore represent mean conditions over several thousand years so that the extent to which these data represent the modern conditions needs to be carefully assessed. The echo types have therefore been interpreted with reference to the sidescan sonar data, core data and bottom photographs in terms of the relative degree of sedimentation versus erosion or non-deposition they represent and the local hydrographic process likely to be responsible for their development.

Type	Description	Interpretation
ET1	Semi-prolonged to prolonged high amplitude seabed echo with few or no sub-bottom echos and smooth to wavy microtopography.	High proportion of sand/silt in sediments (Damuth, 1980) Erosional, high-energy conditions
ET2	Sharp, moderate to high amplitude seabed echo with multiple, closely spaced, parallel, continuous low to high amplitude sub-bottom echos. Smooth to wavy micro-topography.	Low proportion of sand/silt in sediments (Damuth, 1980) Pelagic/hemipelagic or contourite sedimentation
ET3	Sharp, low amplitude seabed echo underlain by two closely spaced high amplitude sub-bottom echos and two moderate amplitude echos interspersed with a number of low amplitude reflectors. Smooth (ET3A) to wavy (ET3B) microtopography.	See discussion in text
ET4	High amplitude, hazy reflectors intermittently overlain by a very low amplitude seabed echo.	Moderate proportion of sand/silt (Damuth, 1980) Abyssal plain with fine-grained sediment drape

DSR6 Summary of the echo-character types observed in the Cape Farewell Eirik Drift region.

For a composite section across the drift, the seabed reflector has been picked using ProMAX seismic interpretation software. Analysis of the relative amplitude of the seabed acoustic reflection allows the sedimentary characteristics of the seabed to be estimated, although with a low lateral resolution of the order of several hundred metres *[Szuman et al. 2006]*.

Variations in the intensity of backscatter along sidescan sonar line makat-86 have been interpreted in terms of probable variations in the mean grain size of the surface sediment, in turn reflecting variations in the relative degree of sediment winnowing. Recent studies on continental shelf sediments have shown a strong correlation between the mean grain size of surface sediment and the intensity of acoustic backscatter, with brighter backscatter indicating a larger mean grain size *[Goff et al. 2000; Collier and Brown 2005]. Collier and Brown (2005)* report a positive correlation with a coefficient of 0.73 between the mean backscatter intensity and the mean surface sediment grain size. As most surface sediments on the upper drift, in the region from which line makat-86 was taken, appear to be winnowed sands, this

result is likely to have relevance here. Lineations observed in the sidescan sonar data are considered to reflect current activity [e.g. Kuijpers *et al.* 2003] and are therefore used as current direction indicators.

To corroborate the backscatter and echo-character interpretations, sedimentological data from the tops of three recently recovered cores (TTR13-AT450G, TTR13-AT451G (hereafter TTR13-450 and 451) and D298-P3) and published bottom photographs *[Rabinowitz and Eittreim 1974]* have been used. No evidence of significant loss of surface sediment was observed during the recovery of the cores. The bulk grain size distribution of the upper centimetre of sediment was determined using a Malvern Mastersizer 2000 laser granulometer and is assumed to be representative of modern sedimentological conditions.

The locations of the newly acquired and published geological and geophysical data used in this study are shown in Figure 4b.

DSR 5.2 Holocene Sedimentary Regimes

The depositional regimes present across the Eirik Drift are mapped on Figure 11a and discussed in detail below. For comparison, the high and low-velocity zones of the DWBC, as determined from the D298 hydrographic data, are mapped in Figure 11b along with the region of interpreted high fine sediment load associated with the DSOW and the pathway of the surface, iceberg-bearing East Greenland Current *(from Holliday et al. 2007)*. The proportions of clay minerals present in the surface sediment are also shown *(from Fagel et al. 1997)* as these may be interpreted as a tracer for sediments transported by the DWBC.

The southeastern flank of the main ridge and the southwestern flanks of the upper two secondary ridges above around 2800 m are characterized by a high-

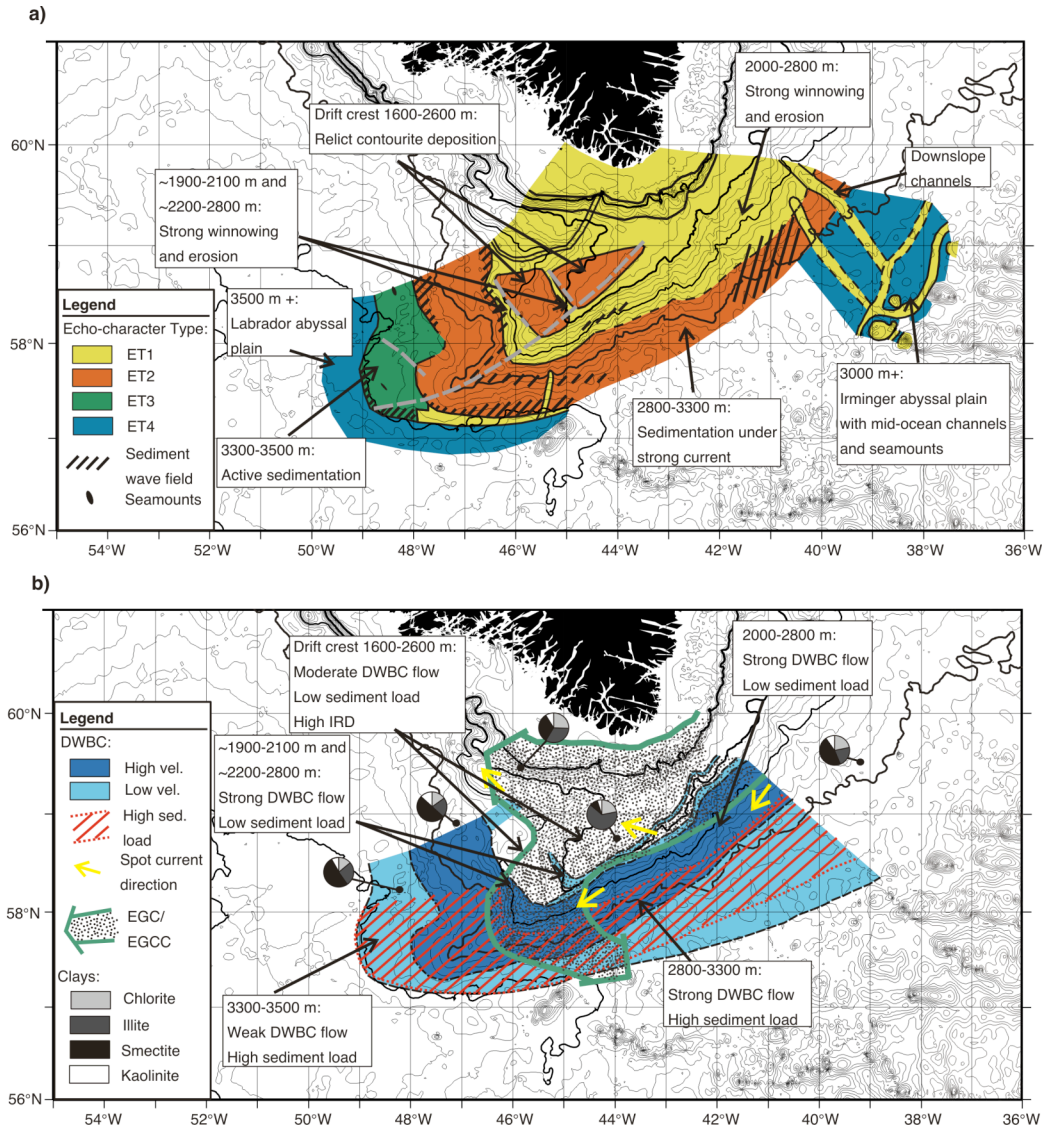

DSR11. a) Spatial distribution of sedimentation regimes determined from echo-character data. The positions of the main and secondary ridge crests are indicated in grey. b) Spatial distribuition of DWBC characteristics determined from the D298 hydrographic data. High velocity areas indicate calculated geostrophic velocity >7.5cm s^{-1} and high sediment load indicates areas with a beam attenuation coefficient >0.42 m^{-1}. The yellow arrows show the direction of deep current flow, determined from spot current measurements, where the velocity exceeded 20cm s^{-1} *(from Rabinowitz and Eittreim 1974)*. The position of the East Greenland Current/East Greenland Coastal Current (EGC/EGCC) is also shown *(from Holliday et al. 2007)*. The pie diagrams show the relative proportions of clay minerals in the surface sediment at various locations across the study area *(from Fagel et al. 1996)*.

amplitude seabed echo that is underlain by a diffuse blackened zone, caused by very high acoustic backscatter, with few or no sub-bottom reflections (Figure 12a). This

echo-character type (ET1) is typical of coarse seabed sediments with a high proportion of sand and silt, resulting from non-depositional or erosional conditions *[e.g. Damuth 1980; Stow et al 2002]*. This is confirmed here by the presence of sandy surface sediments in core TTR13-450 and the rocky seabed (from IRD dropstones) recorded in bottom photograph 1 (Figure 12a). Both the modern and historic hydrographic data show that these upper drift flanks are occupied by the upper portion of the DWBC (Figures 6, 10 and 11b), where the calculated geostrophic velocities are up to 25 cm s^{-1} (Table 3) and are easily capable of producing the coarse, winnowed surface sediments observed, given an input of mixed size IRD from which the mud is removed.

On the northern flank of the main ridge and northeastern flanks of the upper two secondary ridges, the seabed acoustic reflectivity remains high, but the level of acoustic penetration increases and several parallel, laterally continuous sub-bottom echoes are visible (Figure 12a). This echo type (ET2) typically characterises depositional environments with a low proportion (0-5%) of coarse sediments [Damuth, 1980] and is commonly interpreted as representing pelagic or hemipelagic sedimentation, although it is also typical of contourite deposition *[e.g. Damuth 1980; Stow et al. 2002]* .

This spatial pattern of echo type distribution, with ET1 on the steeply sloping drift flanks and ET2 across the crest from the main current pathway (Figure 11a and b), is also observed on other North Atlantic drifts (e.g. the Bjorn and Gardar Drifts - *Bianchi and McCave, 2000*) where it is interpreted to represent winnowing and erosion under strong contour currents along the drift flanks with deposition upslope. However at the Eirik Drift, sandy surface sediments are present within the ET2 zone on the upper northern drift flanks (Figure 12a), suggesting significant winnowing of the fine fraction. This, together with the presence of a condensed Holocene sequence in this area *[Stanford et al. 2006]* , demonstrates that this is not an area of active modern sedimentation. However,

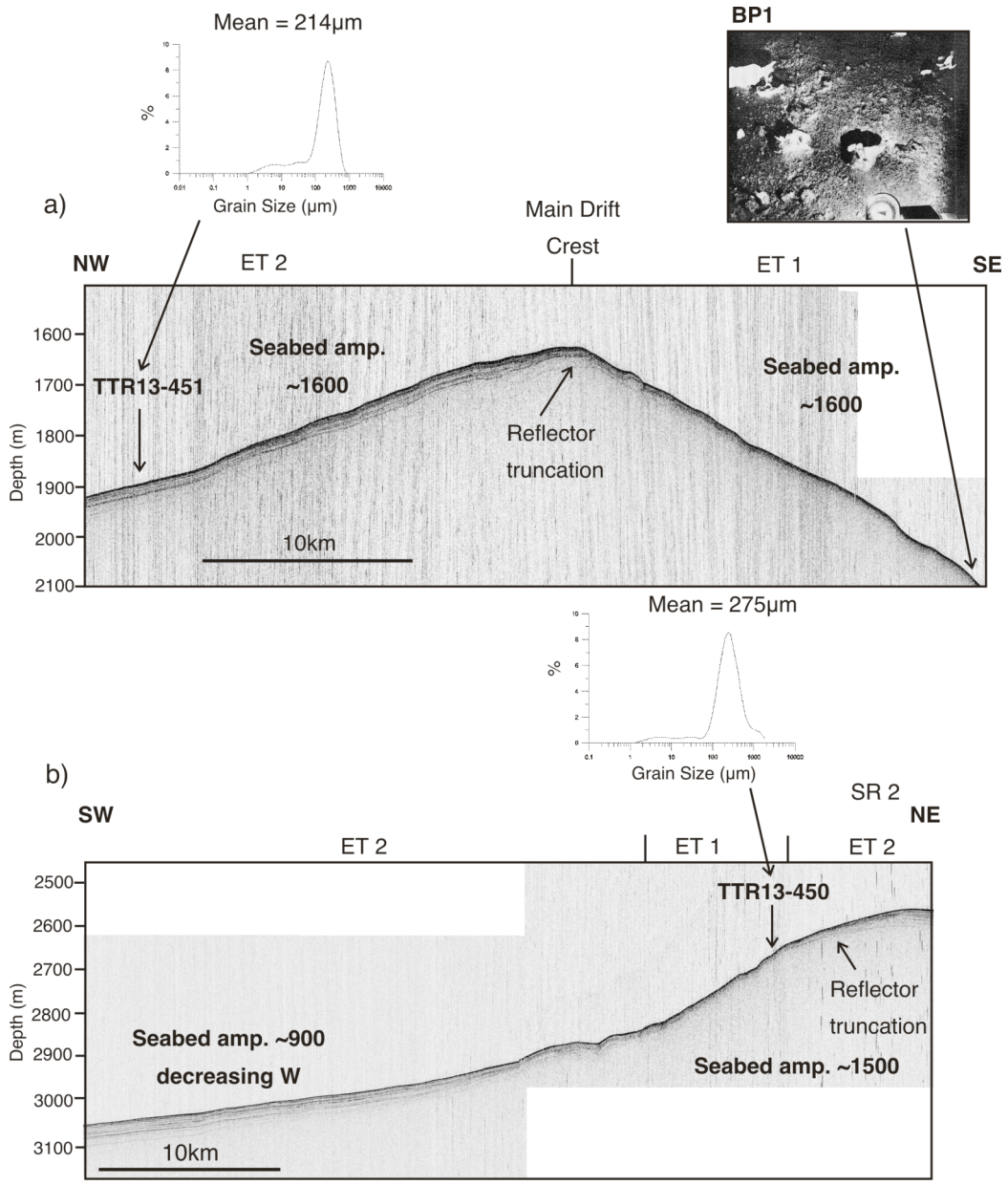

Figure DSR12 Echo characteristics of the upper Eirik Drift. a) Drift crest area with the rocky seabed present to the south of the main drift crest shown by bottom photograph 1 (BP1 – from Rabinowitz and Ettreim 1974) and the presence of sandy surface sediments to the north of the crest shown by the grain-size distribution from the surface of core TTR13-451. b) Section showing the central, most prominent secondary ridge on the northern drift flank, with grain size distribution data from core TTR13-450 close to the upper margin of ET1. The average seabed acoustic reflection amplitude within each of the echo-character zones is also indicated.

the D298 hydrographic data suggest very little current activity in this ET2 zone capable of significant sediment winnowing (Figures 6 and 11b). As discussed in Section 4.3, the geostrophic velocity observed in section D2 in the vicinity of the drift crest may be an underestimation of the actual velocity and spot current measurement data show flow of in excess of 20cm sec^{-1} across the drift crest (Figure 11b).

Beam attenuance data from the D298 hydrographic sections show that the DWBC carries very little sediment above around 2800 m (Figures 6d and 11b), indicating a low lateral sediment input to both the ET1 and 2 zones above this depth. The surface and intermediate waters overlying these upper drift flanks are however occupied by the East Greenland Current (EGC) (Figure 11b), which as a major conduit for icebergs will provide a supply of IRD to this area. This IRD, along with biogenic inputs, forms the only significant source of sediment to the upper drift flanks. The sandy surface sediments observed in both the ET1 and ET2 zones on the upper drift flanks are therefore interpreted to result primarily from the winnowing of these ice-rafted and biogenic sediments, yielding slow sedimentation of a sand-dominated sequence. The relative abundance of clay minerals in the surface sediments from within both of these zones shows a high proportion of illite *[Fagel et al., 1997]* (Figure 11b), which would appear to be a result of this ice-rafted origin.

Sub-bottom reflectors within this ET2 zone are parallel with respect to the seabed and lack obvious truncation, suggesting no significant down-cutting. It seems therefore that the area to the north of the drift crest has been dominantly non-depositional throughout the Holocene, with sediment re-working and winnowing. At the margins of the ET2 zones however, downward truncation of the sub-bottom reflectors toward ET1 zones (Figure 12) suggests a progressively increasing degree of erosion toward the high-velocity current cores.

The presence of secondary ridges to the north of the main ridge crest, each with associated zones of ET1 and ET2 (Figure 11a), suggests the presence of separate DWBC strands in this area. The erosive ET1 zone on the southwest flank of the central secondary ridge occurs at around 2200-2800 m (Figure 11a) and is

associated with the upper part of the main DWBC core (Figure 11b). The upper, minor ridge displays an erosive area between 1900 and 2200 m (Figure 11a). A small, detached strand of contour-flowing current is observed at this depth in both the D298 and historic geostrophic velocity data (Figures 6, 10 and 11b), and water mass characteristics suggest that this is most likely a separated strand of the DWBC (Figure 6b and c). The depth of this current strand is consistent with the flow of North East Atlantic Deep Water 1 (upper ISOW) through the Bight Fracture Zone in the Reykjanes Ridge, described by *Lucotte and Hillaire-Marcel (1994)*.

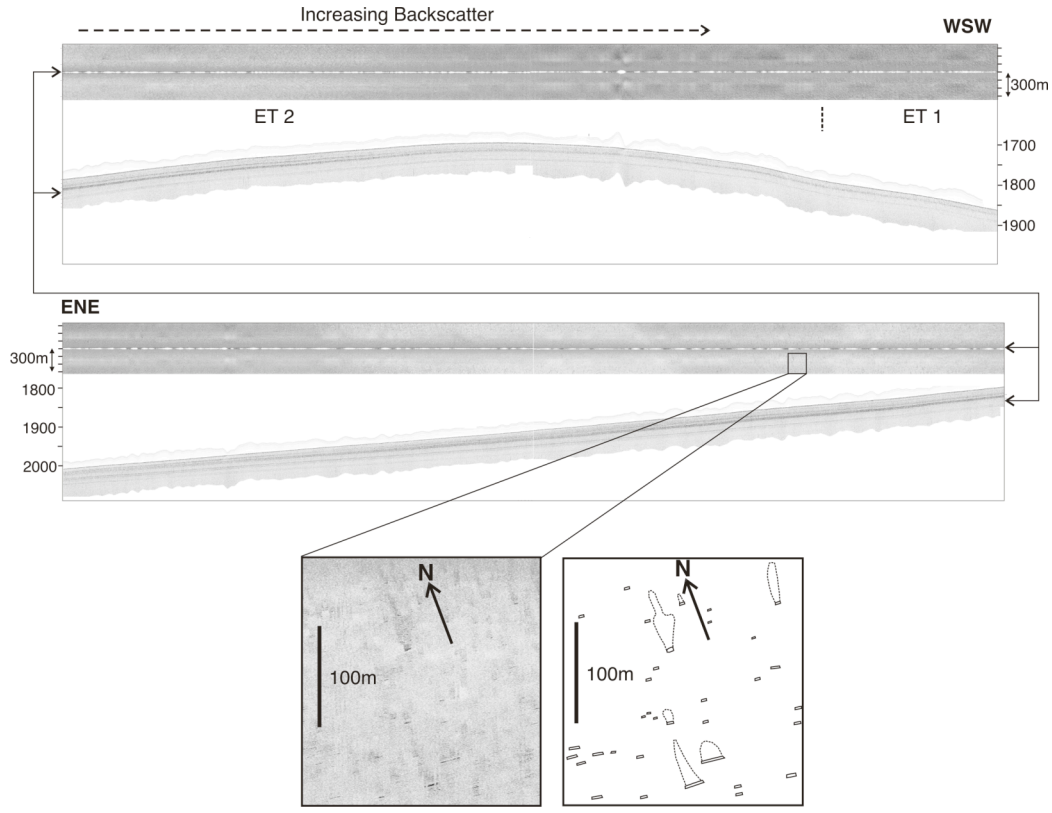

Figure DSR 13 Sidescan sonar line crossing the drift crest, with the corresponding 3.5 kHz section shown below (location shown on Figure 4b). The inset shows the detailed surface texture within the ET2 zone on the northern drift flank, with comet-tail features, highlighted in the adjacent line drawing, indicating unidirectional flow.

Sidescan sonar line makat-86 crosses areas of both ET1 and 2 in the vicinity of the main ridge crest (Figure 13), allowing further interpretation of the sedimentary processes in these zones. A relatively high degree of backscatter and a featureless

surface texture characterise the ET1 zone on the southeastern flank of the drift, while on the northwestern flank, the ET2 zone shows a somewhat lower degree of backscatter and displays distinct surface lineations. The higher backscatter to the southeast of the main drift crest is consistent with the somewhat higher mean grain size observed in this area (Figure 12) and with bottom photographs from within this zone (Figure 12b) that show a rocky seabed with a lack of fine-grained sediments *[Rabinowitz and Eittreim, 1974]*. The observed surface lineations to the north of the drift crest include 'comet-tail' features with high backscatter tails extending up to 100 m to the north and northwest from blocky features a few metres in diameter (Figure 13). These are interpreted to represent coarse lag deposits extending downstream from large glacial boulders similar to those seen in bottom photographs from the Newfoundland Margin *[Carter and Schafer, 1983]*, indicating unidirectional flow. The orientation indicates flow to the north and northwest suggesting flow across the drift crest and supports the inference of significant flow across the drift crest based on the spot current measurement data.

On the lower drift flanks, below about 2800 m, sub-bottom echoes become visible once more (ET2), suggesting that these areas are, or have been, depositional (Figures 12b and 14). Published core data from just below 2800 m on the northern drift flank shows the presence of sandy sediments throughout the Holocene with 30-40% of the bulk sediment greater than 125μm *[Hillaire-Marcel et al., 1994]*. However, bottom photograph 2 from the upper part of this zone on the southeastern flank of the main ridge (Figure 14) indicates the presence of fine-grained sediments at the seabed *[Rabinowitz and Eittreim, 1974]* suggesting ongoing deposition. The seabed acoustic reflection amplitude is somewhat lower here than in the ET2 zone above 2800 m (Figure 12a and b), most likely as a result of finer and less dense surface sediments. Bottom photograph 2 also shows surface lineations indicating a strong current influence, which is also suggested by the pervasive occurrence of low amplitude, symmetrical sediment waves (Figures 11 and 14). The hydrographic data show high DWBC flow velocities in this depth interval, comparable to those within the erosive ET1 zone on the upper drift flanks (Figures 6, 10 and 11b).

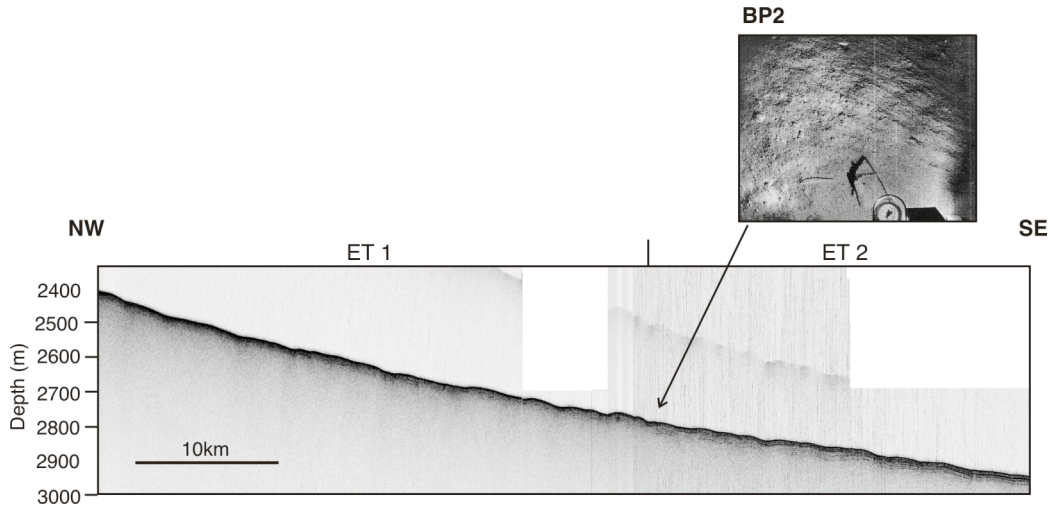

Figure DSR14 Echo characteristics of the deep-water, southeastern flank of the Eirik Drift, with fine surface sediments in the deep ET2 zone shown by bottom photograph 2 (BP2 – from *Rabinowitz and Ettreim, 1974*).

The above identifies a marked difference in the character of surface sediment between the lower and upper drift flanks, despite the similar flow velocities observed over these areas. The lower, more depositional drift flanks corresponds with the region of high oxygen saturation, high beam attenuation and low salinity that represent the sediment-laden DSOW within the D298 hydrographic sections (Figures 6 and 11b). The surface sediment clay mineral data also show the presence of a high proportion of smectites within this lower ET2 zone on both the southern and northern drift flanks, linked to sediment transport by the DSOW *[Fagel et al., 1997]*. On the upper drift flanks however, the only significant sediment sources are IRD and biogenic input. The degree of surface sedimentation associated with the DWBC at the Eirik Drift appears therefore to be controlled by the availability of an abundant lateral sediment supply, rather than by flow velocity alone.

The deep-water drift toe at the base of the northern drift flank is characterised by a distinctive echo-character type (ET3) that consists of a low to moderate amplitude seabed echo underlain by two closely spaced, high amplitude sub-bottom echoes and two moderate amplitude echoes, interspersed with a number of low amplitude reflectors (Figures 15 and 11a).

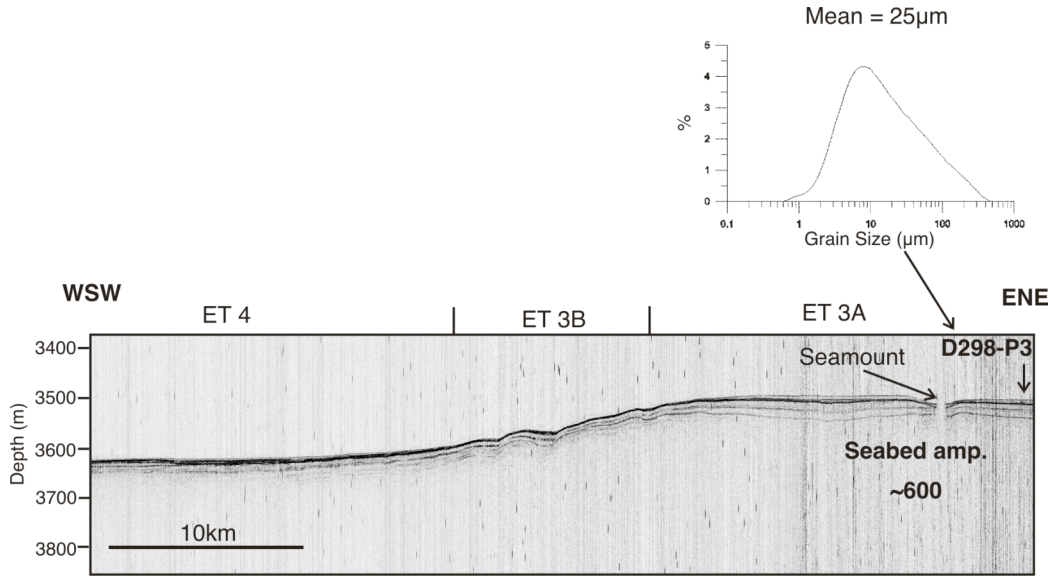

Figure DSR15 Echo characteristics of the deep-water western drift toe and Labrador abyssal plain, with grain size distribution data from core D298-P3.

The upper prominent reflector occurs at approximately 5.5 m below the seafloor in the vicinity of core D298-P2 (depth calculated based on the average p-wave velocity of 1454 m s^{-1} measured in core D298-P2). This depth closely corresponds with the upper boundary of sediments bearing ice rafted debris (IRD) (Figure 16). Comparison of the magnetic susceptibility record with a nearby published, radiocarbon dated record shows this boundary to represent the base of the Holocene *[Stoner et al., 1995]* . The upper transparent unit lying above this reflector is therefore interpreted as the Holocene sequence. The thickness of this sequence, up to 12 m in places, shows that this deep-water area has experienced very active sedimentation at rates of 50-100 cm ka^{-1}. Surface sediments from core D298-P3, from the north of this depositional area, are composed primarily of silt and clay (Figure 15), indicating an environment dominated by the accumulation of fine sediments, suggesting that the active sedimentation in this area continues to the present day.

Moderate to high amplitude discontinuous sub-bottom echoes are observed within the Holocene unit that have a lateral extent of up to 10 km. These discontinuous echoes correspond closely in depth with the thickest and most prominent of the turbidites in core D298-P2 (Figure 16) and are therefore interpreted throughout the study area as turbidites.

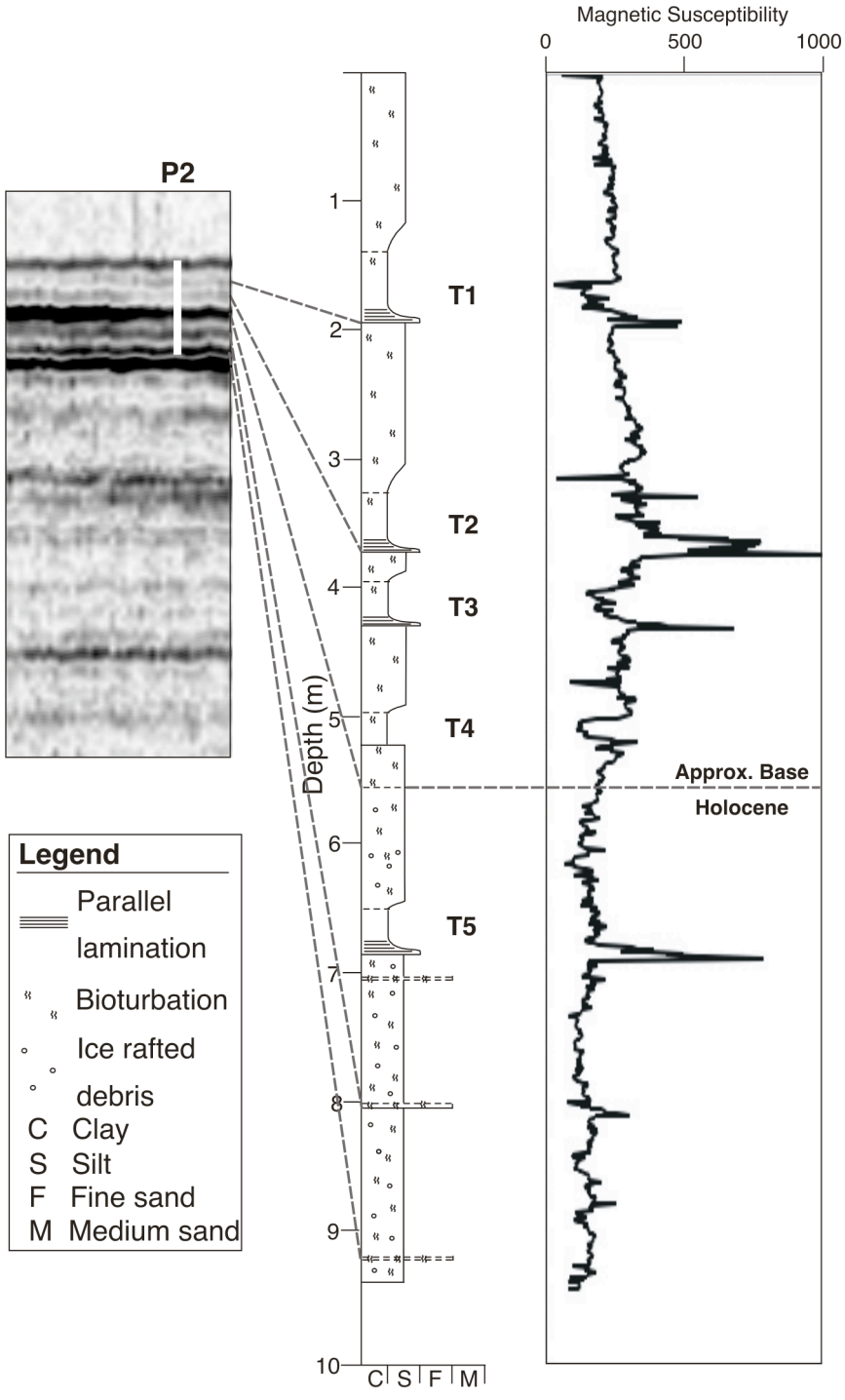

Figure DSR16 3.5 kHz section from the vicinity of core D298-P2 along with the core log and magnetic susceptibility record from D298-P2 showing the probable origin of the observed sub-bottom echoes. T1-T5 = Turbidites 1-5.

Hydrographic data show this deep-water region, between 3300 and 3500 m on the northern drift flank, to be characterised by low DWBC velocities with an intense

bottom nepheloid layer within the DSOW-dominated lower part of the current (Figure 6). Surface clay mineral data also show this area to have a high component of smectites, typical of DSOW-influenced deposition *[Fagel et al., 1997]* (Figure 11b). A combination of low current velocities and abundant lateral sediment supply are therefore the most likely cause of the rapid sedimentation observed in this area. The fact that a thick Holocene sequence is seen only in profiler data from the north of the drift crest indicates that deceleration of the DWBC as it rounds the drift initiates this enhanced deposition.

The abyssal plains of both the Irminger and Labrador Basins are characterised by high amplitude, hazy reflectors that are intermittently overlain by a very low amplitude seabed echo (Figure 15). This echo type (ET4) is interpreted as representing sediments that contain a moderate amount of sand and silt (0-30% - *Damuth, 1980*), intermittently overlain by a thin drape of fine-grained sediments. The very offshore end of hydrographic section D1 shows the low-velocity margin of the DWBC extending out into the centre of the Irminger Basin (Figure 6). The low velocity and moderate sediment load associated with this current margin appear to have allowed limited recent deposition to extend toward the basin centres.

DSR 6. Discussion and conclusions

The Holocene sediment record from the Eirik Drift indicates that recent sedimentation has only occurred down slope of the main DWBC, at the foot of the continental slope. Modern hydrographic data show this to be an area where the current typically has the highest proportion of sediment-laden DSOW. This sediment load can be deposited as the current rounds the drift. However even recent hydrographic data indicate that the structure of the DWBC can vary with warmer current cores of DSOW appearing higher up the drift flanks (Figure 10). Although we would expect such a DSOW core to carry sediment loads capable of deposition, the lack of significant Holocene sedimentation higher up the slope tells us that this can only have been an occasional feature in recent times.

The lack of sedimentation on the drift crest during the Holocene raises the question of the differences between this period and earlier phases of drift construction during the Pliocene and Pleistocene when sediment accumulation did occur on the drift

crest. Significant sediment accumulation during glacial phases of the Pleistocene has been linked to limited current activity *[Hillaire-Marcel et al., 1994]*. The Pliocene however, was characterized by strong DWBC flow in this area *[Arthur et al., 1989]* . Seismic sections show the Pliocene sequence of the drift with pervasive sediment waves and the formation of strongly migrating drift crests that have led to the present drift morphology *[Srivastava et al. 1989; Hunter et al. 2007]*. The most obvious reason for the difference between the Pliocene and Holocene intervals therefore would be a higher sediment supply during the Pliocene, which has been inferred from widespread drift building in the region and may have resulted from local uplift along the Greenland-Scotland Ridge *[Wold, 1994]*. The sequence of drifts found along the path of ISOW, from the Bjorn Drift (Miocene-Quaternary) in the Iceland Basin to the Gloria Drift (Pliocene-Quaternary) in the southern Irminger Basin, suggests that the sediment load carried by the DWBC over the Eirik Drift during this period may have been supplied by a combination of DSOW and ISOW.

Whilst DSOW flows directly from the sill at Denmark Strait to its first major turning point off Cape Farewell, the path of ISOW is more complex. In addition to navigating the bathymetry of the Iceland Basin (resulting in the formation of the Bjorn & Gardar Drifts – Figure 17), it can follow a number of routes between exiting the Iceland Basin and joining the main DWBC. The normally documented route sees ISOW following bottom contours of less than ca. 3000 m from the CGFZ around the Irminger Basin to a confluence with the DSOW driven DWBC to the north of the Eirik Drift. However, the water mass tracer data discussed here support the hypothesis that deeper components of the ISOW/LDW combination flowing out of the CGFZ at depths below 3200 m follow the bathymetry across the Irminger Basin without passing through hydrographic sections set to the south-east from Cape Farewell (Figure 17a) [*McCartney, 1992]. Lherminier et al. (2007)* identify two cores of ISOW flowing south along the south-eastern flanks of the Reykjanes Ridge marked by locally elevated oxygen concentrations. The deeper core is at a depth of around 3500 m in the Maury Channel and has an elevated silicate concentration in excess of 15 µmol/kg. This deep silicate maximum at the foot of the Rekyjanes Ridge has been previously identified further north in the Iceland Basin by *Mann et al. (1973)*. Although *Lherminier et al. (2007)* suggest that this deeper strand is in part due to an Icelandic Basin recirculation, its depth and silicate content is

consistent with our hypothesis of a deeper, more LDW rich, component of ISOW flowing through the deeper reaches of the CGFZ and joining the DWBC well to the south of Cape Farewell.

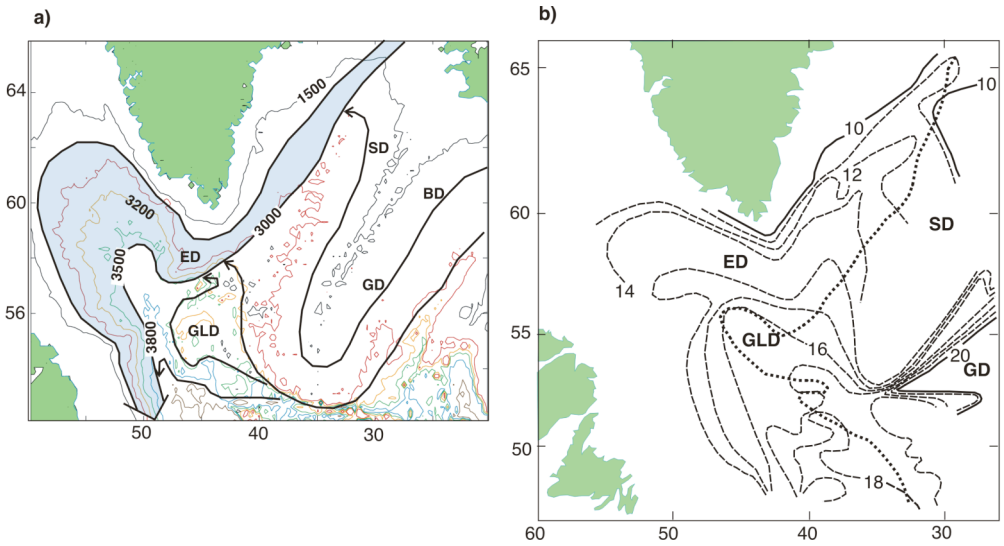

Figure DSR17 a) Schematic representation of the path of the DWBC through the Irminger and Labrador Basins (in blue) with the potential routes by which the ISOW/LDW may join the main DWBC (black arrows). b) Silicate (μmol l^{-1}) of the deep silicate maximum. This occurs above the bottom to the left of the dotted curve and at the bottom to the right of the curve (from McCartney 1992). ED = Eirik Drift; GLD = Gloria Drift; SD = Snorri Drift; GD = Gardar Drift; BD = Bjorn Drift.

Transports have been calculated for the overflow water travelling north along the western side of the Reykjanes Ridge based upon data collected by the *Erika Dan* in early 1962 and corresponding to our sections H1, H10 & H11 *[Worthington and Volkman, 1965]* . These show a reduction in the transport from 7.6 Sv at a latitude of 53°30'N to 2.0 Sv at 59°30'N. The maximum depths in the Irminger Basin at these latitudes are ca. 3600 m and 3100 m, respectively, and the fall in transport corresponds to the increase we calculate on the other side of the Irminger Basin of 3.5 Sv between sections H1 and H10. Although *Saunders (1994)* suggests that the reference levels used by *Worthington and Volkman (1965)* result in an overestimate of the outflow from the CGFZ, these results still provide some support for the hypothesis that the modified ISOW follows different, depth dependent, pathways on exiting the CGFZ according to its potential density relative to the deep/bottom water it encounters in the Irminger Basin. Current meter data presented by *Saunders*

(1994) show a significant westward current flowing through the CGFZ at around 3000 m in the northern channel but without the vertical resolution to identify the flow between 3200 m and 3500 m. Bottom currents above about 3200 m on the western flank of the Reykjanes Ridge will flow north into the Irminger Basin before turning south and joining the DWBC upstream of the Eirik Drift (Figure 17a). Between about 3200 m and 3500 m, the expected flow will first cross the Gloria Drift and then join the DWBC on the Eirik Drift. For flow below about 3500 m, the expected route would be across the southern edge of the Gloria Drift, around the mouth of the Labrador Basin, joining the DWBC off Newfoundland without reaching as far North as the Eirik Drift.

The new silicate concentration data collected during cruise D298 show a very similar pattern to those published by *McCartney (1992)*. *McCartney's (1992)* contour map of the deep silicate maximum (Figure 17b) can be interpreted as showing the pathways of ISOW where the silicate maximum is at the bottom. The point at which the silicate maximum lifts away from the bottom as it is undercut by the denser DSOW marks the offshore extent of the DWBC. This suggests that the deepest component of ISOW barely reaches any of the D298 sections and provides support for the pathway suggested by *McCave and Tucholke (1986)* for ISOW forming the Gloria Drift to the south of the Eirik Drift.

The separate strand of current identified at around 2000 m in both the D298 and historical hydrographic data is consistent with flow of upper ISOW through the Bight Fracture Zone in the Reykjanes Ridge *[Lucotte and Hillaire-Marcel, 1994]* and overlies the southwestern flank of the upper secondary ridge on the northern flank of the Eirik Drift. It has been postulated that the formation of the secondary ridges on the Eirik Drift relates to basement structure *[Hunter et al., 2007]* . However, the coincidence between the location of the upper ridge and a strand of current that is clearly identifiable along the southeast Greenland margin, before any possible influence of local structure at the drift, suggests that the multi-cored nature of the DWBC in this region may also have played a role in the development of the ridges.

The area bounded by Cape Farewell to the north, the CGFZ to the south-east and

Newfoundland to the south-west contains a complex combination of interacting deep currents. By the time the DWBC reaches Newfoundland it has been joined by the majority of the modified ISOW flowing through the CGFZ and its transport is a good indicator of the strength of the global THC. However, the growth in the DWBC transport as it flows around the Eirik Drift is significantly affected by the proportion of ISOW flowing along the different depth/density controlled pathways discussed earlier. The cross-sectional structure of the current will also be affected by the relative densities and water characteristics of the two types of overflow water and the overlying LSW.

We have illustrated how the DSOW core(s) flowing down the Greenland margin can move significantly across the slope over timescales of months (as seen in the hydrographic data from the WOD) and years *[Dickson et al., 1999]* as a result of temperature changes in the surface waters of the Arctic. Similar variations in the ISOW could alter the proportion of water following the different depth-controlled pathways providing a source of short-term variability in the transport of the DWBC over the Eirik Drift and affecting its cross-sectional structure. Some variability in the relative density of ISOW, LSW and DSOW is to be expected as the difference in their travel times from their area of formation to the Cape Farewell region means that the combining flows are sourced from mode waters of different ages.

In conclusion, the transport of the DWBC around the Eirik Drift and the rate of sedimentation in individual locations can be affected by changes in the overflow waters that do not necessarily impact the overall strength of the DWBC as it exits the Labrador Basin and feeds the lower limb of the THC. Although sedimentation patterns reflect average current pathways, even over longer periods, the potentially complex behaviour of the DWBC needs to be considered in the interpretation of paleo-DWBC proxy records from sediment cores.

DSR Acknowledgements

This study was funded as part of the NERC Rapid Climate Change Program under grants NER/T/S/2002/00453 and NER/T/S/2002/00436. The authors wish to thank all those associated with cruises D298, CD159 and TTR-13. The TTR-13 cruise was organised as part of the UNESCO Training Through Research program. The assistance of Dr Simon Dean in the processing of the 3.5 kHz data is also gratefully acknowledged. The cores used in this study are stored at BOSCORF at the National Oceanography Centre, Southampton.

4.4 Appendix To DSR Paper

Considerations When Calculating The Geostrophic Transport Of A Bottom Intensified Current Flowing Across A Sloping Sea Floor

4.4.1 An Introduction To The Dynamic Method For The Calculation Of Geostrophic Velocity

A current flowing in geostrophic equilibrium will have the coriolis force balanced by a lateral pressure gradient at all depths (equation a). The lateral pressure gradient is produced by a combination of the sea surface slope and cross-current variations in the vertical density structure of the water column.

a) $$fv\rho = \frac{dp}{dx}$$

Where f is the coriolis parameter, v the current velocity component perpendicular to the pressure gradient, p the pressure and x the cross-current coordinate.

Geostrophic flow exists for low Rossby numbers (<< 1) which are typically exhibited by relatively slow moving large scale ocean currents. For such currents if we can determine the lateral pressure gradient we can determine the perpendicular component of velocity to a good degree of accuracy.

b) $$\text{Rossby Number, } R_0 = \frac{U}{fL}$$

Where U is a typical current speed and L a typical length scale

Modern CTD data allow us to calculate the vertical density structure at a specific location in high resolution but does not provide any information about the sea surface slope leaving us short of one term in the equation to solve the velocity. However, as the sea surface slope provides a constant component to the pressure gradient throughout the water column, the vertical density structure at two stations is sufficient to deduce the vertical velocity shear between two isobaric surfaces. In equation c) the pressure integrated specific volume anomaly (∂) at each of the stations A and B is calculated from the CTD data. (it is sufficiently accurate to convert pressure simply from depth).

c) $$\overline{V_1} - \overline{V_2} = \frac{1}{Lf} * [\int_{p1}^{p2} \partial_B dp - \int_{p1}^{p2} \partial_A dp]$$

Where L is the station separation and the subscripts 1 and 2 refer to different isobaric surfaces.

The vertical shear structure adjusted against a level of no motion is commonly referred to as the baroclinic component of velocity. If there is no level of no motion then a reference level adjustment needs to be applied. This involves adding a constant velocity throughout the water column based on direct observations (current meters, Doppler profilers etc.) or mass conservation. This addition is often termed the barotropic component.

4.4.2 The Inherent Spatial & Temporal Averaging Effect Of The Dynamic Method

As discussed above the dynamic method produces a velocity that is averaged across the distance between consecutive CTD stations. It also has a temporal averaging affect associated with the response time for geostrophic equilibrium. This is typically of the order of a few days. These affects have both positive and negative implications. When considering current transports it may well be desirable to filter out high frequency

temporal variations and small-scale lateral variations in current strength. However we must take this into consideration when using direct current measurement devices to determine a reference level velocity. Current meters and ADCPs measure instantaneous currents at specific locations. In the case of current meters that provide a continuous record of velocities it is very simple to calculate temporal averages that reflect the geostrophic adjustment period and remove the impact of tides. ADCP data is typically in snapshot form and must be de-tided using tidal models. There is, however, no way of averaging out non-tidal variability of periods shorter than the geostrophic equilibrium timescale. Lateral variations in current strength on a scale smaller than the CTD station spacing can only be tackled by adding more measurement devices. In the case of a mooring array we may typically have an equal number of direct current measurement devices to CTD stations. However more often there will be CTD data and no concurrent direct current measurement data at all. The impact of small-scale lateral variations in current strength on the accuracy of current meter data for determining reference level velocities will be location specific. Ii is clearly a concern in the case of the DWBC off Cape Farewell due to the identification of current cores that appear to move laterally over short-time scales.

4.4.3 The Calculation Of Near Bottom Velocities – The Bottom Triangle Problem

The dynamical method can only calculate the geostrophic shear down to the deepest common CTD data for two stations. This provides no estimate of the velocity in the rectangle below the bottom reading for the shallower station and in the triangle formed above the seabed. Typically physical oceanographers assume that the velocity in this bottom area is either, constant and equal to the velocity calculated for the deepest common readings, or that it increases based upon a constant shear calculated from the velocity profile just above the deepest common observations. However as discussed earlier the geostrophic velocities calculated via the dynamical method are lateral averages and the shears will also be determined from these averages.

We can examine the impact of this lateral averaging in the simple case where the velocity is a linear function of height above the seabed:

d) Velocity, $v(h) = v_{max} - ch$

And hence the vertical shear is a constant

e) Vertical shear, $\frac{dv}{dh} = -c$

Now consider the following 2 station observational array:

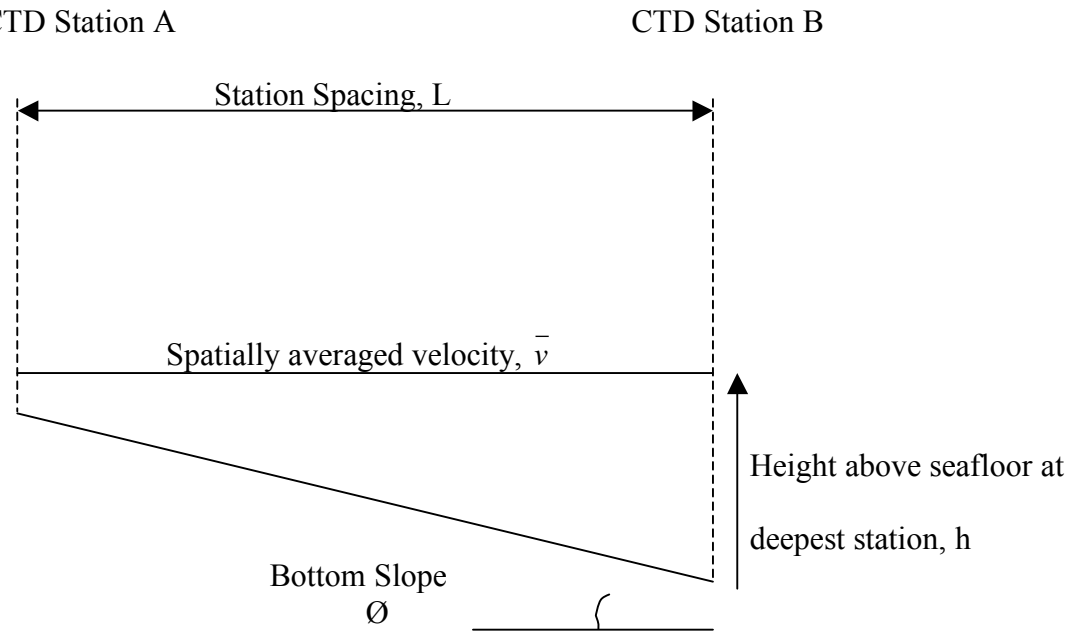

Figure 4.4.1 Schematic of CTD section over sloping bottom

In the area higher than the sea floor at station A (ie where the geostrophic velocity can be calculated from CTD data and h>LtanØ) the spatially averaged velocity will be determined by the average height above the bottom. Based upon the height above the seafloor at station B it is given by:

f) Spatially averaged velocity, $\bar{v}(\mathrm{h}) = v_{\max} - c(h - \frac{L\tan\phi}{2})$

g) Spatially averaged shear, $\frac{d\bar{v}}{dh} = -c$

where LtanØ is the increase in bottom depth between the two stations.

In the simplified case where velocity is a linear function of height above the seabed the shear in the spatially averaged velocity equals the shear in the ordinary velocity. We can now express the bottom triangle transport in terms of the local shear and the spatially averaged velocity at the depth of the seafloor at station A.

Consider a small depth interval in the bottom triangle dh and the associated transport dT. The average velocity is simply determined by the average height (h/2) but the length of the transport element is reduced to h/tanØ. Hence:

h) $\mathrm{dT} = (v_{\max} - \frac{ch}{2}).\frac{h}{\tan\phi}dh$

Integrating equation h) over the height of the bottom triangle gives an expression for the bottom triangle transport:

i) $BottomTriangleTransport, T = \frac{1}{\tan\phi}\int_0^{L\tan\phi} V_{\max}.h - \frac{ch^2}{2}dh$

j) $T = \frac{1}{\tan\phi}[\frac{V_{\max}.L^2\tan^2\phi}{2} - \frac{cL^3\tan^3\phi}{6}]$

Equation j) can then be simplified using the following substitutions:

k) Inter-station increase in depth, H = L tanØ

l) Bottom triangle area, $\Delta = \frac{L^2 \tan\phi}{2}$

To give:

m) Bottom triangle transport, $T = \Delta(V_{max} - \frac{cH}{3})$

As V_{max} is not something that is actually measured it is more useful to substitute for the spatially averaged velocity at the height of the station A seafloor, $\overline{v_A}$. From equation f) this is given by

n) $$\overline{v_A} = v_{max} - c(\frac{L\tan\phi}{2})$$

Combining with equation j) gives:

o) $$T = \Delta(\overline{v_A} + \frac{cH}{6})$$

I.e the transport is given by taking the velocity in the bottom triangle to be the geostrophic velocity at the bottom of the shallower station plus a sixth of the observed shear times the increase in depth between the stations.

In practice current strength is likely to be a non-linear function of depth and also have a dependence upon lateral position. In this case the observed shear in the spatially averaged velocity will become a poorer predicter of the current velocity in the bottom triangle but equation o) provides a starting point for comparison with observations.

4.4.5 Bottom Triangle Methodology And The D298 CTD Data

	Method After Clarke (Sv)	No Bottom triangles (Sv)	Constant velocity (Sv)	0.25* Constant Shear (Sv)	0.5 * Constant Shear (Sv)	Constant Shear (Sv)	Bottom Triangle Transports As % Of Total
D1	5.73	3.91	5.61	5.91	6.20	6.79	30%
D2	9.92	6.74	9.44	9.96	10.48	11.52	29%
D3	8.32	5.49	7.92	8.15	8.38	8.84	31%
D4	6.66	4.80	6.40	6.66	6.93	7.45	25%
D5	6.21	4.23	6.04	6.34	6.65	7.25	30%
D2 to D4 intersect	0.10	0.03	0.08	0.10	0.11	0.14	63%
D2 to D5 intersect	2.77	1.28	2.37	2.62	2.88	3.38	46%
D4 (inc part D2)	6.76	4.83	6.48	6.76	7.04	7.59	25%
D5 (inc part D2)	8.98	5.51	8.41	8.97	9.52	10.63	34%

Table 4.4.1 Geostrophic Transports For The D298 Sections Via Different Methodologies

Table 4.4.1 shows a comparison of the transports calculated for the 5 D298 sections using a variety of bottom triangle methodologies. The results we obtained via the interpolation of the temperature and salinity fields along lines of equal height above the seabed *(after Clarke, 1984)* fall very close to the values obtained using the basic data (on a 100m vertical grid similar to that used in the *Clarke (1984)* method) and assuming the bottom triangle velocity to be a constant given by the lowest calculated geostrophic velocity plus the observed shear extended one quarter of the way to the bottom. The impact of the different methodologies is immaterial for our analysis but our results are encouragingly close to the theoretical answer for a current velocity that decays linearly moving way from the seafloor (equation o).

5 MODELLING STUDIES

5.1 The East Greenland Current System

Modelling The East Greenland Current/East Greenland Coastal Current System

by

David Wilkinson

National Oceanography Centre, Southampton
University of Southampton Waterfront Campus
European Way
Southampton SO14 3ZH, UK

Unpublished

Abstract

The surface current system off southeast Greenland plays a major role in the export of freshwater from the Arctic Basin and Nordic Seas. The main East Greenland Current (EGC) has been recognised for centuries due to its highly visible role as an iceberg highway. In the late 20th century a freshwater jet flowing along the continental shelf between Denmark Strait and Cape Farewell was identified as a separate current, since the EGC is normally found over the continental slope in this region. This inshore, on-shelf current, became known as the East Greenland Coastal Current (EGCC). Although the EGCC was initially considered to be the result of local run-off more recent observations, and a review of historic data, have suggested that it is largely fed by the EGC north of Denmark Strait. Due to the inaccessibility of the region there is still a shortage of the observational data required to gain a full understanding of the dynamics of the EGC current system. High resolution regional modelling provides a means to isolate and investigate the different components of the system and to identify key areas where future observational work should be concentrated. Model results show that a bifurcation of the EGC in the region of Denmark Strait can create an on-shelf strand of the main EGC. The geometry of the shelf edge and the presence of large submarine troughs, extending from the major fjord complexes of the region, can steer and split the EGC in different ways depending on the depth and position of the Polar Front to the north of Denmark Strait. Freshwater runoff from the fjords of southeast Greenland remains trapped close to the coast if the outflow is within a reasonable range of current estimates. Towards Cape Farewell the model runoff combines with the shelf break flow as the shelf narrows. Observational data in this area reveals the near shore current as a surface intensified jet with distinct separation from the shelf break current. This suggests that the local fjords produce surface plumes that do not normally reach the shelf break and therefore have baroclinic Rossby radii of less than a quarter of the local shelf width. However, more investigation is required into the way multiple fjord outflows combine within a small area and there remains little detailed knowledge of current velocities at the mouths of the fjords and the role that the tidal cycle may play.

5.1.1 Introduction

The East Greenland Current (EGC) flows south along the eastern coast of Greenland from the Arctic Basin north of Fram Strait to Cape Farewell in the south. Between Fram Strait and Denmark Strait the EGC carries low salinity surface waters, and intermediate and deep waters of both Arctic and North Atlantic origin [*Rudels et al.*, 2002]. The deeper components of the current are lost crossing the sills at Fram Strait, the Jan Mayen Fracture Zone and Denmark Strait. At the latter the sill depth is only ca. 640m deflecting the deeper components of the current around the Iceland Basin. However the intermediate waters that spill over the sill are still significantly denser than the ambient water masses of the Irminger Basin and so descend rapidly along the bottom of the East Greenland continental slope. These overflow waters are known as Denmark Strait Overflow Water (DSOW) and form the densest part of the Deep Western Boundary Current (DWBC).

Much recent research in the region has concentrated on the overflow waters and their role in driving the lower limb of the global thermohaline circulation (THC). This interest has been stimulated by a growing appreciation of the role the THC plays in shaping global climate [*Rahmstorf*, 2000; *Rahmstorf*, 2002]. In the present mode of the THC deep waters formed in the northern North Atlantic flow across the equator and out through the southern Atlantic. The return flow draws warm surface waters up the full length of the Atlantic warming northwest Europe by around 4.5^{o}C [*Seager et al.*, 2002]. The stability of this mode is dependent upon surface salinities in the northern North Atlantic being higher than those in areas of similar latitude in the Pacific [*Oort*, 1983]. High density North Atlantic Deep Water (NADW) is transported down the full length of the Atlantic and into the other major ocean basins of the world as a result of its high salinity in comparison with Pacific deep waters. NADW is primarily formed from the overflow waters crossing the Greenland-Iceland-Scotland Ridge (DSOW and Iceland-Scotland Overflow Water) with further entrainment as the DWBC travels further south. The density contrast, and hence production, of NADW is reinforced by deep-water formation in the Irminger and Labrador Basins.

It is now commonly accepted that changes in northern North Atlantic salinity can trigger the THC to switch modes resulting in dramatic and rapid climatic shifts [*Broecker*, 2000; *Broecker, et al.*, 1985; *Keigwin and Lehman*, 1994; *Rahmstorf*, 2000]. Palaeoclimate proxies and modelling data suggest that a reduction in northern North Atlantic surface salinity can reduce the density and rate of formation of deep water, which in turn can weaken or even shut down the THC in the region. The influence of meltwater runoff from Greenland on the surface salinity in the deep-water formation areas of the Irminger and Labrador Basins is therefore a topic that requires further investigation. The surface flows of the EGC play a key role in determining the near-surface salinity patterns of the region, yet there is little detailed understanding of how they will react to the accelerating melting of the Greenland ice cap [*van de Wal*, 2003].

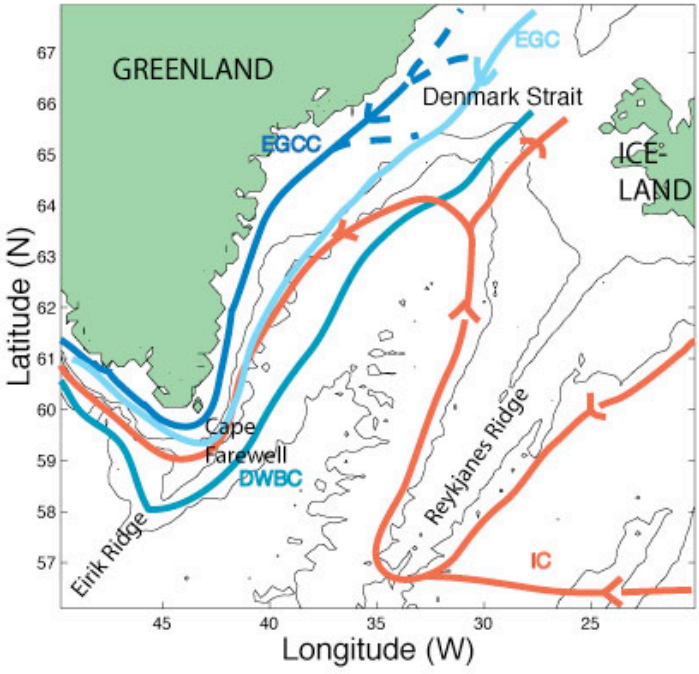

Figure 5.1.1 Map of the South-East Greenland region showing the main ocean currents of the region and the key bathymetric features

The EGC is typically found over the continental slope but to the south of Denmark Strait a separate, lower salinity, current is observed close to the coast over the continental shelf (see figure 5.1.1). During the 20th century this was considered part of the EGC but in the early 21st century it became known as the East Greenland

Coastal Current (EGCC) *[Bacon et al., 2002]*. The EGC/EGCC system is responsible for a significant component of the Arctic freshwater budget. The spot value for the EGCC freshwater transport of 0.06Sv, calculated from a single 1997 section of Cape Farewell, would represent 30% of the net Arctic freshwater gain if seen throughout the year *[Bacon et al., 2002]*.

It is important to understand how the EGCC/EGC system might react to increased meltwater runoff from Greenland, in order to predict the potential impact on rates of deep-water formation in the Irminger and Labrador Basins. Global coupled climate models typically lack the resolution required to accurately represent the dynamics of the complex current system found off southeast Greenland. Although they commonly infer a relationship between regional temperature and surface salinity in the deep-water formation regions, it is possible that any additional freshwater input is trapped in the coastal currents until much further south. A more detailed understanding of the region is required both to predict future climatic change and to properly understand the short-term trends seen in observational data.

It was initially suggested that the EGCC was a seasonal feature driven by run-off from south-eastern Greenland [*Bacon et al.*, 2002]. However, a review of all the available historical, primarily summertime, on-shelf data [*Wilkinson and Bacon*, 2005] failed to reveal the expected relationship between EGCC transport and latitude that would be consistent with this hypothesis. This suggests that a significant component of the EGCC flow originates from north of Denmark Strait. A 2004 RRS James Clark Ross cruise to the area was the first attempt to map the EGCC from north of Denmark Strait to Cape Farewell [*Sutherland and Pickart*, 2008]. Their results show a relatively constant transport for the combination of the EGC and EGCC of about 2 Sv, but with an increase in the freshwater transport of about 60% between Denmark Strait and Cape Farewell. *Sutherland and Pickart* (2008) suggest that the EGCC is formed by a bifurcation of the EGC in the region of Denmark Strait with the resulting flow reinforced by runoff from the southeast Greenland coast. They infer that the proportion of the EGC flow directed onto the shelf is controlled by a combination of topographic steering and wind stress.

Despite this recent work the volume of observational data is still very limited for determining the dynamics of this current system. The purpose of this study is to investigate the roles played by the bathymetry, run-off rate and wind stress in shaping the EGC/EGCC using a high-resolution regional ocean model.

5.1.2 Model & Methodology

The ocean model employed is a high resolution regional implementation of the hybrid coordinate model, HYCOM [*Bleck*, 2002]. The HYCOM model is a development of the isopycnic MICOM model [*Bleck and Smith,* 1990] with hybrid layers in place of isopycnic layers. The hybrid layers switch from isopycnic to depth coordinate as the thickness of the target isopycnic layers fall below a configurable minimum, in this case chosen to be 5m. This provides the advantages of an isopycnic model without the associated loss of vertical resolution in areas with low stratification or where the isopycnic layers outcrop the surface. The present implementation is based upon that used as the ocean component of the CHIME global coupled model [*Megann et al.,* 2009] but with a higher lateral resolution of approximately 5km and a reduced number of vertical layers providing a better trade off between overall resolution and performance for the region covered. In common with CHIME, HYCOM version 2.1.34 is employed with the KPP diapycnal mixing scheme [*Large et al,* 2004] and critical HYCOM parameters of 10^{-4} m^2s^{-1}, background internal wave viscosity, 10^{-5} m^2s^{-1}, background internal wave diffusivity and 0.45, critical bulk Richardson number.

The model domain covers the Irminger Basin, bounded by the Reykjanes Ridge to the east and the Greenland coast to the west. The northern and southern boundaries are chosen to cover the inflow of the East Greenland Current from just north of the Denmark Strait down to Cape Farewell on the southern tip of Greenland. The axes for the horizontal coordinates are rotated to lie approximately along the line of the East Greenland coast and the Reykjanes Ridge with a 330 by 210 grid providing horizontal resolution of about 5km. 10 hybrid layers are used to capture the different water masses involved with the majority used to resolve the near-surface fresh water

front. The target isopycnal densities for these layers are 1025.50, 1025.80, 1026.10, 1026.40, 1026.70, 1027.00, 1027.30, 1027.60, 1027.90 and 1027.99 kg m^{-3}.

In order to investigate the factors shaping the EGC/EGCC system a combination of idealised and realistic bathymetries (see figure 5.1.2) and climatologies is employed. A simplified bathymetry consisting of a 300m deep shelf with a slope descending to 2000m over 85km is used to investigate the degree of topographic steering exerted on various simple current structures. The shelf geometry is chosen to provide a simplified representation of the Greenland Shelf, which broadens in the area of Denmark Strait. The realistic bathymetry employed is derived from the satellite bathymetric dataset of *Smith and Sandwell* (1997).

A boundary zone to the south of Cape Farewell with a straight coastline and a shelf of constant width is used as a southern relaxation zone. An investigation of the impact of the Cape on the flow would require a model domain extending significantly further south and is beyond the scope of this paper. However *Holliday et al.* (2007) have shown that a significant portion of the EGCC is retroflected at the Cape, potentially carrying the impact of any increased freshwater flow into the areas of deep-water formation in the Irminger Basin.

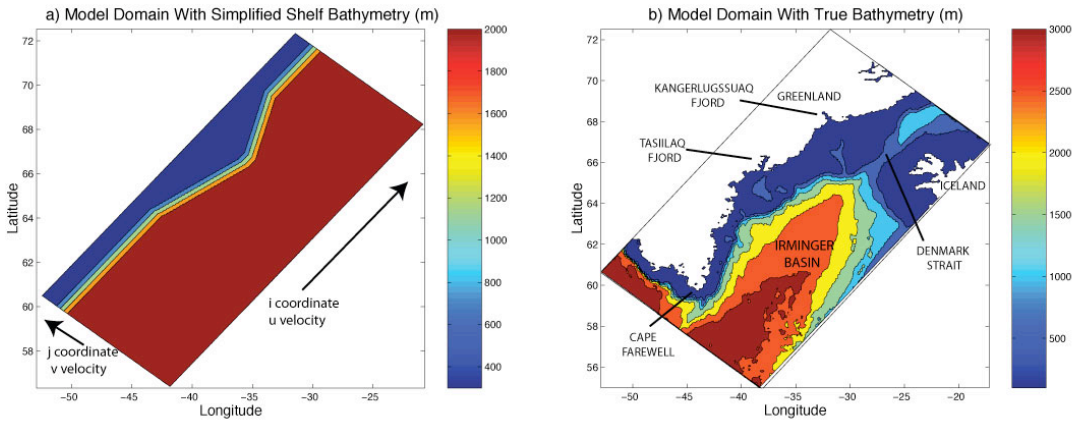

Figure 5.1.2 Example model domains showing the rotated grid a) Simplified bathymetry with 300m deep shelf connected to a 2000m deep ocean via a constant gradient slope. b) Real bathymetry for the Irminger Basin region.

Where a surface intensified baroclinic current is required, a simple analytical frontal model of potential density is used [*Webb*, 1995]. This model has been shown to

provide a good fit to the observational data for the EGCC in the vicinity of Cape Farewell [*Bacon et al.*, 2002] and was used in a historical review of EGCC data [*Wilkinson and Bacon*, 2005]. The potential density ρ(x,z) is a function of distance from the centre of the front and depth and is defined by equations 1 to 4:

$$1) - \rho(x,z) = \rho_0 - \rho_1 f(x,z)$$

$$2) - f(x,z) = 0.5 * (1 + \tanh[\frac{z - z_c(x)}{z_2}])$$

$$3) - z_c(x) = z_1 - z_3(\tanh(\frac{x}{x_1})$$

$$4) - x = x' - x_0$$

where:

z_1 is the mean pycnocline depth

z_2 is the pycnocline thickness

z_3 is the change in pycnocline depth across the front

z_c is the vertical position of the depth of the front

x' is the position with respect to the coast

x_0 is the position of the centre of the front with respect to the shore

ρ_0 is the reference density and is always set to 1028 kg/m^3

ρ_1 is the density difference across the front and is always set to 7 kg/m^3

Having determined the potential density function analytically, salinities are then chosen via an algorithm based on density and depth in order to achieve a low salinity wedge inshore of the front consistent with observational data. Finally potential temperatures are determined from the equation of state for seawater [*Millero and Poisson*, 1981]. The parameters used to determine the frontal structure in the various model simulations referred to throughout the paper are shown in table 5.1.1.

Initialising the model with a climatology based upon this frontal model produces a baroclinic velocity structure but, in the absence of any other forcing, no significant net transport through the water column. The flow is converted to a surface intensified jet using HYCOM's port functionality to add a barotropic component to the current.

Front No	X_0 *(km)*	X_1 *(km)*	z_1 *(m)*	Z_2 *(m)*	z_3 *(m)*
1	120	10	20	70	-40
2	120	30	300	300	-200
3	120	30	500	500	-300
4	160	20	175	220	-120
5	160	30	300	300	-200
6	160	30	500	500	-300
7	120	60	300	300	-200
8	120	60	500	500	-300
9	120	15	500	500	-300

Table 5.1.1 Frontal Model Parameters Used To Define Incoming EGC
(In each case the density difference across the front, σ_1, was set to 7 kg m^{-3})

The port functionality allows the addition of a transport perpendicular to the boundary for each grid point over a specified range along a domain boundary or coastline. The magnitude of the port transports in the region of the front at the northwestern boundary were typically calculated to produce a near zero velocity in the bottom model layer. A similar transport (with the addition of any fjord discharge) is extracted at the southwestern boundary, spread evenly over a wider port width. The initial climatology employed, for the majority of scenarios using the frontal model, has the front at a constant distance from the coast. However the model is only relaxed to the initial climatology in the 14 most northern (I=316 to 329) and 14 most southern (I=2 to 15) rows of grid boxes. This allows the current to adjust to the bathymetry where topographic steering is effective. For shallower currents, where the topographic steering effect is weak, the initial climatology can determine the path of the current for long periods. To investigate the natural progression of shallow currents, alternate model runs were performed using a simply stratified ocean to the south of the relaxation zone.

Low salinity outflows from the two major fjord complexes in the region (Kangerlugssuaq and Tasiilaq) were included in some model runs. In reality fjords dynamics are somewhat complex with the addition of freshwater at the head from melting glaciers driving an exchange at the mouth with the additional complication of tides. For our purposes we have approximated this to a surface output 50m deep with a salinity of 28 and potential temperature of -1 ^{o}C. This provides a surface flow with characteristics at the fjord mouth that correspond to observations for

Kangerlugssuaq Fjord [*Azetsu-Scott and Tan*, 1997] . This flow is achieved by fixing the depth of the fjords to 50m and strongly relaxing the area of the fjord to a constant salinity of 28 and potential temperature of -1^{o}C, combined with a port inflow at the head of the fjord that can be varied as required.

Model Run	*EGC Relaxation*	*Initialisation*	*Fjord Runoff*	*Wind Stress*	*EGC T'port*
1	Barotropic	Simple stratified	None	None	2Sv
2	Barotropic	Simple stratified	None	None	2Sv
3	Barotropic	Simple stratified	None	None	2Sv
4	Barotropic	Simple stratified	None	None	2Sv
5	EGC front 2	Front parallel to coast	None	None	3.9Sv
6	EGC front 3	Front parallel to coast	None	None	10.8Sv
7	EGC front 1	Front parallel to coast	None	None	0.55Sv
8	EGC front 1	Simple stratified	None	None	0.55Sv
9	EGC front 2	Front parallel to coast	None	None	5.0Sv
10	EGC front 3	Front parallel to coast	None	None	6.8Sv
11	EGC front 5	Front parallel to coast	None	None	3.8Sv
12	EGC front 6	Front parallel to coast	None	None	12Sv
13	EGC front 2 plus 2Sv BT	Front parallel to coast	None	None	7Sv
14	EGC front 2	Day 360 of run 9	0.1Sv*2	None	5.2Sv
15	EGC front 2	Day 360 of run 9	0.5Sv*2	None	6.0Sv
16	EGC front 2	Day 360 of run 9	2.0Sv*2	None	9.0Sv
17	EGC front 6	Day 360 of run 12	0.1Sv*2	None	12.2Sv
18	EGC front 6	Day 360 of run 12	0.5Sv*2	None	13.0Sv
19	EGC front 2	Day 600 of run 14	0.1Sv*2	0.02 Nm^{-2} anticyclonic	5.2Sv
20	EGC front 2	Day 600 of run 14	0.1Sv*2	0.02 Nm^{-2} cyclonic	5.2Sv

Table 5.1.2 Main characteristics of model runs employed

The majority of the model runs have excluded wind stress, concentrating on the roles of the bathymetry and the nature of the EGC front. However, observational data has shown a relationship between wind stress and the strength and depth of the EGCC [*Sutherland and Pickart,* 2008]. Therefore the final model runs were designed to compare the impact of cyclonic (the prevailing case in the sub-polar gyre) and anti-cyclonic wind stress on the established domain current system. A full list of model runs is shown in Table 5.1.2.

5.1.3 Results

The aim was to build complexity into the model starting with an idealised bathymetry and climatology (but initially no wind stress or fjord runoff) and gradually building in more realistic features in order to better understand the role played by the various components of the system. Of particular interest were the relationship between the EGCC and the EGC (i.e. is the EGCC a branch of the EGC or a separate current driven by southeast Greenland run-off) and the roles of bathymetry, wind stress and run off in shaping the two currents.

Barotropic Flow Over Simplified Topography

The most basic simulations varied the position of a barotropic current, with respect to the continental slope of the simplified bathymetry (fig. 5.1.2a), flowing in a simple stratified ocean. The stratification was chosen to be similar to that observed beyond the boundary current region north of the Denmark Strait with a cold, low salinity surface layer. Figure 5.1.3 shows the impact of bathymetric steering on currents initiated at different point with respect to the slope. In each case the current at the inflow port was 5 grid points wide (ca 25km) and carried a total of 2Sv. Increasing the transport by a factor of 10 had no significant impact on the resulting patterns of flow.

The barotropic currents are strongly controlled by the bathymetry. In model run 1, where the current is initiated over the shelf, it remains trapped on the shelf with very little leakage over the slope. Similarly where the current is initiated over the deep ocean basin it is prevented from crossing the slope and is steered around the broadened area of the shelf. This is expected as, without external forcing, steady state motion is only possible along potential vorticity contours [*Gill*, 1982]. The potential vorticity, Q is given by the ratio of the Coriolis parameter, f to the depth. Although f is proportional to the sine of the latitude within the model domain changes in the depth are dominant and potential vorticity contours approximate to isobaths. More precisely, in order to conserve potential vorticity, the depth will need to reduce in line with f moving equatorwards. Between the latitudes of 70^{o} and 60^{o} f reduces by 15% so there should be a slight tendency for the flow to move

shorewards as it progresses south. In practice the topographic steering effect is weakened by stratification [*Gill*, 1982] and other types of forcing must also be considered. The more complex model simulations are designed to investigate these interactions.

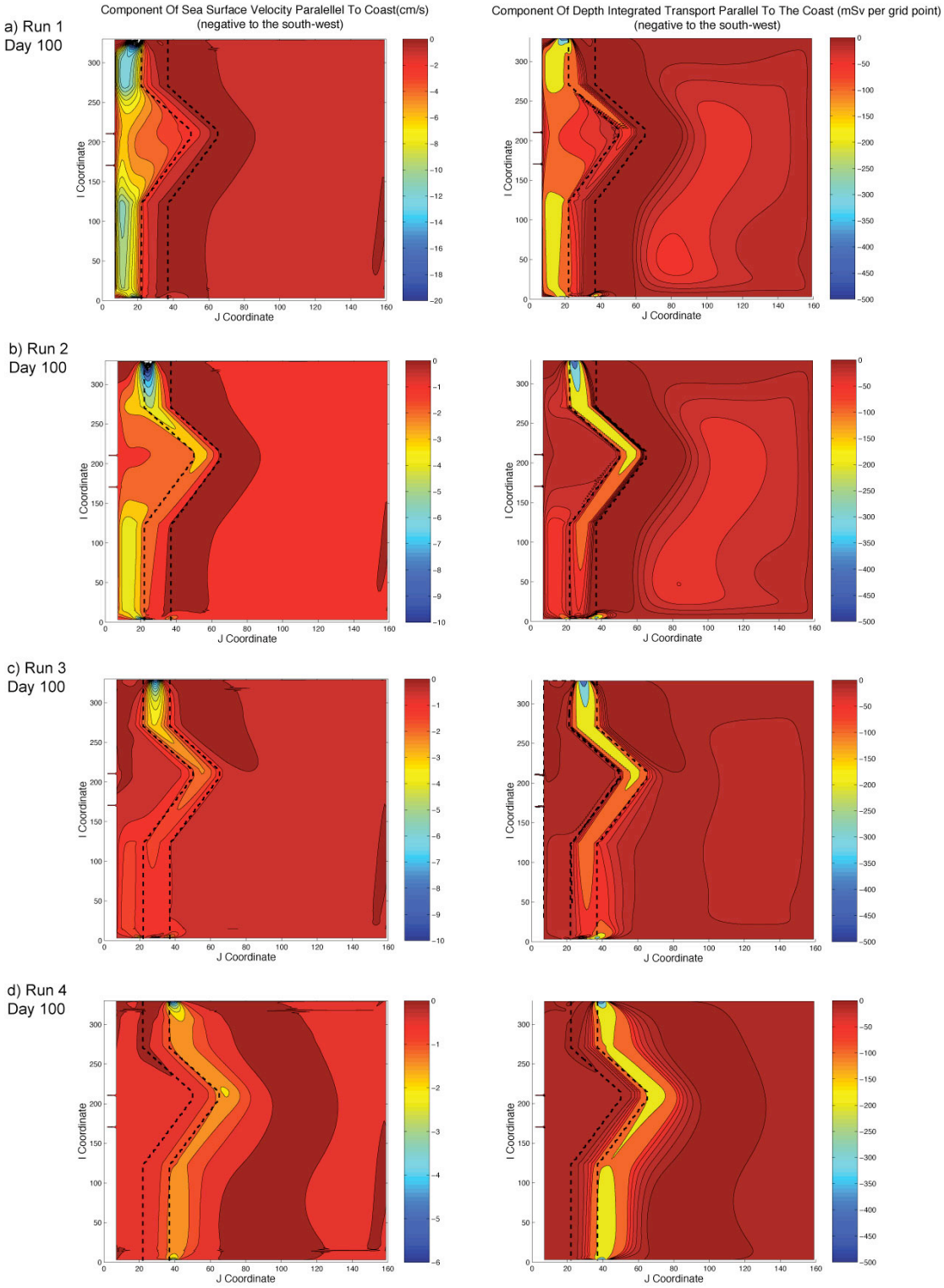

Figure 5.1.3 The impact of a simplified shelf bathymetry on a 2Sv barotropic current of 25km width initiated at different positions with respect to the slope a) on the shelf b) on the inside of the slope c) on the outside of the slope d) offshore of the slope. Note: The 300m and 2000m isobaths are shown as dashed lines.

The EGCC and EGCC are surface intensified currents produced by the freshwater front that lies over the continental slope to the north of Denmark Strait. Observational data from the World Ocean Database [*Conkright, et al.*, 2002] (figure 5.1.4) shows that the front north of Denmark Strait, where the shelf is at its narrowest, is located over the middle of the slope. The clear potential density signature of the front is seen to extend to about 300m depth, although the shape of the front is still discernible in the isopycnals down to at least 500m.

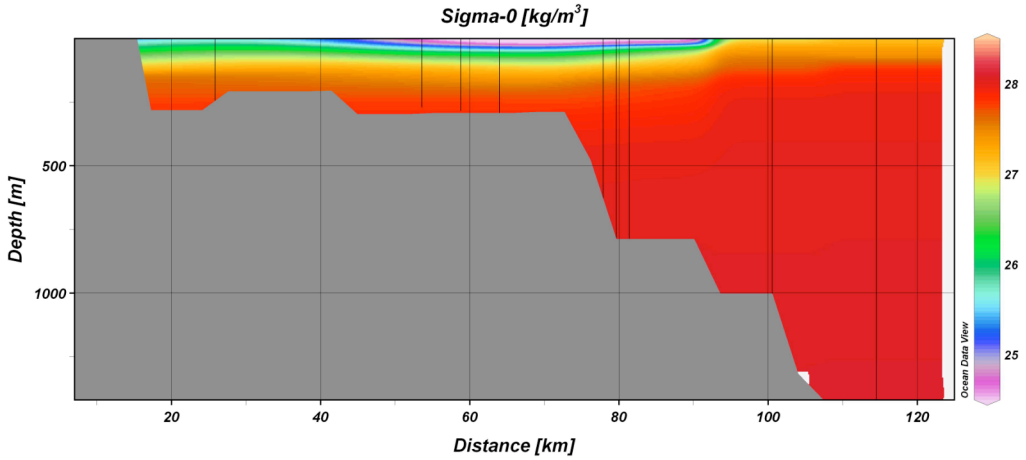

Figure 5.1.4 Plot of potential density along a section taken perpendicular from the East Greenland coast at a latitude of 68.5°N. The section is based upon an average of the available data in the World Ocean Database 2005.

The observational section shown in fig. 5.1.4 corresponds to the northeastern boundary of the model domain. Model runs 5 and 6 simulate the observational data by relaxing the north–eastern boundary to a climatology that positions the EGC front over the middle of the continental slope. They contrast the southward evolution of a 300m deep front (based upon the *Webb* (1995) mean pycnocline depth parameter) with one that is 500m deep. Sample results are shown in figure 5.1.5. The transport injected at the northeastern boundary of 3.9Sv, to achieve a near zero bottom layer velocity, is reasonably consistent with the observation values for the EGC [*Bacon*, 1997; *Sutherland and Pickart*, 2008]. The deeper current has a rather high transport of 10.8Sv. For this reason the 300m deep front lying over the middle of the slope (front 2 in table 5.1.1) is considered the quasi-realistic scenario throughout the study.

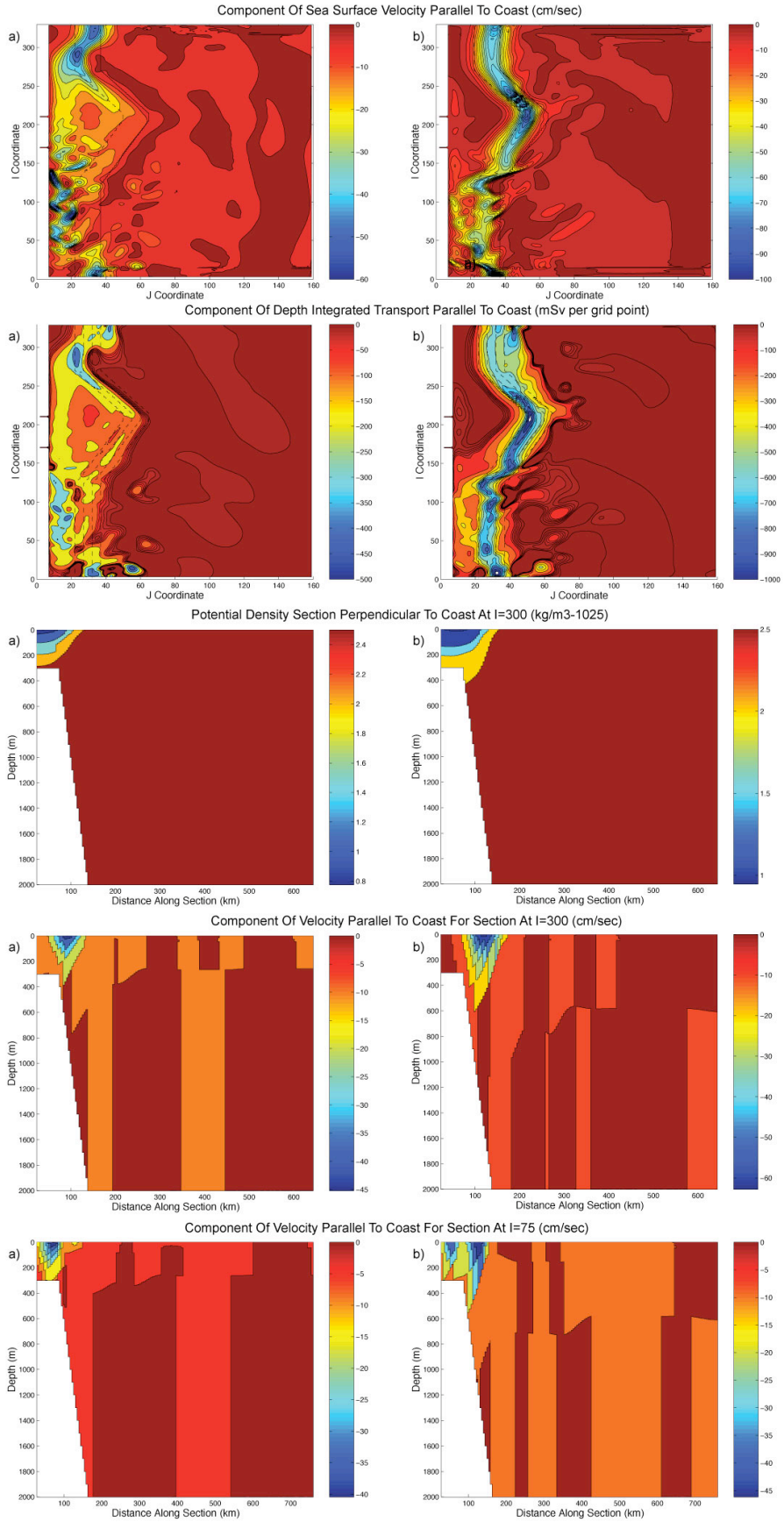

Figure 5.1.5 Current characteristics for two baroclinic currents of different depths and strengths: a) Run 5, day 360; b) Run 6, day 360

In model run 5 the shallower current is clearly subject to weaker bathymetric steering than either the deeper baroclinic current (model run 6) or barotropic current (model runs 1 to 4). A less expected feature is seen when the shelf narrows in the south at i=75 (fig. 5.1.5a). The shallower current recombines into a single jet lying over the shelf with the along slope component detaching from the bathymetry due to inertial overshoot. The deeper current of model run 6 (fig. 5.1.5b) follows the slope around the widening shelf but is split at the point the shelf turns left to run parallel to the coast. A weaker on-shelf jet is formed due to inertial overshoot while the main current continues along the slope. Inertial overshoot occurs when the topograhic steering torque is insufficient for the current to follow a sudden change in direction of the bathymetry. In this case the momentum of the current takes it on to the shelf as the slope turns to the left.

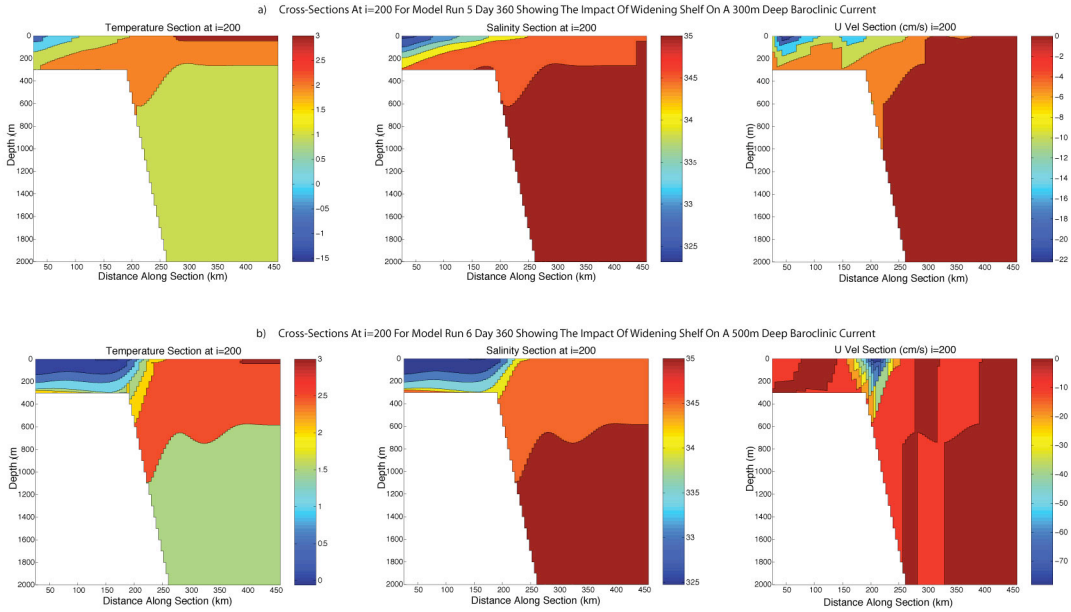

Figure 5.1.6 Detailed sections at i=200 for model runs 5 and 6 (day 360) showing the impact of the widening shelf on the path and structure of the quasi-realistic EGC

Looking in more detail at the structure of the currents at the widest point of the shelf (figure 5.1.6), we see that in run 5 the surface current is split in two but even the offshore strand still resides primarily over the shelf. The higher transport over the slope is due to a more barotropic current with less defined surface intensification. The deeper current (model run 6) essentially extends fully to the bottom of the inner slope at a depth of between 500 and 600m.

Model runs 5 and 6 demonstrate that a key factor in determining the downstream evolution of the EGC is the depth to which the front, and therefore the current, penetrates. Where the current extends to the seafloor, its path is similar to that of the barotropic currents in model runs 1 to 4, being heavily topographically steered. Shallower currents are less influenced by the bathymetry, other than by the coastline itself. A very shallow current, with a mean pycnocline depth of 20m (model run 8), starting over the slope turns right and becomes trapped against the coast as a result of the Coriolis effect outweighing topographic steering (figure 5.1.7). The behaviour of the shallow current is more dependent upon the starting climatology than the deeper equivalents. In model run 8 the current flows into a simple stratified ocean, whereas in run 7 the initialisation is to a 20m deep front running parallel to the coast (in a similar fashion to the other runs). In the second case, at model day 100, there is only limited topographic steering effect but there is also only a small move towards the coast. The initial climatology is able, to some extent, to keep the current flowing parallel to the coast. Although there is evidence that this is not a stable equilibrium, and the shallow current will eventually move to the coast, this behaviour will impact how the current will react to short-term changes in depth and strength.

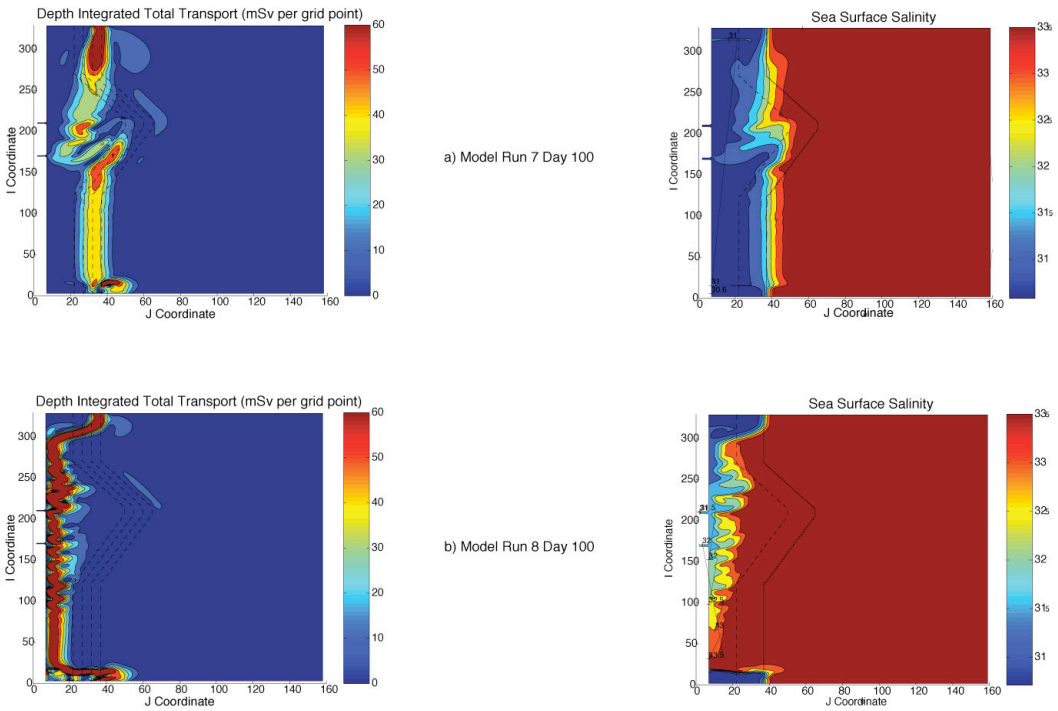

Figure 5.1.7 The southward evolution of a shallow current initiated over the continental slope when flowing into a basin with an established frontal structure (model run 7) and one with a simple stratified structure (model run 8)

Baroclinic Flow Over Realistic Bathymetry

Building in the next layer of realism we apply the quasi-realistic 300m deep over-slope front used in model run 5 to a realistic bathymetry (model run 9 – fig. 5.1.8). The bathymetry is taken from *Smith and Sandwell* (1997) with the addition of a southern relaxation zone, as discussed in section 5.1.2. There are obvious differences from the similar idealised bathymetry run. Possibly the most significant difference can be attributed to the effect of the troughs in the shelf that extend from the major fjord complexes in the region, the Kangerlugssuaq Fjord (KF located at ca. i=260) and the Tasiilaq Fjord (TF located at ca. i=170). At the Kangerlugssuaq Trough (KT) the flow is temporarily split with the inner branch following the bathymetry of the trough (fig. 5.1.8). Around 35% of the flow moves inshore at KT although it largely recombines with the offshore strand after the trough. The Tasiilaq Trough (TT) diverts a similar proportion of the flow inshore but in this case the split is more permanent with the inshore strand reaching the inner shelf where it remains. The more pronounced impact of the TT can be attributed to the fact that the inshore pathway is in line with the shelf break to the north and is supported by the inertia of the current. Further south the two current strands come together again as the shelf narrows. Although the two strands are in contact at i=60, it is still true that the inner component of the current is over the shelf whilst the outer remains over the slope.

Model runs 10 to 13 investigate the impact of changing the starting position, depth and barotropic component of the current (figure 5.1.9). The deeper, stronger current in model run 10 shows a greater tendency to follow the isobaths around the fjord troughs. However the more obvious change is that the current patterns appear more confused, particularly towards the south. This may, in part, be due to the greater transports associated with the deeper current but is also due to the interaction between stronger topographic steering and the complex bathymetry in the region of the 400m isobath. Moving the front 40km further offshore whilst keeping the shallower 300m mean isopycnal depth (model run 11) has a less significant impact, although the offshore strand of the current is more distinct from the inshore at southern latitudes (i=60 &120 on the cumulative transport plots – fig. 5.1.9).

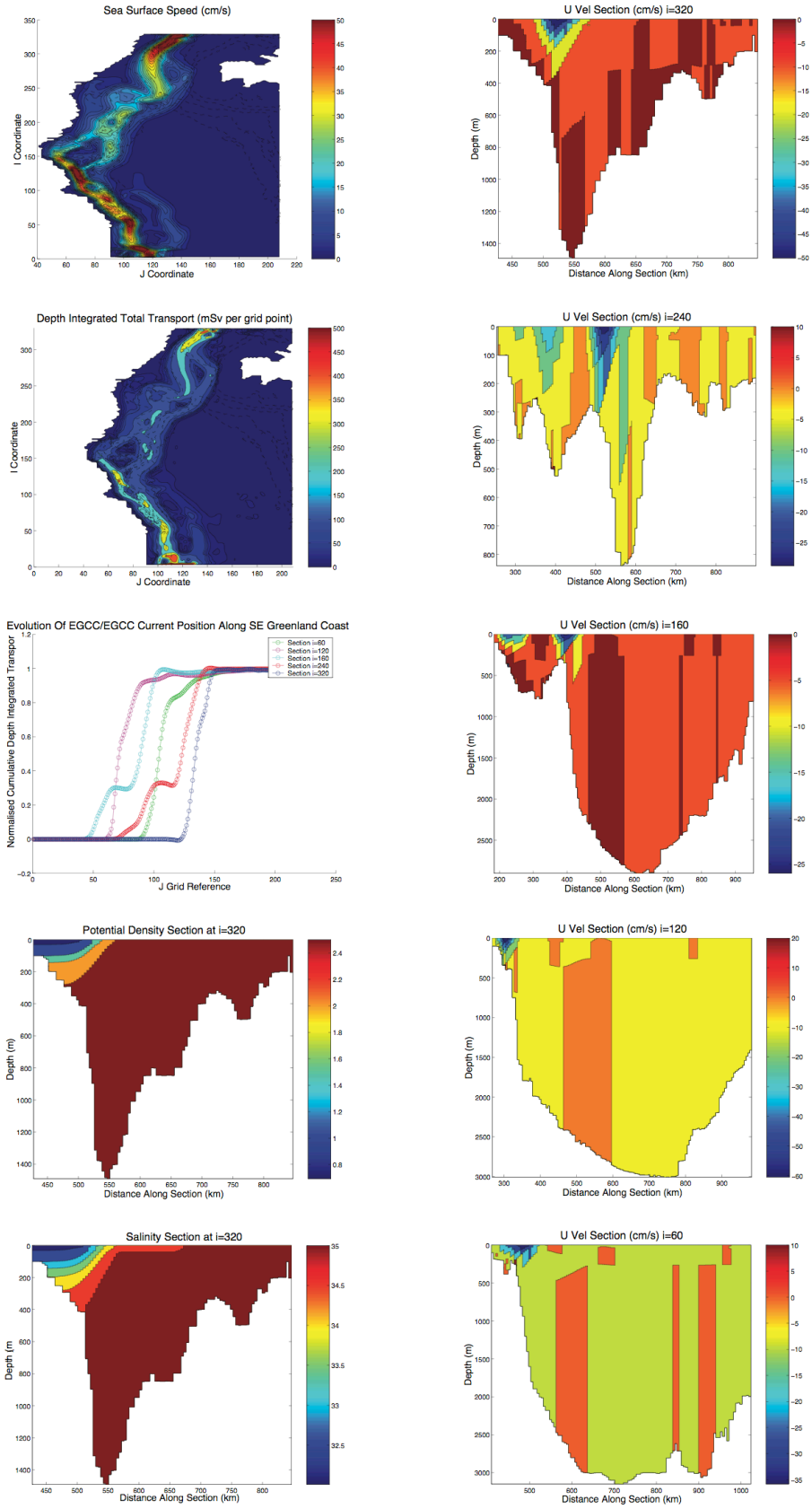

Figure 5.1.8 Spatial evolution of a 300m deep current flowing over realistic topography Model run 9, Day 360

Deepening the front and moving it 40km offshore has a much clearer impact (model run 12). In this scenario the offshore pathway is totally dominant as a result of the greater topographic steering effect and the greater water depth in which the front is created at the northeastern boundary. The current is almost entirely found in a narrow band over the full length of the model domain although a small inshore strand is still generated at the TT. The main current is seen to deviate slightly at the mouths of the two troughs as it is forced to closely follow the isobaths. The simpler, predominantly single, path followed by the current can be attributed to the dominant topographic steering torques that occur when the main front extends to the ocean floor at the northeastern boundary in the region of the 500m isobath. The 500m isobath follows a relatively straight path, while the 400m isobath (approximately associated with the more inshore fronts of runs 9 and 11) is far more affected by the main troughs and other features on the edge of the continental shelf. For currents following shallower isobaths, there are tighter corners to negotiate where the topographic steering effect has to compete with the inertia of the current. This results in the generation of multiple strands that interweave. With the simplified bathymetry (model runs 5 and 6) changing the front depth alone was sufficient to favour either the inshore or offshore pathway. The realistic bathymetry confuses matters due to the significant differences in the complexity of the paths of the different isobaths between 300 and 600m.

In model run 12 the current has a high transport of 12Sv. However it would be possible to construct a scenario with a deep penetrating front of lower density gradient (i.e. with a higher salinity and density on the coastal side of the front) that would follow a similar path but with reduced current velocities and transports. An alternative way to increase the topographic steering effect for a smaller increase in total transport is to add a barotropic component to the current (model run 13). This is the same scenario as in model run 9 except that a barotropic flow of 2Sv has been added across the main width of the current. As a result both the offshore slope current and those strands following the bathymetry around the two main troughs are better defined on the total transport and surface current speed plots (fig. 5.1.9). The highest surface currents are seen following the troughs onto the shelf whilst the offshore strand is less surface intensified but still carries a higher overall transport

per km of cross-section. Total transport is split fairly evenly between the two and recombines as the shelf narrows approaching Cape Farewell.

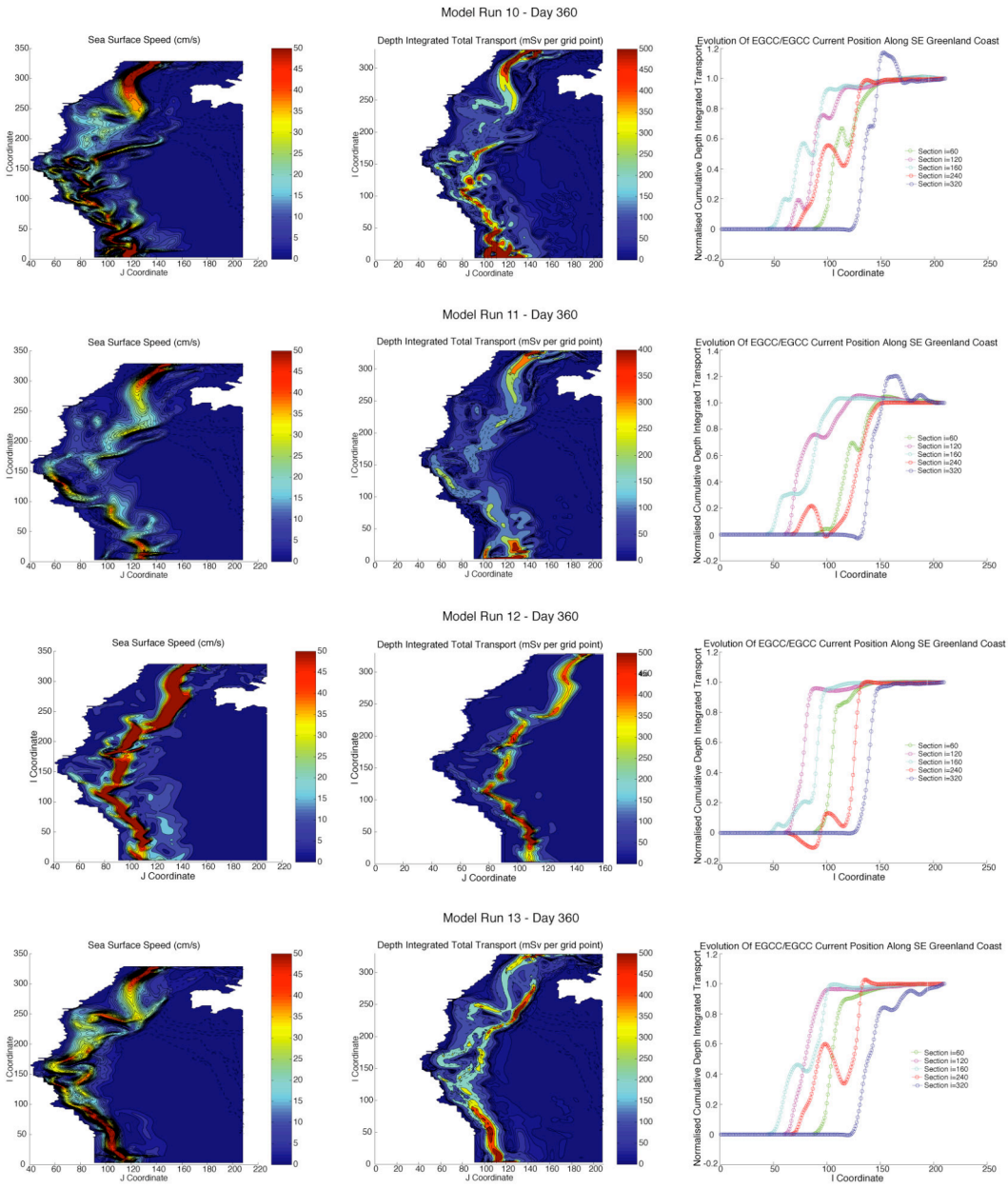

Figure 5.1.9 Contrasting the differing southward evolution of baroclinic currents of different depths, strengths and starting positions

The Role Of Local Fjord Output

Although model runs 9 to 13 demonstrate some of the features of the current system we see in observational data (primarily a bifurcation of the current in the region of Denmark Strait and a strengthening of the inner branch in the region of Tasilaaq Fjord) they all produce a main current further south that recombines over the slope. However observational sections have consistently shown a strong freshwater jet on the narrow shelf region just to the north of Cape Farewell [*Bacon et al.*, 2002; *Sutherland and Pickart*, 2008; *Wilkinson and Bacon*, 2005]. To achieve a similar flow we need to consider the role of freshwater runoff from the southeast Greenland coast.

Model run 14 introduces fjord run-off to the same quasi-realistic EGC set-up as used in runs 5 and 9. In this scenario the output from the two major fjord complexes (KF and TF) is set to 0.1Sv with a salinity of 28. This corresponds to a freshwater flux of 0.02Sv per fjord (based upon a reference salinity of 35). The total of 0.04Sv is comparable with summertime estimates of the freshwater flux in the EGCC; 0.06Sv [*Bacon et al.*, 2002], 0.01 to 0.1Sv [*Wilkinson and Bacon*, 2005] and 0.04 to 0.12Sv [*Sutherland and Pickart*, 2008]. Run 14 represents a best estimate of the present-day summer situation on the assumption that south-east Greenland runoff is responsible for about 50% of the freshwater flux of the EGCC and can be approximated by two equal point sources. Passive tracers are used to track the flow of the different freshwater components of the resultant current system. Tracer 1 is kept at a constant 100% where the salinity is below 32 in the northern relaxation zone. Similarly the outflows from KF and TF are strongly relaxed to 100% for tracers 2 and 3 respectively through the use of local relaxation zones. In all other areas the tracer values are initialised to 0 with no subsequent relaxation. Figure 5.1.10 shows the initial spreading of tracers 2 and 3 from the fjords after 10 days of output. Although the figure shows the surface concentration of tracer1 the concentrations of tracers 2 and 3 are effectively 100% minus the tracer 1 concentration for the regions surrounding the respective fjord mouths.

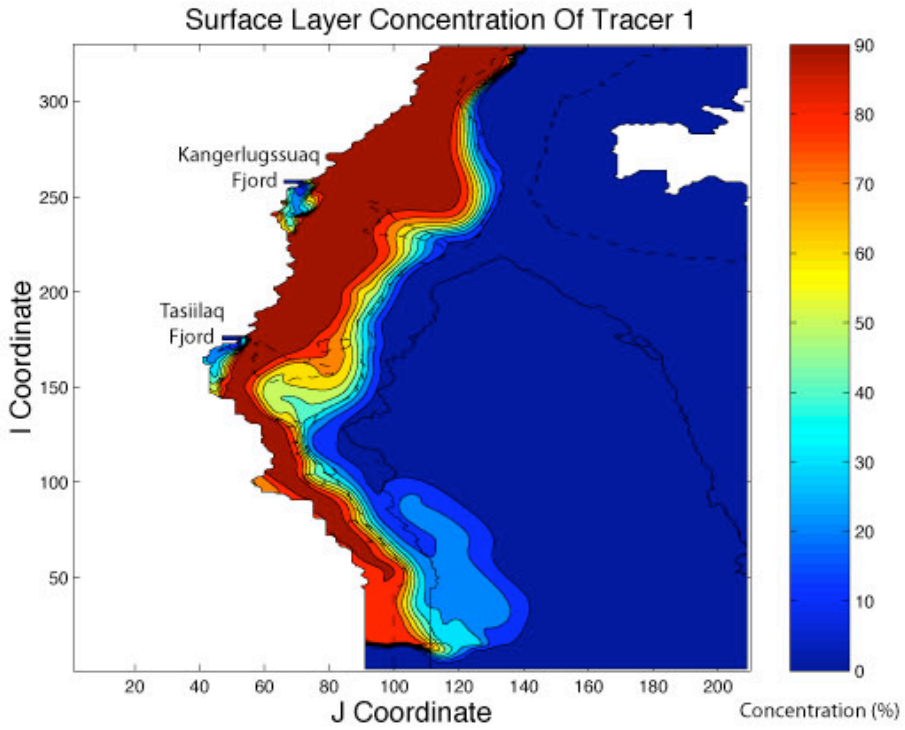

Figure 5.1.10 Tracer 1 surface concentration: Model run 14, day 370
(10 days after the introduction of fjord outflow)

Comparing the results from run 14, day 600 (figure 5.1.11) with those from model run 9 (figure 5.1.8) we can see that the fjord run-off has had little impact on the main flow of the EGC. The surface tracer data shows how the runoff is trapped closely to the coast (figs. 5.1.11g&i). In the wider areas of the shelf (i=240 & 160) the runoff forms an inshore extension to the on-shelf strand of the EGC. Further south at i=120 the impact is to broaden and shallow the single current that lies over the shelf and inner edge of the slope (fig. 5.1.11h). By i=60 the form of the current is largely indistinguishable from that in run 9 though the freshwater transport has of course increased (fig. 5.1.11j). Looking in more detail at tracer cross-sections (figure 5.1.12) we can see how the different constituents sit primarily on top of each other forming the density front. Tracer 1, tracking the flow of low salinity water introduced at the northern boundary, shows how this water mass is trapped on the shelf as far south as i=160 (fig. 5.1.12d). However as the shelf narrows, towards Cape Farewell, it spills over the continental slope (figs. 5.1.12g&j). Tracers 2 and 3 show how the fjord outputs do not initially mix. At i=160 tracer 3 is found

predominantly trapped against the coast with the output from the northern fjord further offshore (fig. 5.1.12f). However by i=60 the two outputs have become largely mixed after 240 days of fjord output (figs. 5.1.12k&l).

The very low concentrations of tracer 3 (output from the southern fjord, TF) along the northern section (i=240) are of some interest (fig. 5.1.12c). The low concentrations in the bottom layer on the shelf show that trace amounts of the outflow can travel north in the near stationary bottom layer. The surface concentrations on the eastern domain boundary show the presence of a very weak circulation around the domain edges. The southern boundary ports and relaxation zones were designed to absorb the flow. The very low concentrations of tracer 3 seen in the northern section demonstrate that this has been largely successful.

Model runs 15 to 18 have increased runoff from the two fjord complexes to investigate the potential impact of an increase in melt rate of the Greenland ice cap on the current dynamics. These runs also consider how the situation changes when the main EGC is situated further offshore (runs 17 and 18 are initialised from run 12 with a deeper 500m front located a further 40km offshore). Simply moving the EGC further offshore (fig. 5.1.13c) has little impact. The fjord output behaves in a similar way to run 14, with the stronger offshore EGC simply following the shelf break until the two meet as the shelf narrows in the south. However boosting the output from each fjord to 0.5Sv has a clearer impact on both EGC scenarios (model runs 15 and 18 – figs 5.1.13a&d). In each case the presence of the stronger fjord outflow diverts more of the EGC flow onto the shelf in the region of the two troughs. The tracer data shows that the runoff is still trapped against the coast as it moves south but it is also able to diffuse to the north against the main EGC flow and is seen in low surface concentrations across the width of the shelf in the area of Denmark Strait.

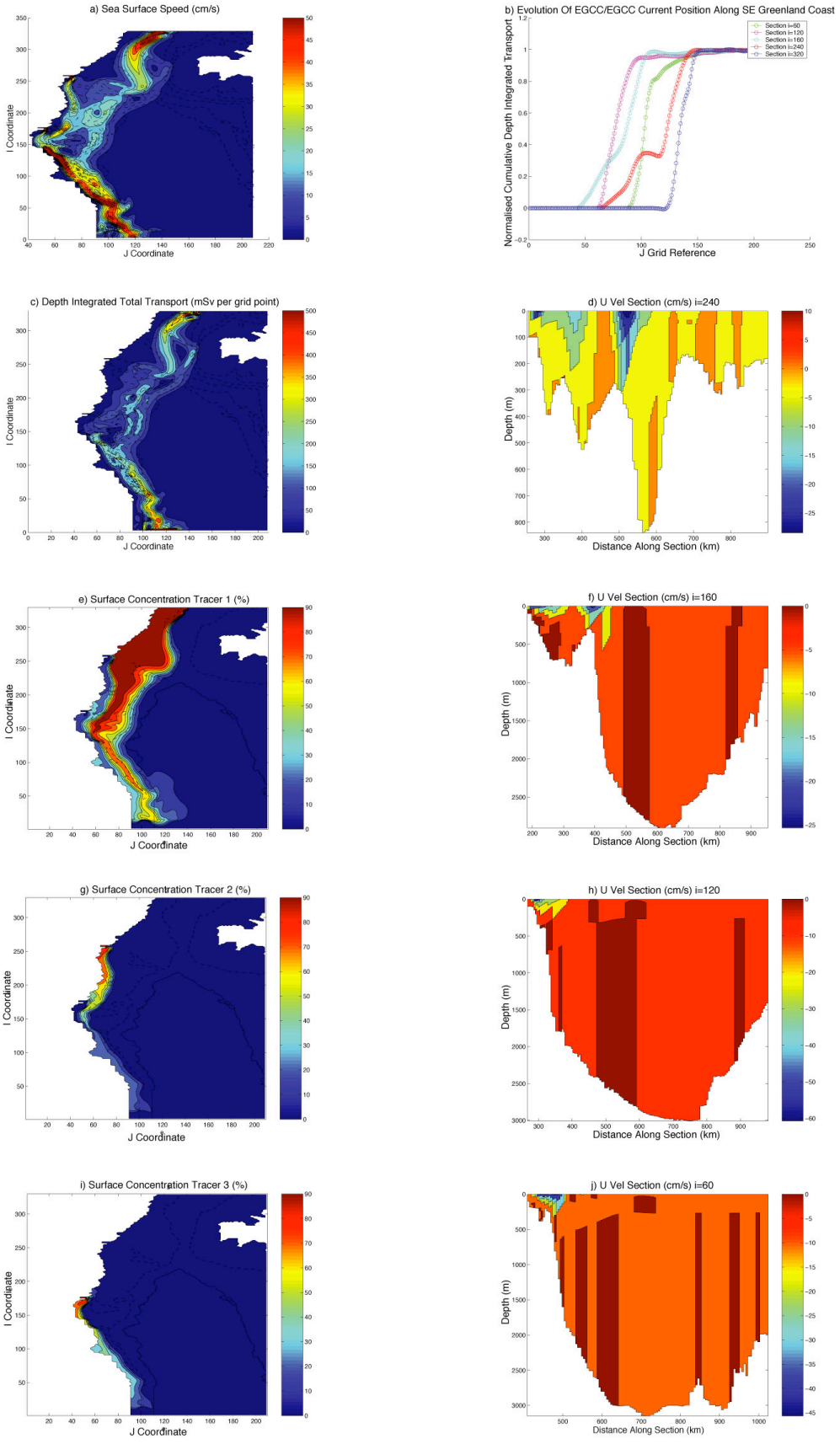

Figure 5.1.11 The impact of fjord runoff of 0.1 Sv, from the two major fjord complexes, on a quasi-realistic EGC. Model run 14 - cumulative run time 600 days

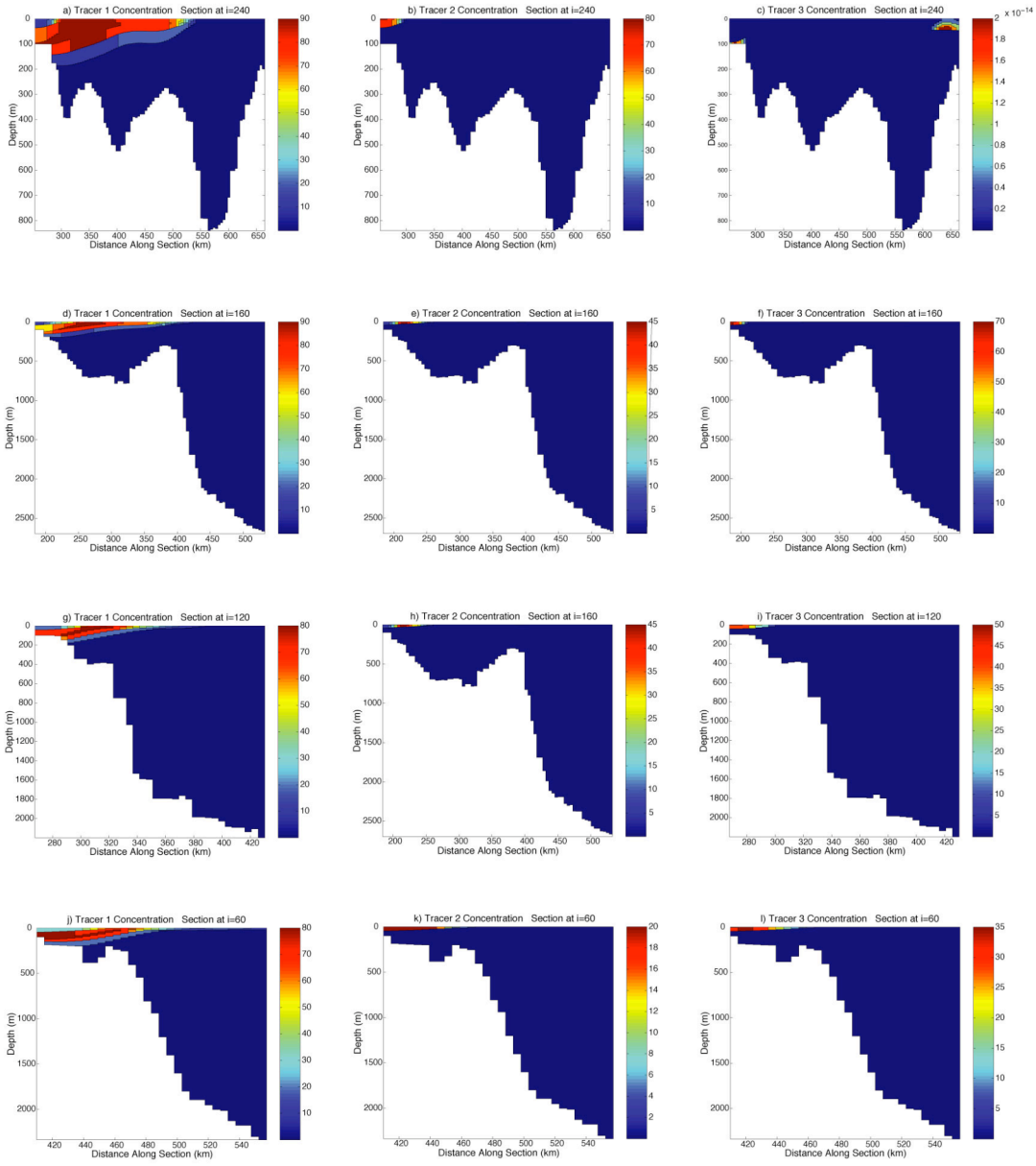

Figure 5.1.12 Detailed cross-sections showing tracer concentrations across the Greenland shelf. Model run 14 - cumulative run time 600 days

Model run 16 further increases output from the two fjords to 2Sv so that their combined output is approaching the same transport as the EGC using the shallower front of run 9. In this case the output from the northern fjord is seen to leave the coast as it turns to the west just before TF. The cumulative transport plot (fig. 5.1.13b) shows far more eddy activity with the increased fjord output whilst tracer cross-sections (fig. 5.1.13e) show the main concentration of northern EGC water (tracer 1) pushed firmly over the slope by i=160. KF fjord outflow water is also seen

to move primarily over the slope by i=120 with TF water forming the major part of the on-shelf current. Even with this level of output it seems that the fjord outflow is only partially able to escape the shelf and the outflow is some twenty times higher than present-day estimates. However, we have not considered the impact of tides that may periodically reinforce the strength of the outflow.

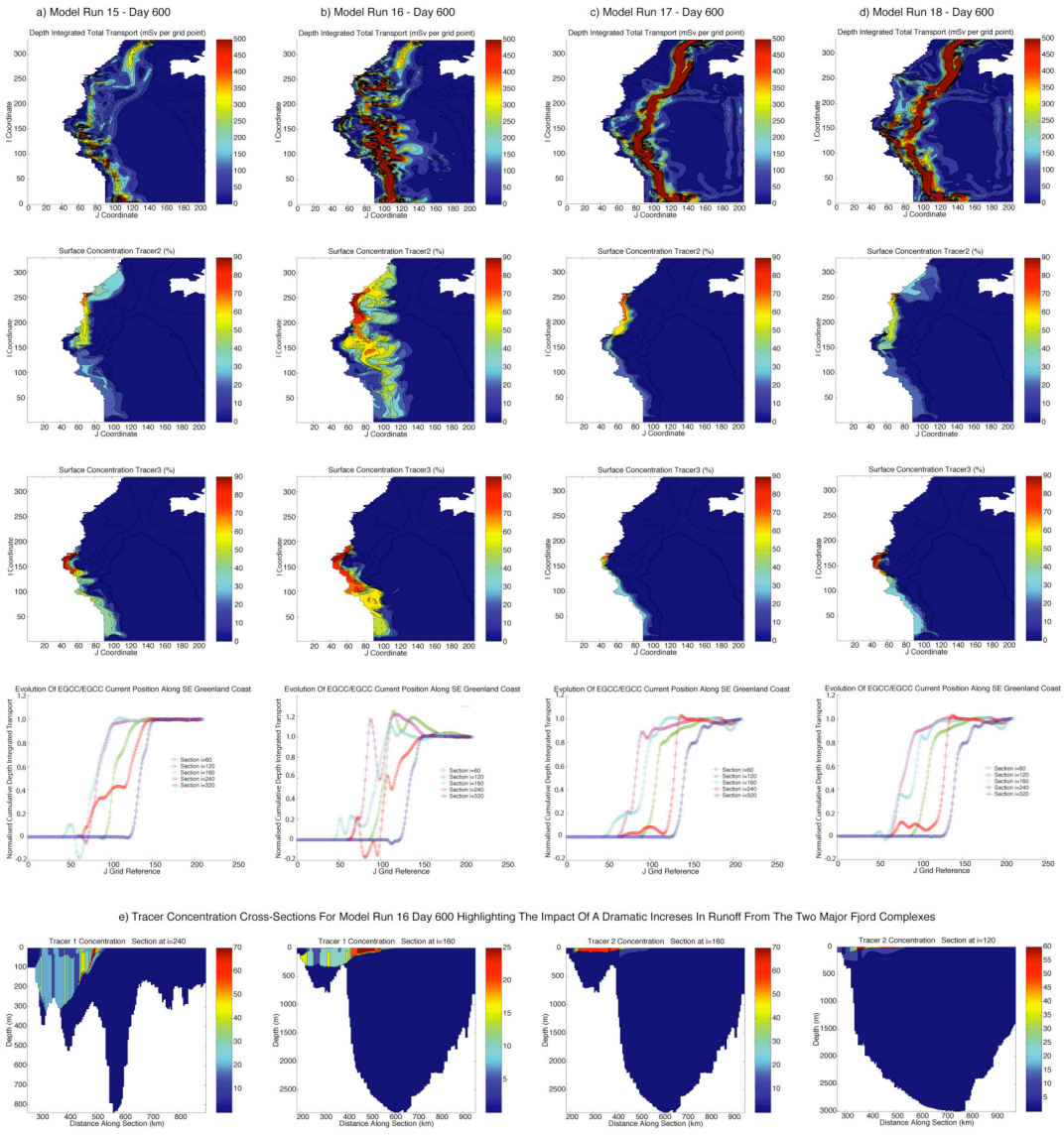

Figure 5.1.13 The impact of increases in fjord runoff on two EGC scenarios

The Role Of Wind Stress

As a final step in building the complexity of the model, to something approaching reality, wind stress was added to the set-up used in model run 14. Two scenarios were run, one with an anticyclonic wind stress pattern (run 19) and the other with a cyclonic pattern (run 20). In each case the maximum stress was chosen to be 0.02 Nm^{-2} based upon typical observed average values in a recent cruise to the area [*Sutherland and Pickart*, 2008]. This corresponds to a wind speed of around 15 km h^{-1}. In both scenarios the wind stress is set to the maximum value over the shelf as far out as j=120, in the case of run 19 it acts towards the north in the direction of the i coordinate whilst in run 20 it acts towards the south. The strength of the wind stress is varied sinusoidally between i=120 and i=210 such that it achieves the maximum value in the opposite direction at the eastern boundary of the model domain. *Sutherland and Pickart (2008)* found that strength and geometry of the current reacted to whether the wind stress was acting to the north (upwelling favourable) or to the south (downwelling favourable).

The cumulative transport plots (fig. 5.1.14a&b) clearly show the wind driven component of the circulation rising as the fetch increases moving to the south. At i=240 there is little impact but by i=60 in model run 19 the on-shelf flow is suppressed by a little over 20% as a result of the northward wind stress. This is compensated for by a southerly flow over the eastern half of the domain. In run 20 the on-shelf transport at i=60 is boosted by a little less, around 18%. The fact that the wind stress superimposes a circulation on the existing flow is of course entirely predictable but the surface tracer plots (fig. 5.1.14) reveal another impact. Tracer 1 and 2 plots for the cyclonic wind stress are almost identical to those for run 14 with no wind stress. However, with an anticyclonic wind circulation opposing the on-shelf current, the current is seen to broaden (fig. 5.1.14a – surface tracer 1). This is due to Ekman transport causing flow to the right of the wind stress driving the higher tracer concentration water away from the coast. This reduces the topographic constraints on the shape of the main current. The main concentration of tracer 1 is clearly displaced to the east so that it lies over a deeper area of the slope with lower concentrations seen to escape beyond into the main Irminger Basin.

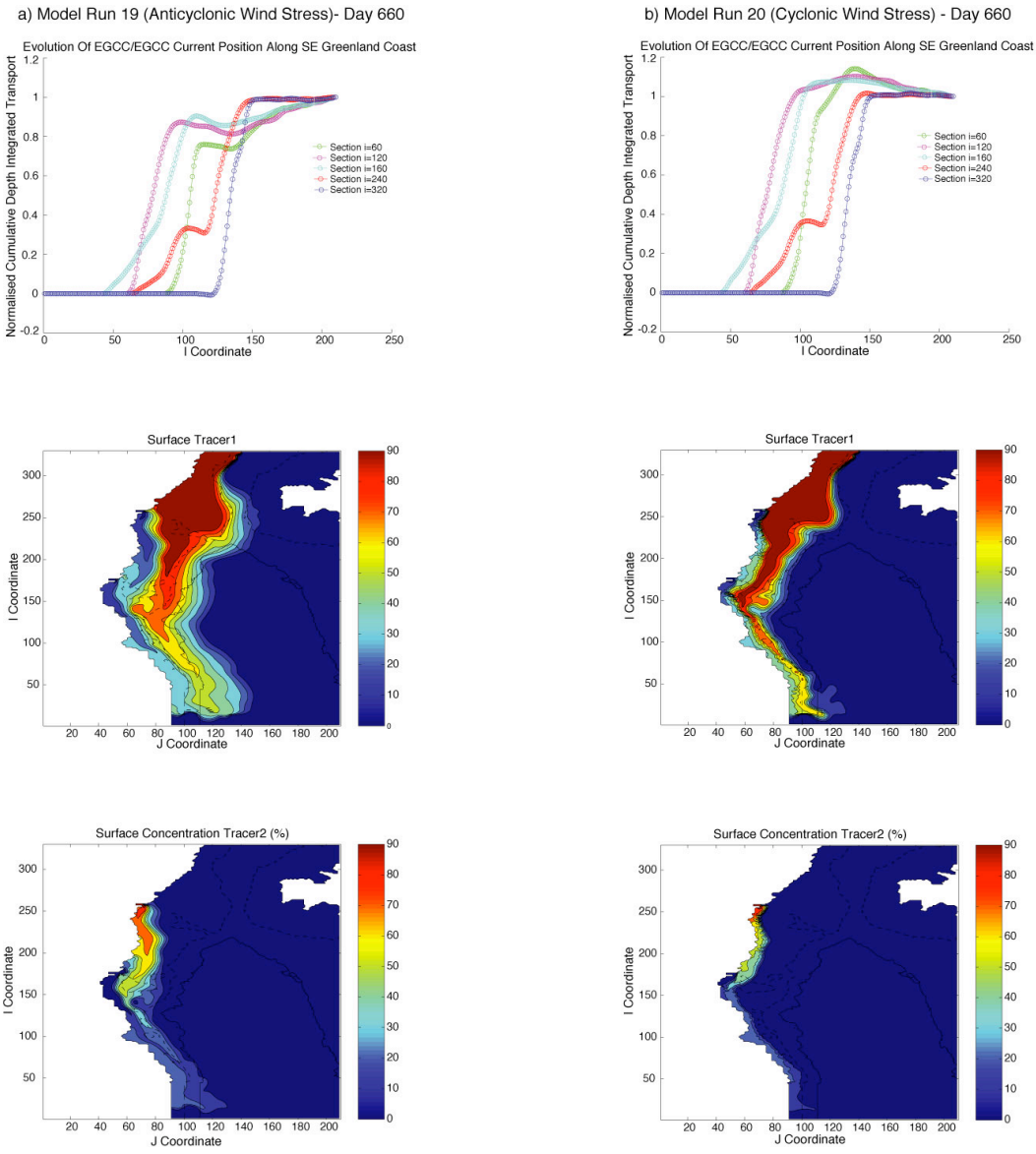

Figure 5.1.14 The impact of wind stress on the EGC/EGCC system

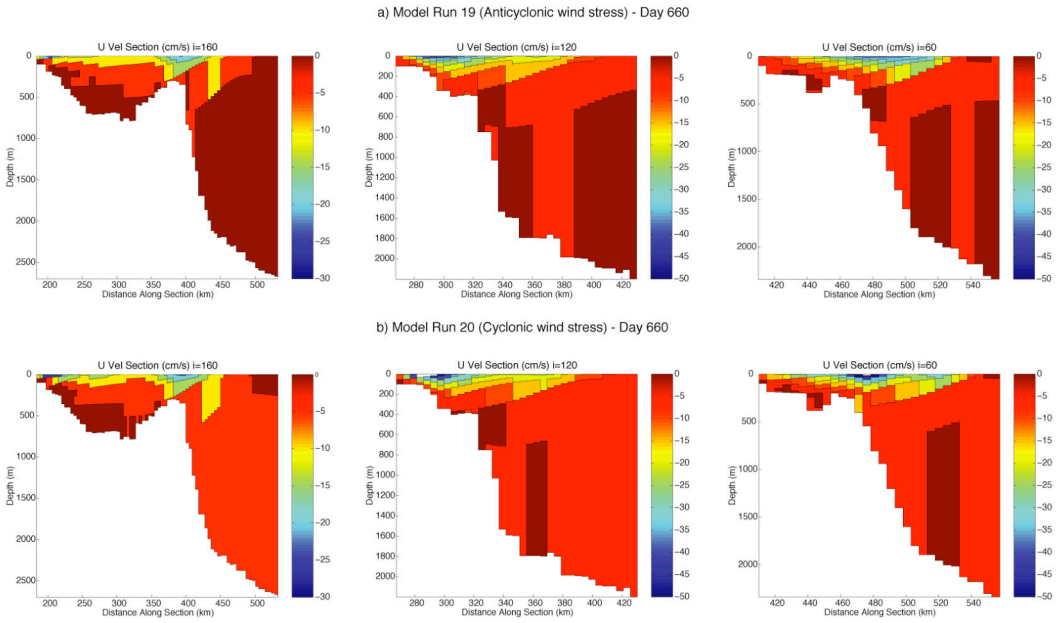

Figure 5.1.15 The impact of wind stress on the cross-sectional structure of the EGC

Cross-sections of the current (fig. 5.1.15) in the two model runs reveal more detail as to how the wind stress affects the form of the flow. Predictably, maximum velocities are increased or decreased depending upon whether the wind stress is reinforcing or reducing the flow. At i=240 the inshore strand of current is weakened in comparison to that at the edge of the shelf in the case of the anticyclonic wind stress (fig. 5.1.15a). Moving south, the cross-sectional plots suggest that the anticyclonic wind stress broadens and shallows the current. However it is also clear that the model lacks both the horizontal and vertical resolution to investigate this phenomenon in detail.

5.1.4 Discussion

The use of model simulations employing a combination of simplified, quasi-realistic bathymetries and climatologies provides an insight into the role played by the various bathymetric, atmospheric and oceanographic components in shaping the EGC/EGCC current system. Although the remote location of the EGC system has historically restricted oceanographic research in the region there are many buoyant coastal currents to be found in more accessible parts of the world. Observational and modelling studies of similar coastal currents [*Gangopadhyay and Robinson,*

2002], in addition to those focussing on the EGC system, can usefully be compared to the results of this study.

The simplified HYCOM model runs confirm the expected influence of the bathymetry on the path of the EGC. The path of a barotropic current is strongly controlled by the bathymetry. Geophysical fluid dynamic theory predicts that a barotropic current should follow lines of constant potential vorticity in the absence of forcing [*Hough, 1897*]. The potential vorticity is calculated as the ratio of the Coriolis parameter to the depth (f/H). For a flat bottomed ocean potential vorticity contours follow lines of latitude but with the complex bathymetry around the Greenland shelf break the variation in depth dominates and potential vorticity contours more closely follow the isobaths.

Strong topographic steering of barotropic currents has been observed in many locations around the world. On the eastern seaboard of North America the shelf break current flowing from the Scotian Bank to the Georges Bank is typically seen to follow the bathymetry around the Northeast Channel at the entrance to the Gulf of Maine. However periodically the current breaks free from topographic influences and flows directly across the mouth of the Northeast Channel. *Williams et al.* (2001) employed a finite difference numerical model to investigate the effect of topography on a barotropic shelf-break jet, particularly with respect to corners and channels in the continental shelf. They found that a modelled barotropic shelf-break jet followed the bathymetry around a right angle bend for inflow speeds of up to 2m/s. Similarly the flow followed the bathymetry around narrow channels with slope widths of 55km. This channel geometry was chosen to represent the Northeast Channel into the Gulf of Maine. The occasional flows across the channel mouth could not be replicated in their barotropic jet model and *Williams et al.* (2001) suggested that the switch to the alternative pathway could be triggered by increased stratification or wind stress. On a larger scale the Antarctic Circumpolar Current (ACC) is also seen to diverge from potential vorticity contours [*Marshall,* 1995]. The ACC would not pass through the Drake Passage if it were constrained to follow potential vorticity contours. *Marshall* (1995) was able to replicate the observed circulation circumnavigating the Antarctic continent in an analytic model by introducing stratification with a quiescent bottom layer. The role of stratification in reducing the

strength of topographic steering is widely accepted (e.g. [*Gill,* 1982]) but it is difficult to quantify this effect resulting in the need for regionally specific numerical models to investigate the detailed behaviour of individual coastal currents. The length scales associated with changes in the topography along the East Greenland shelf are relatively large in comparison with the Northeast Channel and so it is consistent with the work of *Williams et al.* (2001) that stratification and baroclinic currents must be introduced in order to see significant divergence between current pathways and isobaths in the model results.

Although a simple barotropic current is well constrained to follow isobaths we can see that a varying width shelf (run 5) can cause a baroclinic current, initially located over the slope, to bifurcate. It is difficult to derive a mathematical relationship between the strength of the topographic steering torque and the depth of the current but the model allows this relationship to be explored. The key bathymetric features affecting the flow in the region are clearly the overall shape of the continental shelf and the troughs extending from the two major fjord complexes (KF and TF). We can see how the combination of frontal position and depth controls the path of the EGC as it flows equatorward. Currents extending to the sea floor, and positioned over the inner slope, will follow around the trough isobaths. Deeper currents located further offshore are locked to the main shelf edge and are largely unaffected by the troughs in the shelf. Very shallow currents will turn into the coast although they can be supported for some time along the front formed by a previously stronger current. The way in which the slope current can split and recombine depending on its exact position and depth highlights the difficulty in trying to define the EGCC as a distinctly separate current from the EGC.

The regional model allows us to use any combination of frontal position and depth although in reality the two may be related and tied to the EGC transport north of Denmark Strait. It seems likely that the EGC further north is also topographically steered and is found over a depth consistent with the frontal depth. However models runs 7 and 8 demonstrate that short-term changes in frontal depth may not result in an immediate response in the position of the current. This creates a problem when interpreting single-point-in-time data and reinforces the need for long-term monitoring arrays.

These results clearly support the hypothesis, proposed by *Sutherland and Pickart* (2008), that the EGC is bifurcated in the vicinity of Denmark Strait as a result of the shelf geometry. For all but the deepest offshore currents a significant proportion of the EGC moves on to the shelf where it broadens in the area of Denmark Strait. Runoff from the fjords is consistently trapped close to the shore and is not seen to reinforce the inner strand of the EGC until south of TF (in the region of i=160 in the model domain). This raises questions about the use of the name EGCC. Is the name appropriate for any current found over the shelf or should its use be limited to a current that is significantly the result of local freshwater runoff? The model results suggest that the on-shelf currents in the region of TF observed in the 1960s [*Malmberg et al.*, 1972] could well be the main EGC with the local runoff trapped closer to the coast. It is regrettable that neither, the Norwegian cruises in the 1960s, nor the 2004 cruise of *Sutherland and Pickart* (2008) crossed the entire shelf and slope in this area in order to ascertain whether there was also a significant current over the slope. If there is not, and the mid-shelf current in the region of TF is simply a continuation of the EGC, then is it sensible to rename it the EGCC? The model results suggest that there is likely to be some flow over the slope and this could be considered the EGC even if it is significantly weaker.

Further south, as the shelf narrows approaching Cape Farewell, the model struggles to replicate the isolated on-shelf current seen in observational data with even the local coastal runoff appearing to merge with the over slope current. This could be due to a lack of resolution given the narrow shelf and shallow depths. Some of the idealised bathymetry runs actually create a better on-shelf current. One possible conclusion that could be drawn from the model results is that the EGCC, as identified by *Bacon et al.* (2002*)*, is primarily driven by local runoff, but that it is not a continuation of the on-shelf flow, further north, more recently considered the EGCC by *Wilkinson and Bacon* (2005) and *Sutherland and Pickart* (2008). Once again this demonstrates the difficulty in distinguishing between the EGCC and EGC, whether by location or by source.

There is a significant body of scientific literature covering buoyant inflows and the resultant plumes, fronts and coastal currents. Although the full spectrum of

observational studies, tank work, analytical and model simulations is covered the research is mainly focussed on smaller scale, isolated riverine inputs. The East Greenland region differs from the more typical areas studied in three key ways. Firstly, there are many sources of freshwater along the coast making it difficult to consider the role of a single discharge in isolation. Secondly, there are multiple fronts interacting within a small area; the local front due to the nearest freshwater source, the low salinity flow from other sources further to the north and the main Polar Front between the outflow from the Arctic Mediterranean and the warmer North Atlantic circulation (the Irminger Current). Finally, the steep shelving coastline and fjord sides are in contrast with the more typical shallow river mouths that discharge a relatively homogeneous output onto gently inclined coastal shelves. Despite these differences it is worth considering, at least qualitatively, how some of the key hypotheses in the literature compare and contrast with the results of this regional model study.

For a homogeneous buoyant discharge flowing into homogeneous shelf waters simple theory predicts three characteristic plume geometries are possible dependent upon on the parameters of the inflow [*Yankovsky and Chapman,* 1997]. The expected plume geometry can be predicted by the relationship between the theoretical maximum dimensions of the plume, horizontal (y_s) and vertical (h_b) and the bathymetry. Where the expected maximum depth of the plume, h_b, is less than the depth of the river mouth and its coastal shelf a surface advected plume results. Bottom advected plumes form when the isobath corresponding to h_b is further offshore than y_s. Intermediate plumes occur when the h_b isobath is inshore of y_s.

Yankovsky and Chapman (1997) derived expressions for the two keys parameters controlling the extent of a simple plume as follows:

$$y_s = 2(3g'h_0 + v_i^2)/(2g'h_0 + v_i^2)^{1/2} f \qquad h_b = (2Lvh_0 f/g')^{1/2}$$

Where: g' is the reduced gravity

h_0, L and v_i are the depth, width and velocity of the buoyant inflow

f is the Coriolis parameter

Illustrative values of these two parameters for a low salinity plume in the vicinity of the south-east Greenland shelf are shown in table 5.1.3. The predicted surface extent of the plume is approximately four baroclinic Rossby radii.

No.	Fresh Water Input (Sv)	Inflow Sal.	Inflow Temp. (C)	Inflow Velocity (m/s)	Inflow Depth (m)	Inflow Width (m)	Inflow T'port (Sv)	h_b (m)	y_s (m)	Baroclinic Rossby Radius (m)
1	0.02	0	0	0.13	10	25,000	0.02	4.45	52,587	12,392
2	0.02	28	-1	0.13	50	25,000	0.10	22.83	51,199	12,065
3	0.02	30	0	0.13	70	25,000	0.14	32.21	50,807	11,973
4	0.02	32	0.5	0.13	119	25,000	0.23	54.89	50,178	11,825
5	0.02	33	1	0.13	177	25,000	0.35	84.22	48,851	11,512
6	0.02	34	1.2	0.13	350	25,000	0.70	183.85	44,504	10,487
7	0.01	28	-1	0.27	12.5	25,000	0.05	16.14	25,681	6,033
8	0.1	28	-1	0.13	250	25,000	0.50	51.05	114,465	26,978
9	0.2	28	-1	0.13	500	25,000	1.00	72.19	161,874	38,153
10	0.02	28	-1	0.03	250	25,000	0.10	22.83	114,460	26,978

Table 5.1.3 Example plume dimensions after *Yankovsky and Chapman* (1997) for a plume flowing into an ambient water mass of density 1027.8 kg m^{-3} at 65° latitude

Scenarios 1 to 6 in table 5.1.3 illustrate the potential variation in plume geometry with a fixed freshwater flux but different degrees of mixing and exchange in the fjord. The highlighted scenario corresponds to the low salinity flux used in the weaker fjord output model runs. Although the model allows some mixing and exchange within the fjord clearly the parameterisation of the fjord dynamics chosen for this study are destined to produce surface plumes. The choice of this parameterisation is a based upon observational data from Kanferlugssuaq Fjord [*Azetsu-Scott and Tan,* 1997]. As the large fjords in the region, and their associated cross-shelf troughs, have depths in excess of 400m it is extremely unlikely that there would ever be a sufficient combination of freshwater and mixing to develop a bottom controlled plume within the region of the trough. However as the resultant coastal current leaves the trough and turns along the coast it encounters shelf waters of between 100 and 200m in depth. Although there is greater potential to produce a plume front extending the full depth of the shelf on leaving the region of the trough this would still require somewhat greater inflows and mixing than seen in the observational data. This supports the hypothesis that the near shore baroclinic component of the EGC identified by *Malmberg et al.* (1972) could be driven by

local runoff while the mid-shelf current with a baroclinic component is more likely to be a bifurcation of the EGC.

Predicted plume geometry also provides an insight into why the model simulation fails to replicate the separate near-shore baroclinic jet in the vicinity of Cape Farewell. The use of a fjord parameterisation that produces a surface plume is unlikely to be the problem. A bottom-controlled plume would require too large an inflow and would produce a current with a barotropic component. The likely explanation is that the southern fjord flow used in the simulations was too large and the regional input would have been better represented by a larger number of smaller inflows. Scenario 2 in table 5.1.3 shows a predicted plume extent of around 50km, thus positioning its offshore edge in the region of the shelf break near Cape Farewell. However reducing the freshwater flux by a factor of two, with a corresponding reduction in thickness (scenario 7 in table 5.1.3), produces a plume with a maximum theoretical extent of only 26km, sufficiently small to produce a distinctly separate coastal current. The way in which multiple fjord outputs of different strengths might combine along the East Greenland coast is a subject that justifies further investigation.

The work of *Azetsu-Scott and Tan* (1997) looking at oxygen isotope ratios in the KF and KT can also be used to support some of the modelling results. They identified three water masses based upon oxygen isotope ratios: glacial meltwater, Polar Water carried by the EGC and North Atlantic Water. Their plots of near surface water isotope ratios show mixing between the first two occurring within the fjord and out to a distance of about 50km from the fjord mouth. From 50km to 250km offshore the isotope ratio is fairly constant before changing again crossing the polar front. These distances help define the extent to which the runoff penetrates the shelf (50km) and the position of the main EGC (50km to 250km offshore). These figures compare well with the results of model run 14 (fig. 5.1.11). The high concentrations of tracers 1 and 2 at i=240 coincide almost exactly with the oxygen isotope data. This suggests that the quasi-realistic run with fjord output of 0.1Sv is a good representation of the current situation, at least in the vicinity of KT. However as discussed in the previous paragraph the near shore current in the vicinity of Cape Farwell may be driven by more localised inflows with smaller plumes. Future

oxygen isotope studies along the length of the southeast Greenland shelf could provide the answer as to which parts of the EGC/EGCC system are fed by which freshwater sources.

Much of this paper has concentrated on a qualitative interpretation of the model output. The high quantity of numerical output available would support a more quantitative approach. However there are a number of weaknesses that it seems necessary to address before moving to a more detailed style of analysis:

Additional observational data

Observational data are required to setup the model's initial state, to define the boundary conditions and to test the accuracy of the model output. The available data comprise a limited number of sections (less than 100) that inadequately sample the current system from both a spatial and temporal viewpoint. To build up a good time series requires significant investment over a long period, but we can better define the initial state and present day boundary conditions by concentrating on the key areas identified by the model simulations. New observational data could help us better understand: the position and depth of the Polar Front north of Denmark Strait, the outflow from the major fjord complexes (including the impact of the tidal sequence on current velocities) and the transport distribution across the full width of the shelf and slope just to the south of Denmark Strait.

Modelling Refinements

The model domain employed has weaknesses both in terms of spatial coverage and resolution. Retroflection of the current at Cape Farewell *[Holliday et al.,* 2007*]* could have potentially significant impacts on surface salinity in the Irminger Basin and could cause a recirculation that impacts the EGC system further north. The spatial resolution in the region of the EGC has been shown to be insufficient both where the shelf is narrow and shallow and when looking at the impact of wind stress on the depth and breadth of the current. Unfortunately with constraints on run time we can only improve one of the two at the expense of the other. The ideal solution is a variable mesh model that can change the resolution in a given area to suit the

dynamics at the time. This is much more efficient, as in much of the domain there is only limited activity and only low resolution is required. Such models are really only in the development phase but it would be possible to gain some of the benefit by using the nesting facility already available within HYCOM. A high-resolution shelf and slope model could be embedded within a lower resolution model of the Irminger and Labrador Basins.

The simulations in this study were all based upon idealised climatologies that excluded the other main currents of the area, the Irminger Current and DWBC. The simplified scenarios are of great benefit in understanding the role of specific components of the system (e.g. bathymetry, runoff and wind stress). To improve the realism of the simulation it is necessary to add further detail to the initial climatology and introduce the effects of tidal mixing. Such an approach would benefit from the additional observational data and more advanced modelling techniques already discussed.

6 CONCLUDING REMARKS

6.1 Overview

As discussed in chapter 3.2, the development of oceanographic sensors has dramatically increased the amount of data that can be collected by observational oceanographers. However, it remains true that the ocean is very much still under-sampled both from a spatial and temporal point of view. This is particularly the case in inhospitable and difficult to access areas such as the Irminger and Labrador Basins. The combination of new oceanographic and sedimentary data from the Eirik Ridge region, off Southern Greenland, has the potential to reveal some aspects of the relationship between climate change and North Atlantic Deep Western Boundary Current variability. Unfortunately this relationship is not a simple one and there are a number of component problems to address before considering the region's role in the global climate system.

When looking in more detail at the spatial and temporal variability of an ocean current it is necessary to consider the inherent averaging effects of the different techniques employed to measure current strength. The more modern direct current speed detectors (such as ADCPs and current meters) appear to have clear advantages over non-direct approaches such as the dynamic method. However, direct current measurement has the disadvantage of being spatially very localised and, in the case of the ADCP, also temporally very specific. The work of *Dickson et al.* (1999) on the DWBC has shown how lateral movements in current position can complicate the interpretation of data collected by a finite number of current meters placed at intervals across the expected path of the flow. The dynamic method has the advantage of inherent spatial and temporal averaging determined by the station separation and the response time of the isopycnals. However, the dynamic method only provides velocity shear data and a reference velocity is required to determine absolute velocities and current transports. Ideally this reference velocity would be determined by a reasonably dense network of current meters placed across the path of the current. Unfortunately this type of setup is very expensive and so is rarely available. The use of sedimentary proxies provides the

most extreme averaging as it looks at depositional characteristics with a typical resolution of decades. For this reason it can appear easier for the palaeoceanographer to draw broad conclusions about changes in past current strength and position than it is for the modern day physical oceanographer to talk with authority about changes taking place over periods varying between months and decades. Without large quantities of continuous, high spatial resolution data the observational scientist is exposed to the problem of capturing isolated data points that do not reflect the mean flow in the area. Unfortunately palaeo-data alone does not enable us to gain the level of detailed understanding of ocean dynamics required to confidently predict future interactions between the ocean current and earth climate systems. By comparing ocean current proxies and water mass characteristics with climatic indicators it is possible to make rational deductions about how the two interact which allow qualitative judgements about future changes in climate and ocean circulation to be made. In order to make accurate predictions of climate change in an age of anthropogenic CO_2 emission driven global warming a more quantitative understanding of the dynamics of the system are required. The required predictive capability requires reliable Earth system models that have been tuned against modern day observations and palaeo-reconstructions.

In an attempt to overcome the limitations of the individual oceanographic techniques the results presented in this thesis bring together all the available sources of observational data, thus constraining their interpretation to the greatest possible extent. Regional computer modelling has been used to further substantiate the resultant observation-based theories and to provide a more detailed understanding of the system dynamics.

6.2 Summary Of Results

The interpretation of historic hydrographic data for the East Greenland Shelf, presented in chapter 4.2, involved some major assumptions. An assumed level of no motion at the ocean floor was combined with a theoretical frontal model in order to estimate freshwater fluxes. Despite the degree of uncertainty introduced by these assumptions the analysis still provides convincing evidence that the EGCC is not primarily driven by runoff from southeast Greenland, as had been previously suggested [*Bacon et al,* 2002]. Subsequently the results of a 2004 James Clark Ross cruise [*Sutherland & Pickart,* 2008], aimed specifically at investigating the EGCC, revealed the structure and spatial evolution of the current in much more detail. Although these results revealed some of the shortcomings of the assumptions made in *Wilkinson and Bacon* (2005), they concluded that the EGCC was primarily a bifurcation of the EGC rather a result of local South-East Greenland runoff. Combining the results of the two papers provided the starting point for the regional modelling study covered in chapter 5.1. These modelling simulations help develop a more detailed understanding of the interactions between the shallow current system and the bathymetry. They clearly demonstrate how a single surface intensified current positioned over the slope can bifurcate as a result of the geometry of the shelf break. The complex on shelf bathymetry resulting from the troughs formed at the mouths of the region's fjords further complicates the behaviour of the resultant multi-current system. The model results suggest that the relative strengths of the on-shelf (EGCC) and slope (EGC) currents are influenced by the position and depth of the EGC just to the south of Denmark Strait. The way in which runoff from South-East Greenland interacts with the established EGC/EGCC system is also dependent upon the position, strength and structure of the EGC entering the region.

The study of the deep current system benefitted from new data collected on a research cruise specifically tailored to the requirements of this work. Cruise D298 provided high resolution hydrographic, water tracer and sedimentary data collected from carefully chosen locations. This data was subject to a multi-disciplinary analysis with Dr. Sally Hunter providing the sedimentology input.

The analysis of the transmissivity data confirms that, in the modern ocean, the highest sediment load in the DWBC is carried by the DSOW component. This could be expected given the shorter and more direct route that DSOW travels between the GIS ridge and Eirik Drift when compared with ISOW. However, the likelihood that this would also have been true during the main drift-building period must be considered when utilising Eirik Drift sedimentary data as proxies for DWBC strength in the region. Our results showing the different depth dependent pathways are something of a departure from conventional thinking and, if based upon hydrographic data alone, some of the assumptions could easily be challenged. However, when combined with the tracer data analysis, the overall argument becomes much more persuasive and was well received by the reviewers acting on behalf of Deep Sea Research. The depth dependent pathway hypothesis suggests a complex relationship between deep current strength at individual locations around the Eirik Drift and the overall DWBC strength further south off Newfoundland. It is the latter which is significant in determining the strength of THC and so we need to gain a good understanding of these relationships if we wish to make associations between local deep current strength in the Irminger Basin, THC strength and global climatic patterns. Attempting to infer North-Atlantic, and even global scale, circulation dynamics is difficult from a very localised dataset and the hypotheses should be tested against observational data from further a field and against model simulations. I had originally hoped to investigate the hypotheses proposed in the observational study using a series of HYCOM scenarios. Unfortunately the modelling work was delayed by about a year due to problems with the implementation of the HYCOM model. As a result the deep current modelling work was restricted to a single proof of concept run rather than a series of runs that would allow the complexity of the simulation to be built up in a similar way to that employed in the surface current system modelling study (chapter 5.1).

The HYCOM domain employed for the proof of concept run covered the northern North Atlantic from just north of the Greenland-Iceland-Scotland Ridge down to the latitude of the Grand Banks of New Foundland (see fig. 6.2.1). The model domain was set up with a 306 by 260 horizontal grid and 20 hybrid layers providing a horizontal

resolution of approximately 10km. The bathymetry was taken from the satellite bathymetric dataset of *Smith and Sandwell* (1997) and the initial climatology from *Levitus* (1998) with the exception of a homogeneous deep-water reservoir in the Arctic Mediterranean.

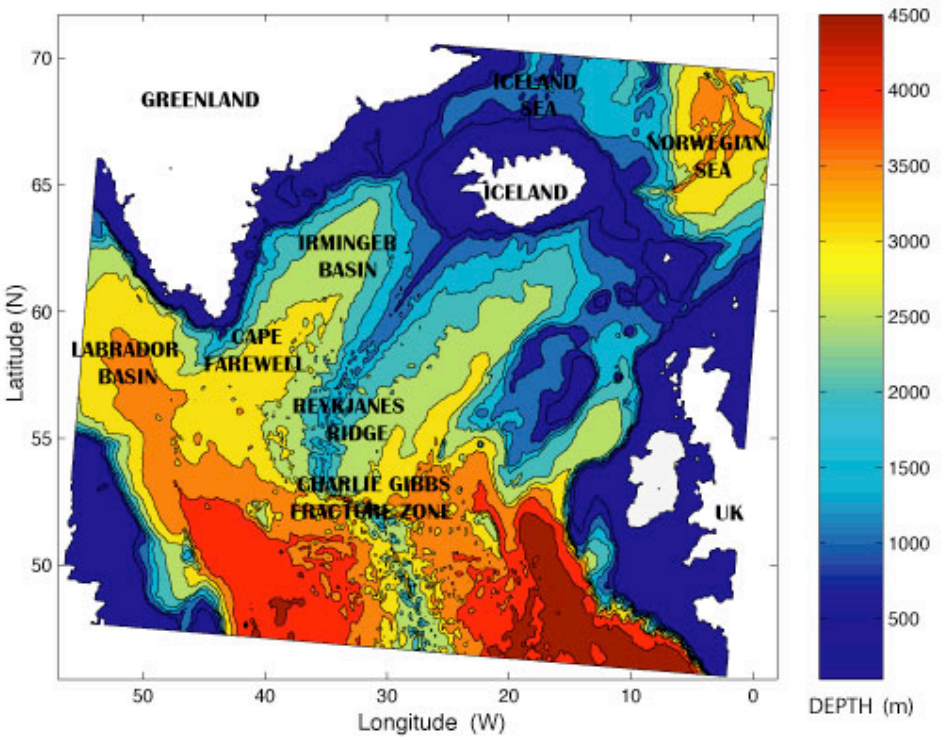

Figure 6.2.1 North Atlantic model domain with *Sandwell and Smith* (1997) bathymetry and key geographic features.

The aim of the run was to reproduce and track the flow of overflow water crossing the GIS Ridge. For simplicity the reservoir of dense water in the Arctic Mediterranean, that drives the overflows, was represented by a homogeneous water mass (salinity 35 and temperature -2^{o}C) extending down from a depth of 500m. The pathways followed by the overflow waters are marked by contours of bottom layer temperature after a 720 day run (figure 6.2.2).

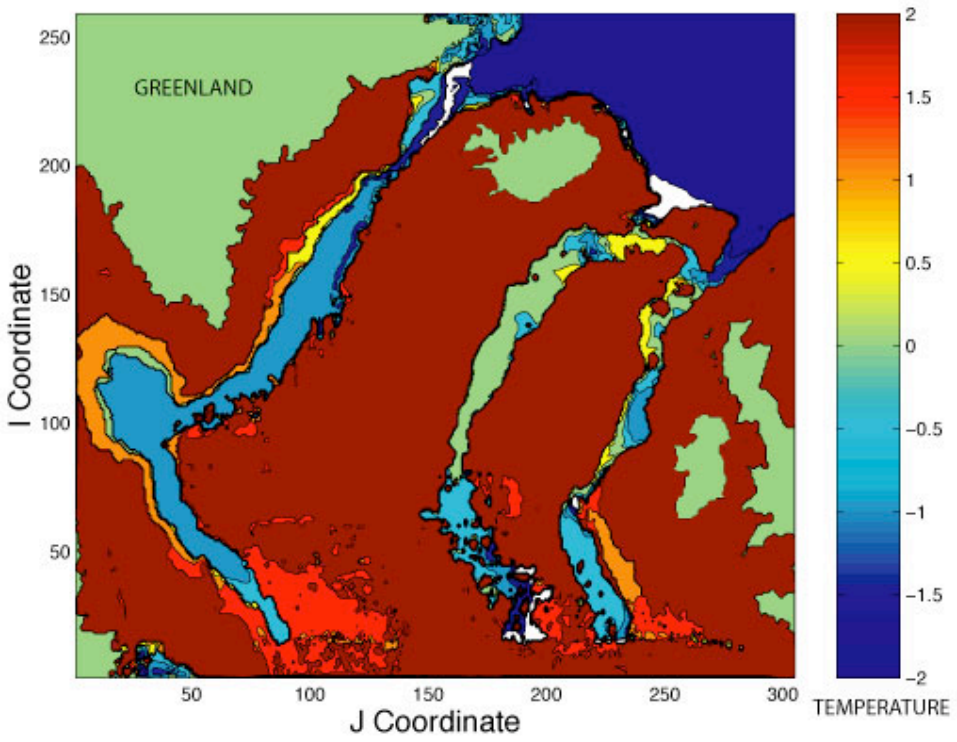

Figure 6.2.2 Contour map of bottom layer temperature after 720 days. The northern reservoir temperature was set to -2^{o}C and the interface depth to 500m

Transport times for DSOW to Cape Farewell and ISOW to the Charlie Gibbs Fracture Zone are of the order of 6 months. These times are at the lower end of estimates from tracer data [*Smith et al.,* 2005*; Smethie and Swift,* 1989]. The pathway of DSOW is in reasonable agreement with observational data, although a large proportion of the coldest water flows directly across the Labrador Basin rather than following the shallower depth contours of the continental slope. However, the flow of ISOW shows two clear departures from observations. Firstly there is no flow of ISOW through the CGFZ. In figure 6.2.2 the strand of ISOW flowing along the eastern flank of the Reykjanes Ridge turns slightly to the southeast as it passes the CGFZ and proceeds towards the southern Atlantic. Secondly the main overflows passing through the Faeroes-Shetland Channel proceed directly south rather than flowing to the west and then south along the flanks of the Reykjanes Ridge. This strand of ISOW creates a flow parallel and to the east of that coming off the flank of the Reykjanes Ridge.

The departure of these results from observations could be due to the use of an excessively dense northern reservoir with too great a density contrast to the ambient waters of the northern North Atlantic. The resultant current patterns are still of some interest as they could represent extreme examples of the density dependent pathways discussed in *Hunter et al.* (2007). Unfortunately, the lack of any ISOW flowing into the Irminger Basin makes it impossible to investigate some of the more subtly different pathways suggested by *Hunter et al.* (2007). A detailed investigation of the model is required to achieve a more realistic simulation (discussed further in section 6.3).

In conclusion, I suggest that both the surface and deep current systems off Southern Greenland are more complex than initial studies suggested. In particular the tendency for spatial movement in current paths must be considered when interpreting both modern physical oceanographic data and palaeo-data. Improving our understanding of this crucial component of the climate system will require the iterative development of modelling and observational research. The results presented in this thesis may well pose more questions than they answer, however these questions identify many areas for future research and these are discussed in the next section.

6.3 Future Work

In order to better understand the circulation of the northern North Atlantic, and its role in global climate change, advances in both observational physical oceanography and numerical modelling are required. The results and experiences of this doctoral research project present avenues for future research in the development of general techniques and specific regional studies.

Observational oceanographers using numerical modelling to support their research would benefit from a robust, state of the art, regional model with well-developed user interfaces. For the purposes of studying the current system off southeast Greenland a user-friendly variable mesh or adaptive mesh model would be particularly useful. Such a tool would have been able to cut the time taken on the modelling in this thesis by a factor of about ten as well as producing higher resolution results.

There is potential to better understand how current velocity datasets drawn from different sources (current meters, ADCPs and geostrophic velocity shears) relate to each other. There is little in the literature comparing data gathered via these different techniques. Using the different observational tools to collect synchronous, high resolution time series data for a range of reasonably small, and easily accessible areas would provide a better understanding of adjustment periods and the inherent temporal and spatial averaging effects of the different techniques.

Looking more specifically at the Greenland region, the results of the surface current studies highlight particular areas where further observational data collection is required. There is little detailed knowledge of the current dynamics at the mouths of the major fjord complexes and a general lack of good time series data across the shelf. Although *Azetsu-Scott and Tan* (1997) collected water property data in the Kangerlugssuaq Fjord they lost their current meter as a result of ice movement. The model runs, discussed in chapter 5, represent the South East Greenland coastal freshwater runoff with only two major fjords. The significance of this assumption could be tested using model

simulations that vary the number of inflows and its accuracy by the collection of more detailed observational data in and around the regions fjords. Modelling simulations also suggest that an important area to study is the region of the Polar Front, just to the south of Denmark Strait. It would be valuable to track the position and depth of the Front together with the associated current structure to analyse how any variations in this area are reflected in the current system further south.

The deep current studies have inferred basin scale and wider circulation patterns from data collected mainly around the Eirik Drift. The resultant hypotheses concerning the role of changing overflow water characteristics on the pathways followed by the deep currents in the northern North Atlantic could be tested and refined by the collection of further observational data and the study of high-resolution model simulations of the region. Ideally a new observational program would collect data from a number of key regions in the northern North Atlantic. Areas of particular interest include the overflow zones of the Greenland-Iceland-Scotland Ridge, the Charlie Gibbs Fracture Zone and Eirik Ridge. Data would need to be collected over intervals that take allowance of the transit times between the different locations. To collect sufficient data to build time series for the region would be a significant undertaking but there are smaller scale projects that could be undertaken at the individual locations along the suggested pathways of the deep flows. Modelling studies present a cheaper way to test these hypotheses. A regional model implementation capable of resolving the different pathways and actually representing the overflow dynamics is required. The early results using HYCOM, discussed previously, show some promise but also major deviations from the observed circulation. A more comprehensive modelling study is required that builds up the complexity of the simulations in terms of bathymetry and climatology. This will allow a more detailed understanding of the roles played by the various components of the system to be built up culminating in a more realistic simulation of the present day circulation. Once this has been achieved it will be possible to explore how changes in the properties of the Arctic Mediterranean reservoir impact upon the overflow rates and the deep current pathways in the northern North Atlantic. Of particular interest would be how changes in the characteristics of the northern reservoir

influence the deep current pathways in the northern North Atlantic and the resulting impact on the correlation between the strength of the DWBC at Cape Farewell and its strength further south off New Foundland. This correlation is of key importance when assessing the value of DWBC strength off Southern Greenland as a proxy for the strength of the global thermohaline circulation. Moving beyond a regional ocean model it would be valuable to use a global coupled model allowing changes in the Arctic Mediterranean basin to be induced with climatic variations than rather being forced with oceanic boundary conditions. Such a model could be used to recreate palaeo-circulations and to investigate the potential impact of global warming. To develop a global coupled model with the required resolution to accurately represent the particular features of interest in the northern North Atlantic will require efficient variable mesh modelling combined with advances in computing power if runs times are to be of a practical length.

7. REFERENCES

Aagaard, K. and E. C. Carmack (1989). "The Role Of Sea Ice And Other Fresh Water In The Arctic Circulation." Journal Of Geophysical Research **94**: 14485-14498.

Aagaard, K. and P. Greisman (1975). "Toward new mass and heat budgets for the Arctic Ocean." Journal Of Geophysical Research **80**: 3821-3827.

Aagaard, K., J. H. Swift, et al. (1985). "Thermohaline circulation in the Arctic Mediterranean Seas." Journal Of Geophysical Research **90**: 4833-4846.

Aagard, K. and L. K. Coachman (1968). "The East Greenland Current north of Denmark Strait." Arctic **1**: 181-200.

Alvarez, M., F. F. Perez, et al. (2004). "Physical and biogeochemical transports in the North Atlantic subpolar gyre." Journal Of Geophysical Research **109**(C03027).

Arthur, M., S. P. Srivastava, et al. (1989). Seismic stratigraphy and history of deep circulation and sediment drift development in the Baffin Bay and the Labrador Sea. Proceedings of the Ocean Drilling Program, Scientific Results. S. P. Srivastava, M. Arthur, B. Clement and e. al. College Station, TX, Ocean Drilling Program. **105:** 957-988.

Azetsu-Scott, K. and F. C. Tan (1997). "Oxygen isotope studies from Iceland to an East Greenland Fjord: behaviour of glacial meltwater plume." Marine Chemistry **56**: 239-251.

Bacon, S. (1997). "Circulation and fluxes in the North Atlantic between Greenland and Ireland." Journal of Physical Oceanography **27**: 1420-1435.

Bacon, S. (1998). "Decadal variability in the outflow from the Nordic Seas to the deep Atlantic Ocean." Nature **394**: 871-874.

Bacon, S. (2002). "The dense overflows from the Nordic Seas into the deep North Atlantic." ICES Marine Science Symposia **215**: 148-155.

Bacon, S. (2006). "RRS Discovery Cruise 298, 23 Aug - 25 Sep 2005. Cape Farewell and Eirik Ridge (CFER-1). National Oceanography Centre, Southmapton, Cruise Report No 10, 113 pp."

Bacon, S., W. J. Gould, et al. (2003). "Open-ocean convection in the Irminger Sea."

Geophysical Research Letters **30**: 1246.

Bacon, S., G. Reverdin, et al. (2002). "A Freshwater Jet On The East Greenland Shelf." Journal Of Geophysical Research **107**: 5 .1 - 5.8.

Bacon, S., D. A. V. Stow, et al. (2003). Cape Farewell and Eirik Ridge: Interannual To millenial thermohaline circulation variability, Southampton Oceanography Centre.

Bianchi, G. C. and I. N. McCave (1999). "Holocene periodicity in North Atlantic climate and deep-ocean flow south of Iceland." Nature **397**: 515-517.

Bianchi, G. G. and I. N. McCave (2000). "Hydrography and sedimentation under the deep western boundary current on Bjorn and Gardar Drifts, Iceland Basin." Marine Geology **165**: 137-169.

Bleck, R, and L.T. Smith (1990). “A wind-driven isopycnic coordinate model of the North and Equatorial Atlantic Ocean. 1: Model development and supporting experiments.” Journal of Geophysical Research **95**: 3273-3285

Bleck, R. (2002). "An oceanic general circulation model framed in hybrid isopycnic-Cartesian coordinates." Ocean Modelling **37**: 55 -88.

Blindheim, J. (1968). "Hydrographic investigations in the Irminger Sea in the years 1954-1964." Fiskeridir. Skr., Ser. Havunders **14**: 72-97.

Box, J. E. (2002). "Survey of Greenland instrumental temperature records 1873-2001." International Journal Of Climatology **22**: 1829-1847.

Boyle, E. A. and L. D. Keigwin (1987). "North Atlantic thermohaline circulation during the past 20,000 years linked to high-latitude surface temperature." Nature **330**: 35-40.

Broecker, W. S. (1991). "The great ocean conveyor." Oceanography **4**(2): 79-89.

Broecker, W. S. (2000). "Abrupt climate change: casual constraints provided by the palaeoclimate record." Earth Science Reviews **51**: 137-154.

Broecker, W. S., D. M. Peteet, et al. (1985). "Does the ocean-atmosphere system have more than one stable mode of operation." Nature **315**: 21-25.

Bruce, J. G. (1995). "Eddies southwest of the Denmark Strait." Deep-Sea Research I **42**(1): 13-29.

Bryan, F. (1986). "High latitude salinity and interhemispheric thermohaline circulations." Nature **323**: 301-304.

Carmack, E. C. (1972). On the hydrography of the Greenland Sea, University of Washington**:** 186.

Carter, L. and C. T. Schafer (1983). "Interaction of the Western Boundary Undercurrent with the contintal margin off Newfoundland." Sedimentology **30**: 751-768.

Chamberlin, T. C. (1906). "On a possbile reversal of deep-sea circulation and its influence on geologic climates." Journal of Geology **14**: 363-373.

Chough, S. K. and R. Hesse (1985). "Contourites from the Eirik Drift, south of Greenland." Sedimentary Geology **41**: 185-189.

Clarke, R. A. (1984). "Transport through the Cape Farewell Flemish Cap section." Rapp. P.V. Reun. Cons. Int. Explor. Mer **185**: 120-130.

Clarke, R. A., J. H. Swift, et al. (1990). "The formation of Greenland Sea Deep Water: Double diffusion or deep convection?" Deep Sea Research **37**: 687-715.

Collier, J. S. and C. J. Brown (2005). "Correlation of sidescan backscatter with grain size distribution of surficial seabed sediments." Marine Geology **214**: 431-449.

Conkright, M. E., J. I. Antonov, et al. (2002). World Ocean Database 2001 Volume 1: Introduction. Washington DC, US Government Printing Office.

Cooke, S. and E. J. Rohling (1999) "Stable Isotopes In foramniferal carbonate shells" Modern Foramnifera 239-258.

Damuth, J. E. (1975). "Echo character of the western equatorial Atlantic floor and its relationship to the dispersal and distribution of terrigenous sediments." Marine Geology **18**: 17-45.

Damuth, J. E. (1980). "Use of high-frequency (3.5-12kHz) echograms in the study of near-bottom sedimentation processes in the deep sea: A review." Marine Geology **38**: 51-75.

Dansgaard, W. and e. al (1982). "A new Greenland deep ice core." Science **218**: 1273-1277.

Dickson, B., J. Meincke, et al. (1999). "Possible predictability in overflow from the Denmark Strait." Nature **397**: 243-246.

Dickson, B., I. Yashayaev, et al. (2002). "Rapid freshening of the deep North Atlantic Ocean over the past four decades." Nature **416**: 832-837.

Dickson, R. R. and J. Brown (1994). "The production of North Atlantic Deep Water: Sources, rates and pathways." Journal of Geophysical Research **99**(C6): 12,319-12,341.

Dickson, R. R., E. M. Gmitrowicz, et al. (1990). "Deep water renewal in the northern North Atlantic." Nature **344**: 848-850.

Dietrich, G. (1957). "Hydrographic Details Of The Waters South-West Of Iceland In July 1957." Annales Biologiques **14**: 22-23.

Eden, C. and J. Willebrand (2001). "Mechanism of interannual to decadal variability of the North Atlantic circulation." Journal of Climate **14**: 2266-2280.

Fagel, N., C. Hillaire-Marcel, et al. (1997). "Changes in Western Boundary Undercurrent outflow since the Last Glacial Maximum, from smectite/illite ratios in deep Labrador Sea sediments." Paleoceanography **12**(1): 79-96.

Fagel, N., C. Robert, et al. (1996). "Clay mineral signature of the NW Atlantic Boundary Undercurrent." Marine Geology **130**(1-2): 19-28.

Faugeres, J.-C. and D. A. V. Stow (1993). "Bottom-current-controlled sedimentation: a synthesis of the contourite problem." Sedimentary Geology **82**: 287-297.

Fiadeiro, M. E. and G. Veronis (1983). "Circulation and heat flux in the Bermuda Triangle." Journal of Physical Oceanography **13**: 1158-1169.

Fischer, J., F. A. Schott, et al. (2004). "Boundary circulation at the exit of the Labrador Sea." Journal Of Physical Oceanography **34**: 1548-1570.

Flodvik, A., K. Aagaard, et al. (1988). "On The Velocity Field Of The East Greenland Current." Deep Sea Research **35**: 1335-1354.

Ganachaud, A. and C. Wunsch (2000). "Improved estimates of global ocean circulation, heat transport and mixing from hydrographic data." Nature **408**: 453-456.

Gangopadhyay, A. and A.R. Robinson (2002). “Feature-oriented regional modeling of oceanic fronts.” Dynamics Of Atmospheres And Oceans **36**: 201-232

Gardner, W. D., P. E. Biscaye, et al. (1985). "Calibration and comparison of the LDGO

nephelometer and the OSU transmissometer on the Nova Scotian Rise. ." Marine Geology **66**: 323-344.

Gill, A. E. (1982). Atmosphere-Ocean Dynamics. San Diego, Academic.

Goff, J. A., H. C. Olson, et al. (2000). "Correlation of side-scan backscatter intensity with grain-size distribution of shelf sediments, New Jersey margin." Geo-Marine Letters **20**: 43-49.

Gordon, A. L. and e. al (1992). "Climate variability and the Atlantic Ocean." Eos **73**: 161-165.

Grootes, P. M., M. Bender, et al. (1994). "Climatic Significance of the Greenland ice core records." pp 11-12 in The Atlantic Climate Change Program (ed. A-M Wilburn) Princeton,, NJ: NOAA Geophysical Fluid Dynamics Laboratory. 179pp.

Gross, T. F. and A. J. Williams (1991). "Characterisation of deep-sea storms. ." Marine Geology **99**: 281-301.

Heezen, B. C., C. D. Hollister, et al. (1966). "Shaping of the continental rise by deep geostrophic contour currents." Science **152**: 502-508.

Hillaire-Marcel, C., A. de Vernal, et al. (1994). "Isotope stratigraphy, sedimentation rates, deep circulation and carbonate events in the Labrador Sea during the last ~200ka." Canadian Journal of Earth Sciences **31**: 63-89.

Hiscott, R. N., M. Cremer, et al. (1989). Evidence from sedimentary structures for processes of sediment transport and deposition during the post-Miocene time at sites 645, 646 and 647, Baffin Bay and the Labrador Sea. Proceedings of the Ocean Drilling Program, Scientific Results. S. P. Srivastava, M. Arthur, B. Clement College Station, TX, Ocean Drilling Program. **105:** 53-63.

Holliday, N. P., A. Meyer, et al. (2007). "Retroflection of part of the east Greenland current at Cape Farewell." Geophysical Research Letters **34**(L07609): doi: 10.1029/2006GL029085.

Hollister, C. D. and I. N. McCave (1984). "Sedimentation under deep-sea storms." Nature **309**: 220-225.

Hough, S. S. (1897). "On the application of harmonic analysis to the dynamical theory of the tides. Part I. On Laplace's oscillations of the first species', and on the

dynamics of ocean currents." Philos. Trans. R. Soc. London, Ser. A **189**: 201-257.

Houghton, J. T. et al (2001). Climate Change 2001: the scientific basis. Contributions of Working Group 1 to the Third Assessment Report of the Intergovernmental Panel on Climate Change Climate Change 2001: The Scientific Basis Cambridge: Cambridge University Press.

Hunter, S. H., D. Wilkinson, et al. (2007). "Deep western boundary current dynamics and associated sedimentation on the Eirik Drift, Southern Greenland Margin." Deep-Sea Research I **54**(12): 2036-2066.

Hurrell, J. W. (1995). "Decadal trends in the North Atlantic Oscillation regional temperatures and precipitation." Science **269**: 676-679.

Innocent, C., N. Fagel, et al. (1997). "Sm-Nd signature of the modern and late Quaternary sediments from the northwest North Atlantic: Implications for deep current changes since the Last Glacial Maximum." Earth and Planetary Science Letters **146**: 607-625.

Jacobi, R. D. and D. E. Hayes (1982). Bathymetry, microphysiography and reflectivity characteristics of the West Aftican margin between Sierra Leone and Mauritania. Geology of the Northwest African Continental Margin. U. von Rad, K. Hinz, M. Sarnthein and E. Seibold. Berlin, Springer-Verlag**:** 182-212.

Keigwin, L. D. and S. J. Lehman (1994). "Deep circulation change linked to HEINRICH event 1 and Younger Dryas in a middepth North Atlantic core." Paleoceanography **9**: 185-194.

Kilworth, P. D. (1979). "On "chimney" formation in the ocean." Journal Of Physical Oceanography **9**: 531-554.

Knudsen, M. (1899). "Hydrography. The Danish Ingolf Expedition, 1(2):23-161. Bianco Luno, Copenhagen, 192pp ".

Kuijpers, A., S. R. Troelstra, et al. (2003). "Late Quaternary sedimentary processes and ocean circulation changes at the southeast Greenland margin." Marine Geology **195**(1-4): 109-129.

Lacan, F. and C. Jeandel (2004). "Denmark Strait Water Circulation Traced By

Heterogeneity In Neodymium Isotopic Compositions." Deep-Sea Research Part 1 **51**: 71-82.

Large, W.G., J.C.McWilliams et al. (1994). “Oceanic vertical mixing: a review and a model with a non-local boundary layer parameterization. Review of Geophysics **32**(4) 363-403

Latif, M. et al (2000). "Tropical stabilisation of the thermohaline circulation in a greenhouse warming simulation." Journal Of Climate **13**: 1809-1813.

Lavender, K. L., R. E. Davis, et al. (2000). "Mid-depth recirculation observed in the interior Labrador and Irminger seas by direct velocity measurements." Nature **407**: 66-69.

Lazier, J., R. Hendry, et al. (2002). "Convection and restratification in the Labrador Sea, 1999-2000." Deep-Sea Research I **49**(10): 1819-1835.

Lazier, J. R. N. (1973). "The renewal of Labrador Sea water." Deep-Sea Research **20**: 341-353.

Levitus, S., T. P. Boyer, et al. (1998). "World Ocean Database 1998. Volume 1: Introduction: NOAA Atlas NESDIS 18, 346pp."

Lherminier, P., H. Mercier, et al. (2007). "Transports across the 2002 Greenland-Portugal Ovide section and comparison with 1997." Journal of Geophysical Research.

Lohmann, K. (1999). Gezeitenkorrektur von schiffsgestuetzten Stroemungsmessungen. Kiel, University of Kiel.

Lucotte, M. and C. Hillaire-Marcel (1994). "Identification et distribution des grandes masses d'eau dans les mers du Labrador et d'Irminger." Canadian Journal of Earth Sciences **31**: 5-13.

Maier-Reimer, E. and U. Mikolajewicz (1989). "Experiments with an OGCM on the cause of the Younger-Dryas." In: Oceanography, A. Ayala-Castanares, W. Wooster and A. Yanez-Arancibia, eds, UNAM Press, Mexico 87-100: 87-100.

Malmberg, S. A., H. G. Gade, et al. (1972). Current Velocities And Volume Transports In The East Greenland Current Off Cape NordenskjoldIn August-September 1965. International Sea Ice Conference, Reykjavik, National Research Council

of Iceland.

Manabe, S. and R. J. Stouffer (1988). "Two stable equilibria of a coupled ocean-atmosphere model." Journal Of Climate **1**: 841-867.

Manighetti, B., I. N. McCave, et al. (1995). "Chronology of climate change:Developing age models for the Biogeochemical Ocean Flux Study cores." Paleoceanography **10**: 513-525.

Mann, C. R., A. R. Coote, et al. (1973). "The meridional distribution of silicate in the western Atlantic Ocean." Deep Sea Research **20**: 791-801.

Marshall, D (1995), “Topographic steering of the Antarctic Circumpolar Current.” Journal Of Physical Oceanography **25**: 1636-1650

Mauritzen, C. (1996). "Production of dense overflow waters feeding in the North Atlantic across the Greenland-Scotland Ridge. Part 1: Evidence for a revised circulation scheme." Deep Sea Research I **43**: 769-806.

McCartney, M. (1992). "Recirculating components of the deep boundary current of the northern North Atlantic." Progress in Oceanography **29**: 283-382.

McCave, I. N. (1983). "Particle size spectra, behavior and origin of nepheloid layers of the Nova Scotian Continental Rise." Journal of Geophysical Research **88**: 7647-7666.

McCave, I. N. (2001). Nepheloid layers. Encyclopedia of Ocean Sciences. J. H. Steele, S. S. Thorpe and K. K. Turekian. San Diego, Academic Press. **4:** 1861-1870.

McCave, I. N. (2003). Nepheloid layer, sediment. Encyclopedia of Sediments and Sedimentary Rocks. G. V. Middleton. Dordrecht, Kluwer.

McCave, I. N., B. Manighetti, et al. (1995). "Sortable silt and fine sediment size/composition slicing: Parameters for paleocurrent speed and paleoceanography." Paleoceanography **10**(3): 593-610.

McCave, I. N. and B. E. Tucholke (1986). Deep current-controlled sedimentation in the western North Atlantic. The Geology of North America. P. R. Vogt and B. E. Tucholke. Boulder, Co, Geological Society of America. **Volume M, Western Atlantic Region:** 451-468.

McManus, J. F., R. Francois, et al. (2004). "Collapse and rapid resumption of Atlantic

meridional cirnulation linked to deglacial climate changes." Nature **428**: 834-837.

Measures, C. I. and J. M. Edmond (1992). "The distribution of aluminium in the Greenland Sea and its relationship to ventilation processes." Journal Of Geophysical Research **97**: 17787-17800.

Megann, A.P., A.L. New et al. (2009). “The sensitivity of a coupled climate model to its ocean component.” Journal Of Climate (submitted)

Millero, F. J. and A. Poisson (1981). "International one-atmosphere equation of state of seawater." Deep Sea Research **28A**: 625-629.

Millwood, L. D., D. L. Hawkins Jr., et al. (2002). Data report: Utilizing colour reflectance analysis as a carbonate concentration proxy. Proceedings of the Ocean Drilling Program, Scientific Results. C. Richter. College Station, TX, Ocean Drilling Program. **181**.

Mosby (1962). "Water, salt and heat balance of the North Polar Sea and of the Norwegian Sea." Geophys. Norv. **24**: 289-313.

Munchow, A. (2000). "Detiding three dimensional velocity survey data in coastal waters." Journal of Atmospheric and Ocean Technology **17**(5): 736-748.

Ohmura, A. and N. Reeh (1991). "New precipitation and accumulation maps for Greenland." Journal of Glaciology **37**: 140-148.

Oort (1983). Global Atmospheric Circulation Statistics 1958-1973 Professional Paper 14, NOAA.

Pickart, R. S. (1992). "Water Mass Components Of The North Atlantic Deep Western Boundary Current." Deep-Sea Research **39**: 1553-1572.

Pickart, R. S., M. A. Spall, et al. (1997). "Mid-depth ventilation in the western boundary current system of the sub-polar gyre." Deep Sea Research **44**: 1025-1054.

Pickart, R. S., F. Straneo, et al. (2003). "Is Labrador Sea Water formed in the Irminger basin?" Deep Sea Research I **50**: 23-52.

Pickart, R. S., D. J. Torres, et al. (2002). "Hydrography of the Labrador Sea during active convection." Journal Of Physical Oceanography **32**: 428-457.

Piepgras, D. J. and G. J. Wasserburg (1987). "Rare earth element transport in the

western North Atlantic inferred from Nd isotopic observations." Geochimica et Cosmochimica Acta **51**: 1257-1271.

Rabinowitz, P. D. and S. L. Eittreim (1974). "Bottom current measurement in the Labrador Sea." Journal of Geophysical Research **79**(27): 4085-4090.

Rahmstorf, S. (2000). "The thermohaline circulation: a system with dangerous thresholds?" Climate Change **46**: 247-256.

Rahmstorf, S. (2002). "Ocean circulation and climate during the past 120,000 years." Nature **419**: 207-214.

Reid, J. L. (1994). "On The Total Geostrophic Circulation Of The North Atalantic Ocean: Flow Patterns, Tracers, And Transports." Progress In Oceanography **33**: 1-92.

Rignot, E. and P. Kanagaratnam (2006). "Changes in the velocity structure of the Greenland ice sheet." Science **311**(5763): 986-990.

Rooth, C. (1982). "Hydrology and ocean circulation." Oceanography **11**: 131-149.

Ross, C. K. (1984). "Temperature-salinity characteristics of the 'overflow' waters in Denmark Strait during OVERFLOW 73." Rapp. P.V. Reun. Cons. Int. Explor. Mer **185**: 111-119.

Rudels, B., E. Fahrbach, et al. (2002). "The East Greenland Current And Its Contribution To The Denmark Strait Overflow." ICES Journal Of Marine Science **59**: 1133-1154.

Rudels, B., H. J. Friedrich, et al. (1999). "The Arctic Circumpolar Boundary Current." Deep-Sea Research II **46**: 1023-1062.

Sarnthein, M. and e. al (1994). "Changes in east Atlantic deepwater circulation over the last 30,000 years: Eight time slice reconstructions." Paleoceanography **9**: 209-267.

Saunders, P. M. (1981). "Practical Conversion Of Pressure To Depth." Journal Of Physical Oceanography **11**: 573-574.

Saunders, P. M. (1994). "The flux of overflow water through the Charlie Gibbs Fracture Zone." Journal Of Geophysical Research **99**.

Schlosser, P., G. Bonisch, et al. (1991). "Reduction of deepwater formation in the

Greenland Sea during the 1980's; evidence from tracer data." Science **251**: 1054-1056.

Schmitz, W. J. (1996). On the World Ocean Circulation: Volume 1: Some global features/North Atlantic circulation.

Schmitz, W. J. and M. S. McCartney (1993). "On the North Atlantic circulation." Reviews of Geophysics **31**(1): 29-49.

Schott, F. A., R. Zantopp, et al. (2004). "Circulation And Deep-Water Export At The Western Exit Of The Subpolar North Atlantic." Journal Of Physical Oceanography **34**: 817-843.

Seager, R., D. S. Battisti, et al. (2002). "Is the Gulf Stream responsible for Europe's mild winters." Quarterly Journal of the Royal Meteorological Society **128**: 2563-2586.

Smethie, W. M. and J. H. Swift (1989). "The tritium:krypton-85 age of the Denmark Strait overflow water and Gibbs Fracture zone water just south of Denmark Strait. ." Journal of Geophysical Research **94**: 8265-8275.

Smith, J. N., E. P. Jones, et al. (2005). "Iodine 129/CFC 11 transit times for Denmark Strait Overflow Water in the Labrador And Irminger Seas." Journal of Geophysical Research **110**: C05006.

Smith, W. H. F. and D. T. Sandwell (1997). "Global sea floor topography from satellite altimetry and ship depth soundings." Science **277**: 1956-1962.

Spinrad, R. and J. R. V. Zaneveld (1982). "An analysis of the optical features of the near-bottom and bottom nepheloid layers in the area of the Scotian Rise." Journal of Geophysical Research **87**(9533-9561).

Srivastava, S. P., K. E. Louden, et al. (1989). Results of detailed geological and geophysical measurement at ODP Sites 645 in Baffin Bay and 646 and 647 in the Labrador Sea. Proceedings of the Ocean Drilling Program, Scientific Results. S. P. Srivastava, M. Arthur, B. Clement and etal. College Station, TX, Ocean Drilling Program. **105:** 891-919.

Stanford, J. D., E. J. Rohling, et al. (2006). "Timing of meltwater pulse 1a and climate responses to meltwater injections." Paleoceanography **21**(4).

Stefansson, U. (1962). "North Icelandic Waters." Rit. Fiskidelidar.

Stommel, H. (1961). "Thermohaline convectionwith two stable regimes of flow." Tellus **13**: 224-230.

Stoner, J. S., J. E. T. Channell, et al. (1995). "Magnetic properties of deep-sea sediments off southwest Greenland: Evidence for major differences between the last two deglaciations." Geology **23**(3): 241-244.

Stow, D. A. V., J. E. Armishaw, et al. (2002). Holocene contourite sand sheet on the Barra Fan slope, NW Hebridean margin. Deep-Water Contourite Systems: Modern Drifts and Ancient Series, Seismic and Sedimentary Characteristics. D. A. V. Stow, C. J. Pudsey, J. A. Howe, J.-C. Faugeres and A. Viana. London, Geological Society. **Memoir 22:** 99-119.

Stramma, L., D. Kieke, et al. (2004). "Deep water changes at the western boundary of the sub-polar North Atlantic during 1996 to 2001." Deep-Sea Research Part 1 **51**: 1033-1056.

Strass, V. H., E. Fahrbach, et al. (1993). "Formation Of Denmark Strait Overflow Water By Mixing In The East Greenland Current." Journal Of Geophysical Research **98**: 6907-6919.

Sun, S. and R. Bleck (2001). "Atlantic thermohaline circulation and its response to increasing CO2 in a coupled atmosphere-ocean model." Geophysical Research Letters.

Sutherland, D. A. and R. S. Pickart (2008). "The East Greenland Coastal Current: Structure,variability, and forcing." Progress in Oceanography **78**(1): 58-77.

Swift, J. H. (1984). "The circulation of Denmark Strait and Iceland-Scotlan overflow waters in the North Atlantic." Deep Sea Research **31**: 1339-1355.

Swift, J. H. (1986). The Arctic Waters. The Nordic Seaa. B. G. Hurdle. New York, Springer-Verlag**:** 129-154.

Swift, J. H. and K. Aagaard (1981). "Seasonal transitions and water mass formation in the Iceland and Greenland seas." Deep Sea Research **28A**: 1107-1129.

Swift, J. H., K. Aagaard, et al. (1980). "The contribution of the Denmark Strait overflow in the deep North Atlantic." Deep Sea Research **27A**: 29-42.

Swift, J. H. and K. P. Koltermann (1988). "The origin of the Norweigan Sea Deep Water." Journal Of Geophysical Research **93**: 3563-3569.

Szuman, M., C. Berndt, et al. (2006). "Seabed characterization through a range of high-resolution acoustic systems - a case study offshore Oman." Marine Geophysical Researches **27**: 167-180.

Talley, L. D. and M. S. McCartney (1982). "Distribution and circulation of Labrador Sea Water." Journal Of Physical Oceanography **12**: 1189-1205.

van de Wal, R. S. W. (2003). Greenland Modelling. Mass Balance of the Cryosphere: Observations and Modelling of Contemporary and Future Changes. J. L. Bamber and A. J. Payne. Cambridge, Cambridge University Press**:** 437-457.

van de Wal, R. S. W., W. Boot, et al. (2008). "Large and rapid melt-induced velocity changes in the ablation zone of the Greenland ice-sheet." Science **321**(5885).

Watts, D. R. (1991). Equatorward currents in temperatures 1.8-6.0C on the continental slope in the mid-Atlantic Bight. Deep Convection And Depp Water Formation In The Oceans. P. C. Chu and J. C. Gascard. Amsterdam, Elsevier**:** 183-196.

Webb, D. J. (1995). "The Vertical Advection Of Momentum In Bryan-Cox-Semtner Ocean General Circulation Models." Journal Of Physical Oceanography **25**: 3186-3195.

Weiss, R. (1970). "The solubility of nitrogen, oxygen and argon in water and seawater." Deep Sea Research **17**: 721-735.

Williams, W.J. and G.G. Gawarkiewicz (2001). “The adjustment of a shelfbreak jet to cross-shelf topography.” Deep Sea Research II **48**: 373-393

Wilkinson, D. and S. Bacon (2005). "The spatial and temporal variability of the East Greenland Current from historic data." Geophysical Research Letters **32**(L24618).

Wold, C. N. (1994). "Cenozoic sediment accumulation on drifts in the northern North Atlantic." Paleoceanography **9**(6): 917-941.

Woodgate, R. A., E. Fahrbach, et al. (1999). "Structure and transport of the East Greenland Current at 75ºN from moored current meters." Journal Of Geophysical Research **104**: 18059-18072.

Worthington, L. V. (1969). "An attempt to measure the volume transport of the Norweigan Sea overflow water through the Denmark Strait." Deep Sea Research **16 (Supplement)**: 421-432.

Worthington, L. V. (1970). "The Norweigan Sea as a mediterranean basin." Deep Sea Research **17**: 77-84.

Worthington, L. V. (1976). "On The North Atlantic Circulation." Johns Hopkins Oceanographic Studies **6**: 1-110.

Worthington, L. V. and G. H. Volkman (1965). "The volume transport of the Norwagian Sea overflow water in the North Atlantic." Deep Sea Research **12**: 667-676.

Wust, G. (1935). "The Stratosphere Of The Atlantic Ocean." Wiss. Ergebn. Dtsch.Atlant.Exped. 'Meteor' 6 **1**: 109-288.